A STATISTICAL ASSOCIATING FLUID THEORY FOR POLAR AND ELECTROLYTE FLUIDS

by

Honggang Zhao

Dissertation

Submitted to the Faculty of the

Graduate School of Vanderbilt University

in partial fulfillment of the requirements

for the degree of

DOCTOR OF PHILOSOPHY

in

Chemical Engineering

May, 2007

Nashville, Tennessee

Approved:

Professor Clare McCabe

Professor Peter T. Cummings

Professor Kenneth A. Debelak

Professor G. Kane Jennings

Professor Harold S. Park

Dedicated

To

My Family

ACKNOWLEDGEMENT

I would like to gratefully and sincerely thank Dr. Clare McCabe for her guidance, understanding, patience, and most importantly, her friendship during my graduate studies at both Colorado School of Mines and Vanderbilt University. I am lucky to be her first PhD student. During the past four years, she encouraged me to grow not only as a chemical engineering but also as an independent thinker. For everything you've done for me, Dr. McCabe, I thank you. I would also like to thank all of the members of the McCabe research group, especially Dr. Lixin Sun, Yun Peng and Pedro Morgado for giving me the opportunity to cowork with them.

I would also like to thank my dissertation committee consisting of Dr. Clare McCabe, Dr. Peter T. Cummings, Dr. Kenneth A. Debelak, Dr. G. Kane Jennings and Dr. Harold S. Park. In particular, I am grateful to Dr. Peter T. Cummings for his assistance and guidance in getting my graduate career started on the right foot. Those discussions with him, which I really enjoyed, gave me a lot of inspiration. I believe that his thoughts provided me with the unique opportunity to gain a wider breath of experience while still a graduate student.

I would like to thank the Department of Chemical Engineering at Colorado School of Mines and Vanderbilt University for their valuable supports.

Finally, and most importantly, I would like to thank my family and my parents. Their support, encouragement, quiet patience and faith in me were the undeniable bedrock upon which the past my life have been built. It was under their watchful eyes that I gained so much drive and ability to tackle challenges I have met.

TABLE OF CONTENTS

Page

LIST OF TABLES

Page

LIST OF FIGURES

Page

CHAPTER I

INTRODUCTION AND BACKGROUND

1.1 Introduction

The ability to accurately predict the thermodynamic properties and phase behavior of fluids is central to product and process design, not only in traditional chemical engineering fields such as petroleum refining, but also in environmental and biochemical engineering in purification and separation processes. Since the energy crisis of the 1970s interest in the ability to predict the thermodynamic properties of fluids has grown, with industry increasingly looking for accurate theoretical tools to minimize costs. While many equations of state have been suggested in the literature to correlate and predict the thermodynamics of fluids, they often rely on effective parameters to describe the molecular interactions and so, particularly for complex fluids, have limited applicability. In order to develop a predictive approach to determine the thermophysical properties and phase behavior of complex fluids, the effects of the size, shape and molecular-level interactions need to be explicitly included into the equation of state (EOS). So called molecular based equations of state such as the perturbed hard chain theory and the statistical associated fluid theory (SAFT) have grown in popularity as they explicitly take into account the effect of such interactions and have parameters that directly relate to molecular level physical interactions.

Perhaps the most successful of these molecular-based equations of state (EOS) is the SAFT approach proposed by Chapman [1, 2] and co-workers on the basis of Wertheim's thermodynamic perturbation theory (TPT) [3-6]. An important feature of the

SAFT theory is that it explicitly takes into account nonsphericity and association interactions and provides a powerful method for investigating the phase behavior of both non-associating and associating chain fluids. In the SAFT framework, the free energy can be written as the sum of four separate contributions:

$$\frac{A}{Nk_BT} = \frac{A^{ideal}}{Nk_BT} + \frac{A^{mono}}{Nk_BT} + \frac{A^{chain}}{Nk_BT} + \frac{A^{assoc}}{Nk_BT} \tag{1.1}$$

where N is the number of molecules, k_B Boltzmann's constant, and T the temperature. A^{ideal} is the ideal free energy, A^{mono} the contribution to the free energy due to the monomer segments, A^{chain} the contribution due to the formation of bonds between monomer segments, and A^{assoc} is the contribution due to association. Hence, a SAFT fluid is a collection of monomers that can form covalent bonds; the monomers interact via repulsive and attractive (dispersion) forces, and, in some cases, association interactions [7]. The many different versions of SAFT essentially correspond to different choices for the monomer fluid, and different theoretical approaches to the calculation of the monomer free energy and structure. For an excellent overview the reader is directed to a recent review [8]. In this work we focus on the SAFT-VR approach, which is a recent extension of the theory that describes chain molecules formed from hard-core monomers with attractive potentials of variable range (SAFT-VR) [9, 10], typically a square well. The SAFT-VR equation has been successfully used to describe the phase equilibria of a wide range of industrially important systems; for example, alkanes of low molecular weight through to simple polymers [9, 11-14], and their binary mixtures [15-23], perfluoroalkanes [24-26], hydrogen fluoride [27], boron triflouride [28], water [29, 30], refrigerant systems [31], carbon dioxide [22, 27, 32-34], and electrolyte solutions

[35-38], have all been studied. Further details of the SAFT and SAFT-VR equations of state will be presented in section 1.2.

Although the SAFT equation in its many variations explicitly takes into account the effect of molecular shape, size and hydrogen bonding interactions the effects of long-range interactions, such as ion-ion, ion-dipole, dipole-dipole etc., are typically taken into account in an effective way through the segment size and energy parameters. Since the interactions are not described explicitly in the equation the predictive capability is reduced and often large binary interaction parameters have to be fitted to experimental data. In order to overcome this drawback of the SAFT equation and develop a more predictive approach, in this work, versions of the statistical associating fluids theory (SAFT) will be developed to model polar fluids and electrolyte solutions in which the effects of the long range interactions are taken explicitly into account.

In chapter II, we present a statistical associating fluid theory for potentials of variable range to model dipolar fluids. The new theory (SAFT-VR+D) explicitly accounts for dipolar interactions through a combination of the SAFT-VR approach with integral equation theory. Predictions for the thermodynamic properties and phase behavior of dipolar square-well monomer and chain fluids, in which one or more segments are dipolar, are considered and compared with new computer simulation data. In Chapter III, the SAFT-VR+D approach is extended to study associating dipolar fluids. Predictions for the thermodynamic properties and phase behavior of dipolar associating square-well monomers with one, two and four association sites are considered and compared with new isothermal-isobaric and Gibbs ensemble Monte Carlo simulations data. Finally, the model is applied to model water. In Chapter IV, a SAFT-VR approach is developed to

describe the *PVT* phase behavior of electrolyte fluids, in which the solvent molecules are explicitly described as dipolar associating molecules. Again *NPT* MC simulations are conducted to obtain simulation data to compare to the theoretical predictions. In Chapter V, the SAFT-VR equation is extended to model ionic liquids. The correlations and predictions of the thermodynamic properties for several ionic liquids studied are presented and directly compared to experimental data. Finally, concluding remarks are made and recommendation is discussed in Chapter VI.

1.2 Background

1.2.1 SAFT Equation of State

The development of accurate equations of state firmly based in statistical mechanics is one of the main research fields in chemical engineering, since it allows for an accurate description of the thermodynamic properties of real substances. The first equation of state based on molecular theory was due to van der Waals (vdW). The vdW EOS, which introduces two basic molecular features such as molecular size and attractive interactions, gives a very good first approximation to the properties of real substances. However, some molecules are highly non-spherical and/or possess highly directional attractive forces such as hydrogen bonds, and the van der Waals' approach tends to fail in such cases. In recent years, considerable effort has been made in the development of theories for fluids of associating chain molecules. The most successful theories for such systems originate in the seminal work of Wertheim [3-6]. The statistical associating fluid theory (SAFT) [7, 39] is one such theory. The SAFT approach provides a molecular based EOS that has

been used extensively to correlate and predict experimental results for a wide variety of substances. It is evident from even a brief overview of the recent literature that the SAFT equation is becoming one of the most accurate and versatile tools in the description of fluid phase equilibria. Excellent reviews of the SAFT EOS were recently published by Gubbins and Muller [40] and Economou [41].

As reflected by Figure 1, a SAFT fluid can be considered to be a collection of monomers that can form covalent bonds; the monomers can interact via repulsive and dispersion forces, and, in some cases, association interactions. Since the SAFT EOS has a firm basis in statistical mechanics, the theory offers several advantages. The first advantage is that each of the approximations made in the development of SAFT, such as the chain and association terms, can be tested against molecular simulation results. In this way, the range of applicability of each term in the equation of state can be determined. The second advantage is that we can systematically refine the equation of state by making better approximations or by extending the theory. A third advantage is that the SAFT parameters have real physical meaning. For example, associating or hydrogen-bonding molecules are characterized by association energy and bonding volume (related to the change in entropy on association) [42] which can be determined from spectroscopy or from quantum mechanical calculations.

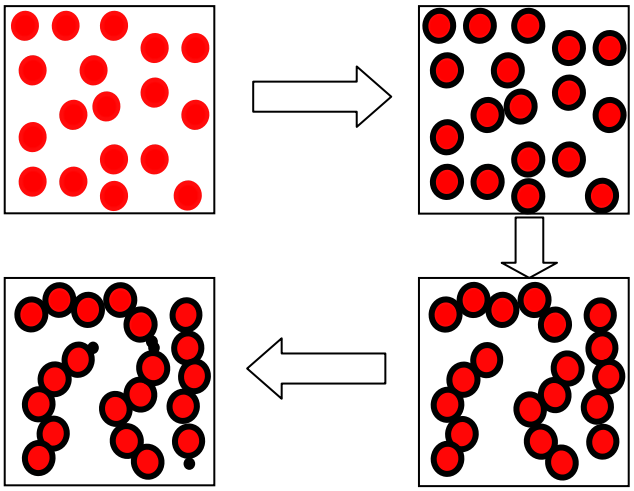

Figure 1: Schematic picture of formation of SAFT chain associating fluids. A collection of hard spheres which interact through dispersion interaction, and those hard spheres tangibly bond together to form chain molecules, then those molecules interact through association interaction.

1.2.2 SAFT-VR Equation of State

In the past decade, several versions of the SAFT equation have been proposed. One of these augmented SAFT EOSs is the SAFT-VR EOS [43, 44], which describes chain molecules formed from hard-core monomers with attractive potentials of variable attractive range (SAFT-VR), typically a square-well potential as given by equation (1.2).

$$u_{ij}^{SW}(r) = \begin{cases} +\infty & \text{if} \quad r < \sigma_{ij} \\ -\varepsilon_{ij} & \text{if} \quad \sigma_{ij} \le r < \lambda_{ij}\sigma_{ij} \\ 0 & \text{if} \quad r \ge \lambda_{ij}\sigma_{ij} \end{cases} \tag{1.2}$$

The general form of the SAFT-VR Helmholtz free energy for associating chain molecules is given by equation 1.1. The addition of the non-conformal parameter characterizing the range of the potential greatly enhances the performance of the equation in describing the phase behavior of real systems. In this theory the dispersion interactions are treated via a

second-order high-temperature perturbation expansion, which provides a more rigorous description of the thermodynamics than found in simpler versions of the SAFT approach, such as the SAFT-HS EOS [45] in which the mean-field approximation was used to describe the attractive interaction between monomer segments. Detailed expressions for each term of the equation 1.1 are presented in turn below.

1.2.2.1 Ideal contribution

The ideal contribution to the free energy is given by

$$\frac{A^{IDEAL}}{Nk_BT} = \ln\left(\rho\Lambda^3\right) - 1 \tag{1.3}$$

where $\rho = N/V$ is the number density of chain molecules, N the number of molecules, V the volume of the system, and Λ the thermal de Broglie wavelength. Since the ideal term is separated out, the remaining terms are as residual free energies.

1.2.2.2 Monomer contribution

The contribution to the Helmholtz free energy due to the monomer segments is

$$\frac{A^{MONO.}}{Nk_BT} = m\frac{A^{MONO.}}{N_sk_BT} = ma^M \tag{1.4}$$

where N_s is the total number of square-well spherical monomers. Within the high temperature perturbation theory of Barker and Henderson, in the inverse of the temperature $\beta = 1/k_BT$, the isotropic term a^M is given by,

$$a^M = a^{HS} + \beta a_1^{SW} + \beta^2 a_2^{SW} \tag{1.5}$$

The isotropic contribution to the free energy is expressed as in the SAFT-VR approach by a^{HS}, the free energy due to repulsive interactions between the hard cores, and a_1^{SW} and a_2^{SW}, the first and second perturbative terms associated with the isotropic attractive energy. The expression of Carnahan and Starling is used for the hard sphere term

$$a^{HS} = \frac{4\eta - 3\eta^2}{(1-\eta)^2} \tag{1.6}$$

where η is the packing fraction, defined as $\eta = (\pi/6)\rho_s\sigma^3$. The first perturbative term of the mean attractive energy corresponds to the average of the monomer-monomer interaction calculated with the hard sphere structure. Using the mean-value theorem we can obtain an expression for a_1^{SW} in terms of an effective packing fraction η_{eff} evaluated at contact [46],

$$a_1^{SW} = -4\eta\varepsilon(\lambda^3 - 1)g^{HS}(1;\eta_{eff}) \tag{1.7}$$

where the Carnahan and Starling equation of state is used to evaluate $g^{HS}(1;\eta_{eff})$.

$$g^{HS}(1;\eta_{eff}) = \frac{1-\eta_{eff}/2}{(1-\eta_{eff})^3} \tag{1.8}$$

For range $1.1 \le \lambda \le 1.8$, the effective packing fraction η_{eff} is described by a function of η and λ, viz

$$\eta_{eff}(\eta,\lambda) = c_1\eta + c_2\eta^2 + c_3\eta^3 \tag{1.9}$$

where the coefficients c_n are given by

$$\begin{pmatrix} c_1 \\ c_2 \\ c_3 \end{pmatrix} = \begin{pmatrix} 2.25855 & 0.249434 & 0.249434 \\ -0.669270 & -0.827739 & -0.827739 \\ 10.1576 & 5.30827 & 5.30827 \end{pmatrix} \times \begin{pmatrix} 1 \\ \lambda \\ \lambda^2 \end{pmatrix} \tag{1.10}$$

The second perturbation term a_2^{SW} is obtained from the first density derivative of a_1^{SW} within the local compressibility approximation

$$a_2^{SW} = \frac{1}{2}\varepsilon K^{HS}\eta\frac{\partial a_1^{SW}}{\partial \eta} \tag{1.11}$$

where K^{HS} is the hard-sphere isothermal compressibility of Percus-Yevick (PY)

$$K^{HS} = \frac{(1-\eta)^4}{1+4\eta+4\eta^2} \tag{1.12}$$

1.2.2.3 Chain contribution

The contribution to the free energy due to chain formation from *m* dipolar square-well monomers is given by,

$$\frac{A^{CHAIN}}{Nk_BT} = -(m-1)\ln y^{SW}(\sigma) \tag{1.13}$$

$y^{SW}(r)$ is the dipolar square-well monomer background correlation function evaluated at hard-core contact,

$$y^{SW}(r) = \exp\left[\beta u^{SW}(r)\right] g^{SW}(r) \tag{1.14}$$

where $g^{SW}(r)$ is the pair distribution function for the square-well fluid. In the SAFT-VR equation, a high-temperature perturbation expansion is used to determine the radial distribution function for the square-well fluid $g^{SW}(r)$

$$g^{SW}(r) = g^{HS}(r) + \beta\varepsilon g_1(r) \tag{1.15}$$

where the radial distribution function $g^{SW}(r)$ at hard-core contact is given by

$$g^{SW}(\sigma^+) = g^{HS}(\sigma) + \beta\varepsilon g_1(\sigma) \tag{1.16}$$

and $g_1(\sigma)$ can be obtained from a self-consistent calculation of the pressure using the Clausius virial theorem and the first derivative of the free energy with respect to the density.

1.2.2.4 Association contribution

Based on the theory of Wertheim, the contribution due to association for *s* sites on a molecule is obtained as [7]:

$$\frac{A^{ASSOC}}{NkT} = \sum_{a=1}^{s}(\ln X_a - \frac{X_a}{2}) + \frac{s}{2} \tag{1.17}$$

where the sum is over all *s* sites of type *a* on a molecule, and X_a is the fraction of molecules not bonded at site *a*:

$$X_a = \frac{1}{1 + \sum_{b=1}^{s} \rho X_b \Delta_{a,b}} \tag{1.18}$$

The function $\Delta_{a,b}$, which characterizes the association between site *a* and site *b* on different molecules, can be written as

$$\Delta_{a,b} = K_{a,b} f_{a,b} g^M(\sigma) \tag{1.19}$$

where, $g^M(\sigma)$ is the contact value of the monomer-monomer radial distribution function, $f_{a,b} = \exp\left(-\psi_{a,b}/kT\right) - 1$ is the Mayer *f* function of the *a*-*b* site-site bonding interaction $\psi_{a,b,}$ and $K_{a,b}$ is the volume available for bonding [47].

CHAPTER II

PHASE BEHAVIOR OF DIPOLAR FLUIDS FROM THE SAFT-VR+D EQUATION OF STATE

2.1 Introduction

Anisotropic interactions can have a significant effect on the thermodynamic properties of fluids, both for fluids of simple spherical molecules such as water to chain-like molecules such as alcohols and ketones. While many equations of state have been used to describe the thermodynamics of these systems, they often rely on effective parameters to describe the molecular interactions, and so have limited applicability beyond the fluids and state conditions to which the parameters were fitted. In order to develop a truly predictive approach for the thermophysical properties and phase behavior of fluids the molecular-level interactions need to be explicitly included into the equation of state.

As discussed in Chapter I, while the SAFT equation in its many variations have been applied to the study of polar fluids, the molecular interactions between the molecules are typically taken into account in an effective way through the segment size and energy parameters [48-51]. In SAFT equations of state that have been specifically developed for polar fluids, dipolar and/or quadrupolar interactions are generally incorporated through the addition of the corresponding terms to equation 1. For the dipolar term, both the μ-expansion proposed by Gubbins and Gray[52], which describes the interaction of dipolar hard sphere fluids using an angular pair correlation function, and the more rapidly converging Padé approximation of Stell and coworkers[53], have been widely adopted. For example, Muller and Gubbins[50] applied the μ-expansion to

describe water as a hard, spherical, associating, dipolar fluid within Wertheim's TPT theory, achieving good agreement with simulation and experimental data and in a SAFT like equation of state for alkanols and water Xu *et al*.[51] applied a Padé approximation to describe dipole-dipole interactions.

A common feature of these equations of state is to treat non-spherical dipolar molecules as spherical dipolar fluids. As a result, the orientation of the dipolar interaction and the possibility of multiple polar sites within a molecule cannot be taken into account. In contrast, Jog et al. [54, 55] developed a SAFT EOS for tangent hard sphere chains with dipoles on alternate segments. This approach was subsequently used by Tumakaka and Sadowski[56] to extend the PC-SAFT EOS to describe mixtures of non-dipolar and polar molecules. Dominik et al.[57] later compared Polar PC-SAFT in which the dipolar contribution of Jog is used with predictions using an alternate dipolar term due to Saggar and Fischer [58, 59], and found that while both approaches yield similar results the parameters for the original Polar PC-SAFT were more physically meaningful. More recently, Gross and Vrabec [60] developed a contribution for dipolar interactions based on third order perturbation theory which uses simulation data for the vapor-liquid equilibria of the two-center Lennard-Jones plus point dipole fluid to determine the model constants. The proposed term has been incorporated into the PC-SAFT equation of state and has been shown to improve the description of pure component and mixture phase equilibria for dipolar fluids over the original PC-SAFT approach.

We note that in the SAFT EOS approaches summarized above, and to the best of our knowledge, in those reported in the literature to date, the inclusion of dipolar

contributions to the equation of state has been limited to adding a dipolar term to the free energy and therefore the structural impact of the dipolar interactions on the thermodynamics and phase behavior has not been considered.

An alternative approach to using perturbation theory to describe dipolar fluids is through integral-equation theory. Wertheim[61] solved the Ornstein-Zernike (OZ) equation using the mean spherical approximation (MSA) closure for dipolar hard spheres and provided analytical expressions for the thermodynamic and structural properties of the model. Patey and Valleau [62] and Verlet and Weis [63] subsequently performed computer simulations for the dipolar hard-sphere system and found that the theoretical MSA harmonic coefficients for dipolar spheres are in good agreement with simulation data far from contact, but are too small at contact. Extensions, such as the optimized random phase approximation (ORPA) [64] and the exponential approximation (EXP) [64], have been proposed to systematically improve the results of the MSA for the pair correlation function of dipolar hard spheres. In particular, the linearized version of the EXP (LEXP), suggested by Verlet and Weis [63], provides considerable improvement for the pair correlation function over the MSA result at contact. Subsequently, Adelman and Deutch [65] in a similar approach to Wertheim, solved the OZ equation for simple polar mixtures, in which the components are restricted to have equal diameters but may have different dipole moments. Although other integral equation theories for dipolar fluids, such as the reference hypernetted chain approximation of Patey and co-workers [66-68], these do not provide analytical expressions and so require numerical solution methods.

Here, we present an equation of state to model chain molecules with one or multiple dipolar sites embedded in specific segments of the chain through a combination

of the MSA theory for dipolar interactions and the statistical associating fluid theory for potentials of variable range (SAFT-VR). We refer to the resulting theory and EOS as SAFT-VR+D. In our model, the dipolar square-well monomer fluid is chosen as the reference fluid within the framework of the SAFT approach. The potential of the reference state therefore consists of two parts: an isotropic square well potential and an anisotropic dipolar potential, for which we use the MSA and the SAFT-VR equation respectively. Although the solution of the MSA for dipolar fluids is approximate, it provides analytical expressions for the thermodynamic and structural properties, thus permitting the development of a SAFT-VR equation of state for dipolar fluids in which the effect of the dipole on the phase behavior is explicitly described in the monomer and chain terms and not simply treated as a perturbation at the level of the monomer. In this work, two specific systems are considered; molecules with a dipole moment embedded in each segment and molecules in which dipole moments are embedded in specific segments.

The remainder of the chapter is organized as follows: in section 2.2 we present the SAFT-VR+D model and theory for dipolar square-well fluids. In section 2.3, details of the molecular simulations performed are presented. Results for the phase behavior of pure dipolar square-well fluids are presented and compared with simulation results in section 2.4. Finally, concluding remarks are made and future work discussed in section 2.5.

2.2 Model and theory

2.2.1 Pure Chain Fluids

We have developed an accurate equation of state to model dipolar square-well fluids through a combination of the SAFT-VR approach and the generalized mean-spherical approximation for dipolar fluids. As in the SAFT-VR approach, non-associating molecules are described by four parameters; the size of the monomer segments σ, the depth ε and range λ of the square-well potential characterizing the attractive dispersion interactions between the monomer segments, and *m* which determines the number of segments tangentially bonded together in the model chain. The inclusion of dipolar interactions into the SAFT-VR EOS introduces three additional parameters; the dipole moment μ and the orientation of the dipoles which is determined by the azimuthal θ and polar ϕ angles of the inter-segment axis along *r,* as shown in Figure 1.[69]

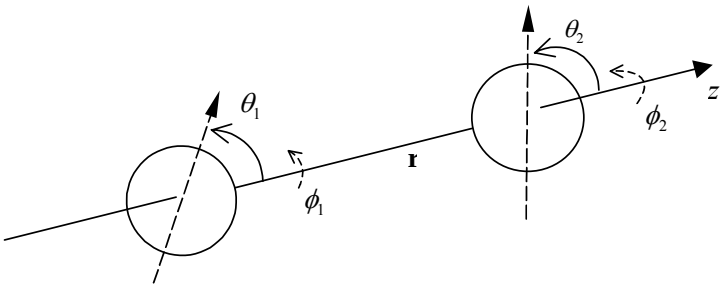

Figure 2: The inter-dipole site coordinate system, with polar axis along *r* [69].

In the SAFT-VR+D approach, the reference fluid is a dipolar square-well fluid with the dipole embedded in the center of the segment from which chain molecules of *m* tangentially bonded segments can be formed, as shown schematically in Figure 2. Each

segment has a hard-core diameter σ and interacts through an intermolecular potential of the form

$$u(\mathbf{r}\boldsymbol{\omega}_1\boldsymbol{\omega}_2) = u^{HS}(r;\sigma) - \varepsilon\phi^{SW}(r;\lambda) + u^{DIPOLE}(\mathbf{r}\boldsymbol{\omega}_1\boldsymbol{\omega}_2) \tag{2.1}$$

Here, $\mathbf{r}$ is the vector between the center of the two monomers, $r = |\mathbf{r}|$ and $\boldsymbol{\omega}_i = (\theta_i, \phi_i)$ is the set of angles defining the orientation of the dipole in monomer *i* (see Figure 1). As in the SAFT-VR equation the monomer-monomer isotropic potential consist of a hard sphere repulsive interaction u^{HS}, defined by

$$u^{HS}(r;\sigma) = \begin{cases} \infty & r < \sigma \\ 0 & r > \sigma \end{cases} \tag{2.2}$$

and an attractive square-well interaction of depth $-\varepsilon$ and shape $\phi^{SW}(r;\lambda)$, where λ is a parameter associated with the range of the attractive forces, *viz*

$$\phi^{SW}(r;\lambda) = \begin{cases} 1 & \sigma < r < \lambda\sigma \\ 0 & r > \lambda\sigma \end{cases} \tag{2.3}$$

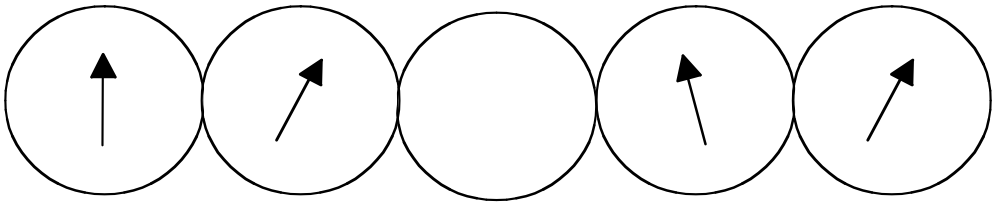

Figure 3: Schematic showing the molecular model used to describe a chain fluid with dipole moments embedded in some segments.

The dipole-dipole potential is a long-range anisotropic interaction, which can be expressed as,

$$u^{DIPOLE}(\mathbf{r}\boldsymbol{\omega}_1\boldsymbol{\omega}_2) = -\frac{\mu^2}{r^3} D(\mathbf{n}_1\mathbf{n}_2\mathbf{r}) \tag{2.4}$$

where

$$D(\mathbf{n}_1\mathbf{n}_2\hat{\mathbf{r}}) = 3(\mathbf{n}_1 \cdot \hat{\mathbf{r}})(\mathbf{n}_2 \cdot \hat{\mathbf{r}}) - \mathbf{n}_1 \cdot \mathbf{n}_2 \tag{2.5}$$

Here $\hat{\mathbf{r}}$ is the unit vector in the direction of $\mathbf{r}$ joining the center of the segments (Figure 1) and $\mathbf{n}_i$ is a unit vector parallel to the dipole moment of segment i.

Within the SAFT framework, the Helmholtz free energy A for N chains formed from m spherical segments, which in this work refers to spherical dipolar square-well segments, can be written in the form

$$\frac{A}{Nk_BT} = \frac{A^{IDEAL}}{Nk_BT} + \frac{A^{MONO}}{Nk_BT} + \frac{A^{CHAIN}}{Nk_BT} \tag{2.6}$$

where A^{IDEAL} is the free energy of the ideal fluid, A^{MONO} is the contribution due to the dipolar square-well monomer, and A^{CHAIN} represents the free energy due to chain formation. We have not included the contribution due to association interactions, as only non-associating (i.e. hydrogen bond type association interactions) dipolar chain molecules are considered in this first extension of the theory.

In order to understand the nature of the MSA solution and its relevance to the current problem, we need to examine it briefly. The MSA for dipolar hard spheres arises from the exact Ornstein-Zernike equation for linear molecules, given by

$$h(\mathbf{r}\omega_1\omega_2) = c(\mathbf{r}\omega_1\omega_2) + \frac{\rho}{4\pi}\int h(\mathbf{r}_{12}\omega_1\omega_3)c(\mathbf{r}_{23}\omega_3\omega_2)d\mathbf{r}_3 d\omega_3 \tag{2.7}$$

where $h(\mathbf{r}\omega_1\omega_2)$ and $c(\mathbf{r}\omega_1\omega_2)$ are the total and direct correlation functions respectively. The total correlation function is related to the pair distribution function $g(\mathbf{r}\omega_1\omega_2)$ by $h(\mathbf{r}\omega_1\omega_2) = g(\mathbf{r}\omega_1\omega_2) - 1$. The MSA closure for a hard core potential states that

$$
\begin{aligned}
h(\mathbf{r}\boldsymbol{\omega}_1\boldsymbol{\omega}_2) &= -1 & r < \sigma \\
c(\mathbf{r}\boldsymbol{\omega}_1\boldsymbol{\omega}_2) &= -\frac{1}{k_B T} u(\mathbf{r}\boldsymbol{\omega}_1\boldsymbol{\omega}_2) & r > \sigma
\end{aligned}
\tag{2.8}
$$

Hence, the MSA for dipolar hard spheres becomes

$$
\begin{aligned}
h(\mathbf{r}\boldsymbol{\omega}_1\boldsymbol{\omega}_2) &= -1 & r < \sigma \\
c(\mathbf{r}\boldsymbol{\omega}_1\boldsymbol{\omega}_2) &= \frac{\mu^2}{k_B T r^3} D(\mathbf{n}_1\mathbf{n}_2\hat{\mathbf{r}}) & r > \sigma
\end{aligned}
\tag{2.9}
$$

Wertheim [61] showed that with this closure the total and direct correlation functions for dipolar hard spheres in the MSA can be written in the simplified form,

$$
\begin{aligned}
h(\mathbf{r}\boldsymbol{\omega}_1\boldsymbol{\omega}_2) &= h_s(r) + h_\Delta(r)\Delta(\mathbf{n}_1\mathbf{n}_2) + h_D(r)D(\mathbf{n}_1\mathbf{n}_2\hat{\mathbf{r}}) \\
c(\mathbf{r}\boldsymbol{\omega}_1\boldsymbol{\omega}_2) &= c_s(r) + c_\Delta(r)\Delta(\mathbf{n}_1\mathbf{n}_2) + c_D(r)D(\mathbf{n}_1\mathbf{n}_2\hat{\mathbf{r}})
\end{aligned}
\tag{2.10}
$$

where $\Delta(\mathbf{n}_1\mathbf{n}_2) = \mathbf{n}_1 \cdot \mathbf{n}_2$ and $h_s(r)$, $h_\Delta(r)$ and $h_D(r)$ and the corresponding direct correlation quantities are functions of r only. Moreover, within the MSA, $h_s(r)$ and $c_s(r)$ are given by their Percus-Yevick (PY) hard-sphere values, and $h_\Delta(r)$ and $h_D(r)$ are calculated from functions arising from the solution of the PY approximation for hard spheres. We point out, however, that much of the Wertheim solution holds true in more general cases. For example, consider the dipolar square-well fluid in the generalized MSA (GMSA):[70, 71]

$$
\begin{aligned}
h(\mathbf{r}\boldsymbol{\omega}_1\boldsymbol{\omega}_2) &= -1 & r < \sigma \\
c(\mathbf{r}\boldsymbol{\omega}_1\boldsymbol{\omega}_2) &= c^{SW}(r) + \frac{\mu^2}{k_B T r^3} D(\mathbf{n}_1\mathbf{n}_2\hat{\mathbf{r}}) & r > \sigma
\end{aligned}
\tag{2.11}
$$

where $c^{SW}(r)$ is the direct correlation for the square-well fluid (i.e., the usual, non-dipolar square-well fluid). With this GMSA closure, the solution of the Ornstein-Zernike equation is given by

$$
\begin{aligned}
h^{DSW}\left(\mathbf{r}\boldsymbol{\omega}_1\boldsymbol{\omega}_2\right) &= h^{SW}\left(r\right) + h_{\Delta}\left(r\right)\Delta\left(\mathbf{n}_1\mathbf{n}_2\right) + h_D\left(r\right)D\left(\mathbf{n}_1\mathbf{n}_2\hat{\mathbf{r}}\right) \\
c^{DSW}\left(\mathbf{r}\boldsymbol{\omega}_1\boldsymbol{\omega}_2\right) &= c^{SW}\left(r\right) + c_{\Delta}\left(r\right)\Delta\left(\mathbf{n}_1\mathbf{n}_2\right) + c_D\left(r\right)D\left(\mathbf{n}_1\mathbf{n}_2\hat{\mathbf{r}}\right)
\end{aligned}
\tag{2.12}
$$

where now $h^{SW}\left(r\right)$ and $c^{SW}\left(r\right)$ are the correlation functions for the square-well fluid and $h_{\Delta}\left(r\right)$ and $h_D\left(r\right)$ are again obtained in terms of hard-sphere Percus-Yevick quantities. This is because the GMSA closure on these quantities is the same as that for the MSA dipolar hard sphere case, namely

$$
\begin{aligned}
h_{\Delta}\left(r\right) &= 0 \qquad r < \sigma \\
h_D\left(r\right) &= 0 \qquad r < \sigma \\
c_{\Delta}\left(r\right) &= 0 \qquad r > \sigma \\
c_D\left(r\right) &= \frac{\mu^2}{k_B T r^3} \qquad r > \sigma
\end{aligned}
\tag{2.13}
$$

Note that $h^{SW}\left(r\right)$ and $c^{SW}\left(r\right)$ can be the exact such quantities or those calculated by some approximate theory (such as perturbation theory). Hence, within the GMSA, the pair distribution function $g^{DSW}\left(\mathbf{r}\boldsymbol{\omega}_1\boldsymbol{\omega}_2\right)$ and Helmholtz free energy of dipolar square-well monomers are given by,

$$
\begin{aligned}
g^{DSW}\left(\mathbf{r}\boldsymbol{\omega}_1\boldsymbol{\omega}_2;\rho,T\right) &= g^{SW}\left(r;\rho,T\right) + h_{\Delta}\left(r;\rho,T\right)\Delta\left(\mathbf{n}_1\mathbf{n}_2\right) + h_D\left(r;\rho,T\right)D\left(\mathbf{n}_1\mathbf{n}_2\hat{\mathbf{r}}\right) \\
A^{DSW}\left(r;\rho,T\right) &= A^{SW}\left(r;\rho,T\right) + A^{DIPOLE}\left(\mathbf{r}\boldsymbol{\omega}_1\boldsymbol{\omega}_2;\rho,T\right)
\end{aligned}
\tag{2.14}
$$

where $g^{SW}\left(r\right)$ is the radial distribution function of the square-well monomer fluid and the state dependence of the quantities on ρ and T is explicitly shown. Detailed expressions for each new term of the SAFT- VR+D equation are presented below, while those in common with the original SAFT-VR equation are given in the section 2 of Chapter I.

2.2.1.2 Monomer contribution

The contribution to the Helmholtz free energy due to the monomer segments is

$$\frac{A^{MONO.}}{Nk_BT} = m\frac{A^{MONO.}}{N_s k_B T} = ma^M \tag{2.15}$$

where N_s is the total number of dipolar spherical monomers. Within the GMSA the excess Helmholtz free energy per monomer a^M, is given by

$$\begin{aligned} a^M &= a^{DSW} = a^{DIPOLE} + a^{Isotropic} \\ &= a^{DIPOLE} + a^{HS} + \beta a_1^{SW} + \beta^2 a_2^{SW} \end{aligned}$$

where a^{DIPOLE} describes the contribution to the free energy due to the anisotropic dipolar interaction and the isotropic term $a^{Isotropic}$ is given by equations (1.5) in section 1.2.

The contribution to the free energy due to the dipolar interaction is obtained from Wertheim's solution of the Ornstein-Zernike equation for dipolar hard spheres with the MSA closure as given by equation (2.9) [61]; the excess free energy due to the dipolar interactions is given by

$$a^{DIPOLE} = -\frac{8}{\eta}\xi^2\left[\frac{(1+\xi)^2}{(1-2\xi)^4} + \frac{(2-\xi)^2}{8(1+\xi)^4}\right] \tag{2.16}$$

where $\xi = \kappa\eta$ and κ is the scaling parameter. κ is determined by y, the so-called strength of the dipolar effect [61]

$$3y = q_{PY}(\kappa\eta) - q_{PY}(-\kappa\eta) \tag{2.17}$$

and is a dimensionless function of density ρ, temperature β and dipole moment μ

$$y = \frac{4\pi}{9}\rho\beta\mu^2 \tag{2.18}$$

q_{PY} is the dimensionless inverse compressibility of Percus-Yevick (PY), given by [61]

$$q_{PY}(\eta) = \frac{(1+2\eta)^2}{(1-\eta)^4} \tag{2.19}$$

2.2.1.3 Chain contribution

The contribution to the free energy due to chain formation from *m* dipolar square-well monomers is given by,

$$\frac{A^{CHAIN}}{Nk_BT} = -(m-1)\ln y^{DSW}(\sigma\boldsymbol{\omega}_1\boldsymbol{\omega}_2) \tag{2.20}$$

$y^{DSW}(\sigma\boldsymbol{\omega}_1\boldsymbol{\omega}_2)$ is the dipolar square-well monomer background correlation function evaluated at hard-core contact,

$$y^{DSW}(\mathbf{r}\boldsymbol{\omega}_1\boldsymbol{\omega}_2;\rho,T) = \exp\left[\beta u^{DSW}(\mathbf{r}\boldsymbol{\omega}_1\boldsymbol{\omega}_2)\right] g^{DSW}(\mathbf{r}\boldsymbol{\omega}_1\boldsymbol{\omega}_2;\rho,T) \tag{2.21}$$

where $g^{DSW}(\mathbf{r}\boldsymbol{\omega}_1\boldsymbol{\omega}_2;\rho,T)$ is the pair distribution function for the dipolar square-well fluid and obtained from the GMSA (equation (2.14)). In the SAFT-VR equation, a high-temperature perturbation expansion is used to determine the radial distribution function for the square-well fluid $g^{SW}(r)$

$$g^{SW}(r) = g^{HS}(r) + \beta\varepsilon g_1(r) \tag{2.22}$$

where the radial distribution function $g^{SW}(r)$ at hard-core contact is given by

$$g^{SW}(\sigma^+) = g^{HS}(\sigma) + \beta\varepsilon g_1(\sigma) \tag{2.23}$$

and $g_1(\sigma)$ can be obtained from a self-consistent calculation of the pressure using the Clausius virial theorem and the first derivative of the free energy with respect to the density.

When compared with the Monte Carlo simulation data of Verlet et al. [63], Wertheim's solution with the MSA closure underestimates the spherical harmonic

coefficients at contact. As discussed in the introduction, extensions such as ORPA, EXP and LEXP have been suggested to improve the description of structural properties. Among them, the LEXP approximation is the most attractive; the LEXP $h_{\Delta}(r;\rho,T)$ and $h_D(r;\rho,T)$ appear the most accurate in comparison with the simulation data, though the LEXP result for $h_s(r)$ shows little improvement over the MSA results. Within the LEXP approximation, the radial distribution function of the square-well monomer is given by

$$g^{DSW}(\mathbf{r}\boldsymbol{\omega}_1\boldsymbol{\omega}_2;\rho,T) = g^{SW}(r;\rho,T)\left(1 + h_{\Delta}(r;\rho,T)\Delta(\mathbf{n}_1\mathbf{n}_2) + h_D(r;\rho,T)D(\mathbf{n}_1\mathbf{n}_2\hat{\mathbf{r}})\right) \quad (2.24)$$

The spherical harmonic coefficients, $h_{\Delta}(r;\rho,T)$ and $h_D(r;\rho,T)$, can be obtained from the analytic solution of the PY approximation for the hard sphere fluid as

$$\begin{aligned} h_{\Delta}(r;\eta,T) &= -2\kappa\left(h_{PY}(-\kappa\eta,r) - h_{PY}(2\kappa\eta,r)\right) \\ h_D(r;\eta,T) &= \kappa\begin{pmatrix} h_{PY}(-\kappa\eta,r) + 2h_{PY}(2\kappa\eta,r) \\ -\int_0^r h_{PY}(-\kappa\eta,r')dr' - 2\int_0^r h_{PY}(2\kappa\eta,r')dr' \end{pmatrix} \end{aligned} \quad (2.25)$$

We note that κ is a function of temperature, which is determined by the strength of the dipolar effect as given by equations (2.17), (2.18) and (2.19). The spherical harmonic coefficient $h_{PY}(\rho;r)$ is obtained by solving the OZ equation with the PY closure by introducing the dimensionless quantities $x = r/\sigma$ and $\bar{q}_{PY}(x) = q_{PY}(x)/\sigma^2$

$$xh_{PY}(x) = -\bar{q}'_{PY}(x) + 12\eta\int_0^1 dx'\bar{q}_{PY}(x')(x-x')h_{PY}(|x-x'|) \quad (2.26)$$

for all $x \geq 0$, where $\bar{q}'_{PY}(x) \equiv d\bar{q}_{PY}(x)/dx$. $\bar{q}_{PY}(x)$ is given by

$$\bar{q}_{PY}(x) = \begin{matrix} \frac{1}{2}a(x^2-1) + b(x-1) \\ 0 \end{matrix} \quad \begin{matrix} x \leq 1 \\ x \geq 1 \end{matrix} \quad (2.27)$$

For $x < 1$,

$$\bar{q}'_{PY}(x) = ax + b \tag{2.28}$$

where

$$\begin{aligned} a &= \frac{1+2\eta}{(1-\eta)^2} \\ b &= -\frac{3\eta}{2(1-\eta)^2} \end{aligned} \tag{2.29}$$

The analytic expression of $h_{PY}(\rho; r)$ at contact can be obtained by setting $x = 1^+$ in equations (2.26) and (2.27)

$$h_{PY}(\eta, \sigma) = \frac{\eta(5-2\eta)}{2(1-\eta)^2} \tag{2.30}$$

Both the LEXP approximation and GMSA are considered in the SAFT-VR+D equation to determine the thermodynamic properties and phase behavior from the Helmholtz free energy of dipolar fluids using standard thermodynamic relations.

2.2.2 Chains with Mixed Dipole Moments

While the expressions given above treat chain molecules formed from dipolar square-well segments, each having the same dipolar strength, we can also consider chain molecules that contain segments with different strength and orientation of dipole moments.

Adelman and Deutch [65] provided an exact solution to the MSA for simple polar mixtures with equal hard sphere radii and differing dipole moment, in which the structure and thermodynamic properties are completely determined from the pure dipolar fluid

result of Wertheim using an effective density $\hat{\rho}$ and dipole moment $\hat{\mu}$. Substituting the effective density and dipole moment into equations (2.16) and (2.25), the Helmholtz free energy and radial distribution function due to dipolar interactions can easily be obtained for chain molecules with mixed dipole moments. The limiting case of chain molecules composed of a mixture of dipolar and non-dipolar segments can also be studied. In their solution of the MSA Adelman and Deutch [65] determined that the pair correlation function of the non-dipolar segments are unaffected by the presence of the dipoles on dipolar segments, and vice versa. This is a direct result of the linearity in the MSA approximation between the direct correlation function and the dipole-dipole interaction as shown in equation (2.9). Hence, in the limiting case of a diatomic dipolar molecule in which the dipole moments of one and/or two of the segments μ_i and/or μ_j are zero, the anisotropic component of the direct correlation function of the dipolar hard sphere and non-dipolar hard sphere is zero. Accordingly, within the GMSA, the pair distribution function $g^{DSW}\left(\mathbf{r}\boldsymbol{\omega}_1\boldsymbol{\omega}_2\right)$ for a square-well diatomic molecule consisting of one dipolar segment (sphere 1) and one non-dipolar segment (sphere 2) reduces to the pair distribution function of non-dipolar molecules $g^{SW}\left(r\right)$ for 3 (g_{12}, g_{21}, g_{22}) out of the 4 possible pair correlation functions. Correspondingly, the Helmholtz free energy due to chain formation in the SAFT-VR+D EOS for chain molecules consisting of dipolar and non-dipolar segments is given by

$$\frac{A^{CHAIN}}{Nk_BT} = -\left(m - m' - 1\right)\ln y^{SW}\left(\sigma\right) - \sum_{\text{bonded dipole pairs } ij} \ln y_{ij}^{DSW}\left(\sigma\boldsymbol{\omega}_i\boldsymbol{\omega}_j\right) \qquad (2.31)$$

where m' is the number of bonds between two dipolar spheres (i.e., equal to the number of terms in the sum). Hence, as in the hetero-SAFT-VR approach [72] the Helmholtz

free energy directly reflects the structure of the chains through explicit dependence on the magnitudes and relative orientation of dipoles in neighboring dipolar segments.

2.3 Computer Simulations

Monte Carlo simulations have been performed to study the thermodynamic properties of dipolar square-well monomer and chain fluids. The simulations were performed in both the isothermal-isobaric (*NPT*) and Gibbs ensembles. Intermolecular and non-bonded intramolecular interactions, except for nearest neighbors along the chain, are taken into account through the dipolar square well potential given by equation (2.1). The reaction field [73-76] method, which has been shown to be adequate to calculate vapor-liquid phase behavior for systems with long-range dipolar potentials [77], is applied to deal with the long-range dipolar interactions. The reaction field approach replaces the molecules beyond a cut-off distance by a dielectric continuum, the effect of which is taken into account by including a new term into the dipolar potential, viz [78]

$$u^{dipole} = \begin{cases} -\left(\frac{\mu_1\mu_2}{r^3}\right) D - \frac{2\left(\varepsilon_{RF}-1\right)}{2\varepsilon_{RF}+1}\frac{\mu_1\mu_2}{r_c^{\,3}} & r < r_c \\ 0 & r \geq r_c \end{cases} \tag{2.32}$$

where r_c is the cut-off distance beyond which the pair potential vanishes and ε_{RF} the dielectric constant of the continuum. In the simulations, the value of r_c is set to 2.5σ, and ε_{RF} to ∞. In both the NPT ensemble and GEMC simulations, the usual periodic boundary conditions and minimum image convention are used. In the NPT ensemble simulations, one cycle consists of three kinds of trial moves: *N* trial displacements of randomly chosen molecules, *N* trial rotations and one volume change. The extent of each trial move is adjusted to give an individual acceptance probability of 30 - 40%. In the

GEMC simulations, particle exchanges between two phases are performed in addition to the three trial moves described above. The traditional Widom particle insertion method is used to achieve particle exchanges. Each simulation was started from an initial configuration in which 128 molecules are placed on a lattice in the simulation box. An initial simulation of 100,000 - 500,000 cycles was performed to equilibrate the system, before averaging for between 500,000 and 2,000,000 cycles. The thermodynamic properties of the system were obtained as ensemble averages and the errors estimated by determining the standard deviation.

Before studying the dipolar square-well fluids of interest in this work, to check the accuracy of our simulation code, we calculated the coexistence curve of several Stockmayer fluids using the GEMC technique and the reaction field method to treat the long-range dipolar interactions. Good agreement was obtained with the results of Smit and co-workers [79], who accounted for the long-range dipolar interactions with the Ewald summation method.

2.4 Results and discussion

We have studied the phase behavior of several dipolar square well monomer fluids (system 1 - 4), several dipolar diatomic fluids with a dipole moment in each segment (system 5 - 12) and dipolar triatomic fluids with one non-dipolar segment (system 13 - 14). The details of these systems are listed in Table 1. Comparisons are made between the theoretical predictions and *NPT* and Gibbs ensemble simulation data in order to validate and test the predictive ability of the SAFT-VR+D EOS for dipolar monomer and

chain molecules. The numerical results of the *NPT* simulations are reported in Tables 2 - 5 and those of the GEMC simulations in Table 6.

Table 1: Model parameters for the dipolar square well monomer and chain fluids studied.

System	ε^*	λ	σ^*	m	$(\mu_1^*)^2$	$(\mu_2^*)^2$	$(\mu_3^*)^2$
1	1	1.5	1	1	0.5	-	-
2	1	1.5	1	1	1.0	-	-
3	1	1.5	1	1	2.0	-	-
4	1	1.8	1	1	1.0	-	-
5	1	1.5	1	2	0.5[a]	0.5[a]	-
6	1	1.5	1	2	0.5[b]	0.5[b]	-
7	1	1.8	1	2	0.5[a]	0.5[a]	-
8	1	1.8	1	2	0.5[b]	0.5[b]	-
9	1	1.5	1	2	1.0[a]	0.5[a]	-
10	1	1.5	1	2	1.0[b]	0.5[b]	-
11	1	1.5	1	2	0.5[b]	0.5[a]	-
12	1	1.5	1	2	1.0[b]	1.0[a]	-
13	1	1.5	1	3	1.0[a]	1.0[a]	0.0
14	1	1.5	1	3	1.0[b]	1.0[b]	0.0

[a] represents parallel dipole moments, [b] perpendicular dipole moments

Table 2: *NPT* MC simulation results for the monomer dipolar fluids studied (systems 1 – 4). The reduced temperature is given by $T^* = kT / \varepsilon_1$, the pressure by $P^* = P\sigma_1^3 / \varepsilon_1$, and the energy is defined per segment as $E^* = E / N_s\varepsilon_1$.

Sys.	T*	P*	η		E*		Sys.	T*	P*	η		E*	
1	1.0	0.2709	0.361	0.009	-5.67	0.18	3	1.4	0.3998	0.325	0.015	-6.42	0.31
		1.4247	0.402	0.008	-6.22	0.16			1.2344	0.368	0.010	-7.22	0.24
		3.2068	0.438	0.007	-6.64	0.14			3.0338	0.412	0.007	-8.05	0.19
	1.2	0.2607	0.308	0.015	-4.67	0.23			5.6074	0.448	0.007	-8.67	0.18
		0.9319	0.357	0.010	-5.49	0.17		1.6	0.8584	0.315	0.013	-6.01	0.27
		2.4438	0.402	0.007	-6.10	0.16			1.9303	0.364	0.010	-6.93	0.23
		4.6508	0.438	0.007	-6.51	0.15			4.0910	0.409	0.008	-7.76	0.21
	1.4	0.6980	0.309	0.013	-4.64	0.22			7.0897	0.446	0.007	-8.40	0.19
		1.6034	0.355	0.010	-5.33	0.17		1.8	0.9291	0.286	0.014	-5.32	0.29
		3.4747	0.401	0.008	-5.98	0.16			2.1609	0.347	0.010	-6.46	0.26
		6.1063	0.439	0.007	-6.44	0.14			4.6056	0.399	0.009	-7.41	0.21
	1.6	1.1400	0.304	0.011	-4.51	0.21			7.9677	0.438	0.009	-8.08	0.21
		2.2812	0.353	0.009	-5.26	0.16		2.0	1.2979	0.283	0.012	-5.13	0.26
		4.5127	0.400	0.007	-5.90	0.15			2.7495	0.335	0.010	-6.02	0.23
		7.5688	0.440	0.007	-6.37	0.11			5.5369	0.396	0.008	-7.20	0.20
2	1.0	0.1114	0.365	0.011	-6.12	0.19			9.3085	0.438	0.007	-7.90	0.18
		1.2336	0.404	0.008	-6.70	0.15	4	1.6	0.2207	0.316	0.013	-7.78	0.31
		2.9901	0.441	0.007	-7.20	0.12			1.2256	0.363	0.010	-8.79	0.23
	1.2	0.1428	0.313	0.016	-5.13	0.26			3.2759	0.414	0.009	-9.94	0.22
		0.7840	0.358	0.010	-5.84	0.18			6.0884	0.456	0.008	-10.81	0.20
		2.2650	0.403	0.008	-6.51	0.15		2.0	1.0840	0.310	0.011	-7.47	0.26
		4.4469	0.440	0.007	-7.01	0.13			2.5606	0.359	0.010	-8.52	0.23
	1.4	0.5893	0.308	0.014	-4.92	0.23			5.3308	0.406	0.009	-9.47	0.21
		1.4658	0.356	0.009	-5.67	0.17			8.9901	0.450	0.007	-10.33	0.19
		3.3072	0.403	0.009	-6.38	0.15		2.4	2.0048	0.305	0.011	-7.25	0.26
		5.9143	0.440	0.007	-6.88	0.13			3.9679	0.355	0.010	-8.29	0.23
	1.6	1.0668	0.309	0.013	-4.98	0.23			7.4716	0.405	0.008	-9.30	0.20
		2.1874	0.357	0.010	-5.75	0.18			11.9877	0.448	0.007	-10.13	0.19
		4.3971	0.402	0.008	-6.43	0.15		2.8	2.9060	0.303	0.011	-7.11	0.26
		7.4351	0.441	0.007	-6.94	0.13			5.3495	0.353	0.008	-8.16	0.21
									9.5795	0.403	0.008	-9.17	0.19
									14.9459	0.444	0.007	-9.96	0.18

Table 3: *NPT* MC simulation results for the diatomic dipolar fluids studied (systems 5 - 10). See Table 1 for details.

Sys.	T*	P*	η		E*		Sys.	T*	P*	η		E*	
5	1.0	0.3721	0.410	0.006	-5.54	0.09	8	2.0	0.7107	0.357	0.008	-7.86	0.18
		1.8525	0.443	0.005	-5.94	0.08			2.9407	0.406	0.006	-8.88	0.15
	1.2	0.0525	0.367	0.009	-4.84	0.13			6.1322	0.449	0.005	-9.73	0.13
		1.1806	0.408	0.006	-5.40	0.10		2.4	0.3873	0.307	0.009	-6.68	0.21
		3.0368	0.442	0.005	-5.82	0.08			1.7620	0.353	0.007	-7.67	0.17
	1.4	0.5640	0.362	0.009	-4.69	0.13			4.6134	0.403	0.006	-8.70	0.15
		2.0010	0.406	0.006	-5.31	0.10			8.5541	0.446	0.005	-9.52	0.13
		4.2329	0.442	0.005	-5.75	0.07		2.8	1.0455	0.304	0.009	-6.54	0.20
	1.6	0.3239	0.308	0.012	-3.87	0.17			2.8189	0.353	0.007	-7.58	0.17
		1.0817	0.358	0.008	-4.57	0.12			6.2931	0.403	0.006	-8.59	0.15
		2.8285	0.404	0.006	-5.22	0.10			10.9833	0.445	0.005	-9.40	0.12
		5.4361	0.442	0.005	-5.69	0.08		3.2	1.7063	0.303	0.008	-6.45	0.19
6	1.2	0.8442	0.404	0.006	-5.72	0.11			3.8792	0.351	0.007	-7.49	0.16
		2.6833	0.441	0.005	-6.21	0.09			7.9769	0.402	0.007	-8.50	0.15
	1.4	0.2966	0.354	0.010	-4.85	0.16			13.4169	0.444	0.005	-9.31	0.13
		1.6745	0.403	0.006	-5.58	0.11	9	1.2	0.9137	0.403	0.006	-5.43	0.11
		3.8872	0.440	0.005	-6.09	0.09			2.7443	0.439	0.005	-5.90	0.08
	1.6	0.1430	0.293	0.013	-3.91	0.19		1.4	0.3591	0.352	0.009	-4.62	0.14
		0.8191	0.353	0.008	-4.74	0.14			1.7418	0.402	0.006	-5.33	0.10
		2.5093	0.402	0.006	-5.47	0.11			3.9480	0.439	0.005	-5.81	0.08
		5.0964	0.440	0.005	-6.00	0.09		1.6	0.1865	0.290	0.015	-3.70	0.20
	1.8	0.4678	0.295	0.012	-3.83	0.18			0.8800	0.351	0.008	-4.52	0.13
		1.3444	0.352	0.008	-4.65	0.14			2.5753	0.401	0.006	-5.25	0.10
		3.3471	0.401	0.006	-5.38	0.11			5.1574	0.439	0.005	-5.75	0.08
		6.3089	0.440	0.005	-5.92	0.09		1.8	0.5116	0.297	0.012	-3.71	0.17
7	2.0	0.9915	0.361	0.008	-7.75	0.17			1.4044	0.351	0.008	-4.47	0.13
		3.2433	0.409	0.006	-8.70	0.14			3.4125	0.400	0.006	-5.18	0.10
		6.4371	0.451	0.006	-9.48	0.13			6.3703	0.440	0.005	-5.70	0.08
	2.4	0.6117	0.315	0.009	-6.70	0.20	10	1.2	0.7878	0.408	0.007	-6.21	0.13
		2.0353	0.358	0.008	-7.59	0.17			2.6037	0.444	0.005	-6.72	0.10
		4.9118	0.407	0.006	-8.55	0.13		1.4	0.2655	0.360	0.009	-5.28	0.15
		8.8584	0.448	0.006	-9.32	0.13			1.6298	0.406	0.006	-6.01	0.12
	2.8	1.2649	0.008	-6.548	0.19	0.31			3.8213	0.443	0.005	-6.53	0.11
		3.0867	0.007	-7.503	0.15	0.36		1.6	0.1211	0.302	0.015	-4.30	0.22
		6.5881	0.006	-8.454	0.13	0.40			0.7974	0.358	0.009	-5.12	0.16
		11.2869	0.006	-9.222	0.13	0.45			2.4750	0.404	0.006	-5.85	0.13
	3.2	1.9221	0.309	0.009	-6.46	0.19			5.0427	0.442	0.005	-6.40	0.10
		4.1429	0.355	0.007	-7.41	0.15		1.8	0.4541	0.303	0.012	-4.18	0.19
		8.2693	0.404	0.006	-8.38	0.13			1.3309	0.356	0.008	-4.99	0.15
		13.7198	0.445	0.005	-9.14	0.12			3.3221	0.404	0.006	-5.74	0.12
									6.2661	0.442	0.005	-6.30	0.11

Table 4: *NPT* MC simulation results for diatomic fluids with different orientation of dipole moments (systems 11 - 12). See Table 1 for details.

System	T*	P*	η		E*	
11	1.2	0.9646	0.404	0.006	-5.48	0.10
		2.8011	0.440	0.005	-5.95	0.08
	1.4	0.4001	0.356	0.009	-4.70	0.14
		1.7903	0.403	0.006	-5.37	0.10
		4.0025	0.440	0.005	-5.86	0.08
	1.6	0.2181	0.298	0.014	-3.82	0.18
		0.9190	0.355	0.009	-4.60	0.14
		2.6218	0.402	0.006	-5.29	0.10
		5.2098	0.441	0.005	-5.80	0.09
	1.8	0.5415	0.298	0.011	-3.74	0.17
		1.4417	0.353	0.008	-4.52	0.13
		3.4571	0.402	0.006	-5.23	0.10
		6.4208	0.441	0.005	-5.74	0.09
12	1.2	0.8322	0.409	0.007	-6.06	0.12
		2.6495	0.444	0.005	-6.56	0.10
	1.4	0.2993	0.360	0.008	-5.16	0.15
		1.6669	0.407	0.006	-5.89	0.12
		3.8606	0.442	0.005	-6.40	0.10
	1.6	0.1449	0.299	0.014	-4.15	0.20
		0.8254	0.359	0.008	-5.02	0.15
		2.5066	0.405	0.006	-5.74	0.12
		5.0766	0.443	0.005	-6.30	0.10
	1.8	0.4737	0.302	0.012	-4.08	0.19
		1.3544	0.355	0.008	-4.88	0.14
		3.3491	0.404	0.006	-5.65	0.12
		6.2955	0.442	0.005	-6.20	0.10

Table 5: *NPT* MC simulation results for diatomic fluids with different orientation of dipole moments (systems 11 - 12). See Table 1 for details.

System	T*	P*	η		E*	
11	1.2	0.9646	0.404	0.006	-5.48	0.10
		2.8011	0.440	0.005	-5.95	0.08
	1.4	0.4001	0.356	0.009	-4.70	0.14
		1.7903	0.403	0.006	-5.37	0.10
		4.0025	0.440	0.005	-5.86	0.08
	1.6	0.2181	0.298	0.014	-3.82	0.18
		0.9190	0.355	0.009	-4.60	0.14
		2.6218	0.402	0.006	-5.29	0.10
		5.2098	0.441	0.005	-5.80	0.09
	1.8	0.5415	0.298	0.011	-3.74	0.17
		1.4417	0.353	0.008	-4.52	0.13
		3.4571	0.402	0.006	-5.23	0.10
		6.4208	0.441	0.005	-5.74	0.09
12	1.2	0.8322	0.409	0.007	-6.06	0.12
		2.6495	0.444	0.005	-6.56	0.10
	1.4	0.2993	0.360	0.008	-5.16	0.15
		1.6669	0.407	0.006	-5.89	0.12
		3.8606	0.442	0.005	-6.40	0.10
	1.6	0.1449	0.299	0.014	-4.15	0.20
		0.8254	0.359	0.008	-5.02	0.15
		2.5066	0.405	0.006	-5.74	0.12
		5.0766	0.443	0.005	-6.30	0.10
	1.8	0.4737	0.302	0.012	-4.08	0.19
		1.3544	0.355	0.008	-4.88	0.14
		3.3491	0.404	0.006	-5.65	0.12
		6.2955	0.442	0.005	-6.20	0.10

Table 6: N*PT* MC simulation results for the triatomic fluids studied (systems 13 - 14). See Table 1 for details.

System	T*	P*	η		E*	
13	1.6	0.6205	0.362	0.007	-4.39	0.11
		2.1968	0.408	0.006	-5.05	0.09
		5.4991	0.455	0.004	-5.65	0.06
	1.8	0.2949	0.305	0.010	-3.57	0.13
		1.0942	0.358	0.007	-4.30	0.10
		2.9655	0.407	0.005	-4.99	0.08
		6.7409	0.456	0.004	-5.60	0.06
	2.0	0.5857	0.308	0.009	-3.56	0.13
		1.5699	0.358	0.006	-4.25	0.10
		3.7365	0.406	0.005	-4.94	0.08
		7.9847	0.451	0.004	-5.57	0.07
	2.2	0.8773	0.306	0.009	-3.48	0.13
		2.0469	0.357	0.006	-4.20	0.10
		4.5089	0.405	0.005	-4.89	0.08
		9.2300	0.454	0.004	-5.52	0.06
14	1.6	0.3556	0.353	0.008	-4.86	0.14
		1.8608	0.403	0.005	-5.62	0.11
		5.1151	0.451	0.004	-6.29	0.08
	1.8	0.1171	0.297	0.011	-3.88	0.16
		0.8380	0.351	0.008	-4.73	0.14
		2.6410	0.399	0.005	-5.49	0.10
		6.3691	0.452	0.004	-6.21	0.08
	2.0	0.4110	0.300	0.010	-3.80	0.15
		1.3202	0.354	0.007	-4.62	0.13
		3.4209	0.400	0.005	-5.39	0.10
		7.6229	0.451	0.004	-6.09	0.08
	2.2	0.7049	0.301	0.009	-3.74	0.14
		1.8023	0.351	0.007	-4.55	0.13
		4.2007	0.402	0.005	-5.33	0.10
		8.8765	0.454	0.004	-6.02	0.08

In Figure 3, we present comparisons of the SAFT-VR+D predictions with molecular simulation results for the *PVT* behavior of monomer fluids with different dipole moments (systems 1 – 3). From the Figure we see that the system with the highest reduced dipole moment (system 3) exhibits the highest density at a given pressure and temperature, as would be expected due to the increase in attractive interactions between the molecules. We observe good agreement between the simulation results and theoretical predictions over a wide range of temperatures and pressures for systems 1 and 2, however the SAFT-VR+D EOS is seen to slightly under-predict the density at a given temperature and pressure for system 3, which has the highest value of the reduced dipole moment.

In order to obtain a more comprehensive understanding of the thermodynamic properties of the systems studied and further test the SAFT-VR+D approach, we also determined the fluid phase diagram for systems 1 and 2. The results are presented in Figure 4 along with the phase diagram for a non-dipolar square-well fluid with the same model parameters (i.e., $\varepsilon^* = 1.0$, $\lambda = 1.5$, $\sigma^* = 1.0$) for comparison. From the Figure we see that as the dipole moment increases the critical temperature of the system increases, due to the increase in the attractive interactions. We also note from the Figure that the SAFT-VR+D equation appears to over estimate the critical point; this is an unavoidable feature of equations of state like SAFT that are based on analytical expressions for the free energy [80]. Away from the critical region we see good agreement between the theory and simulation for system 1 with the lowest dipole moment. For fluids with larger reduced dipole moments, we notice a slight disagreement between the SAFT-VR+D description and simulation data, particularly for the liquid

density at low temperatures. Patey et al. [62] observed a similar trend, in that the GMSA does not provide a good description of the thermodynamic properties of dipolar hard spheres with large dipole moments.

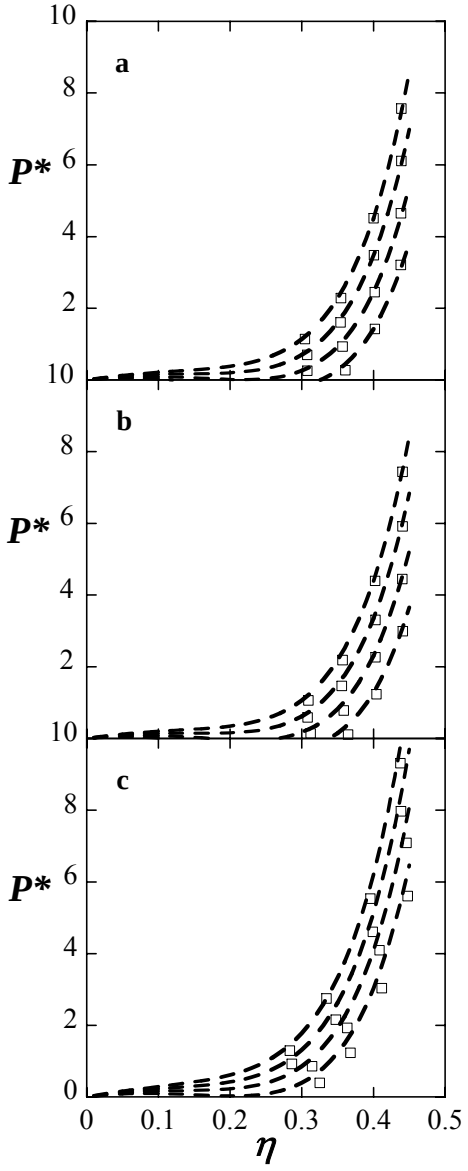

Figure 4: Isotherms for dipolar square-well monomer fluids with $\varepsilon^* = 1.0$, $\lambda = 1.5$, $\sigma^* = 1.0$ and (a) dipole moment $\mu^{*2} = 0.5$, at T* = 1.0, 1.2, 1.4 and 1.6 (from bottom to top), (b) dipole moment $\mu^{*2} = 1.0$, T*= 1.0, 1.2, 1.4 and 1.6 (from bottom to top) and (c) dipole moment $\mu^{*2} = 2.0$, at T* = 1.4, 1.6, 1.8 and 2.0 (from bottom to top). The dashed lines represent predictions from the SAFT-VR+D equation with the GMSA approximation and the squares the NPT-MC simulation data.

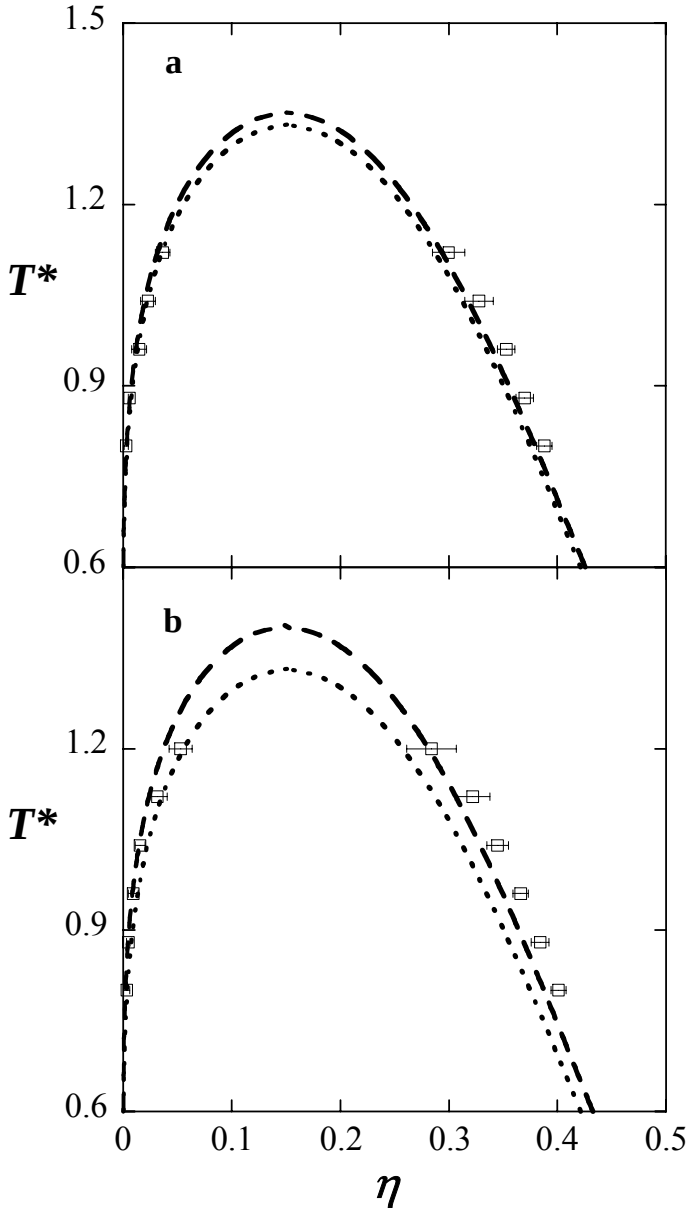

Figure 5: Coexisting densities for dipolar square-well monomer fluids with $\varepsilon^* = 1.0$, $\lambda = 1.5$, $\sigma^* = 1.0$ and dipole moment (a) $\mu^{*2} = 0.5$ and (b) $\mu^{*2} = 1.0$. The squares represent the GEMC simulation data, the dashed lines predictions from the SAFT-VR+D equation with the GMSA approximation and the dotted lines predictions from the SAFT-VR+D equation for $\mu^{*2} = 0$.

In the original development of the SAFT-VR EOS Gil-Villegas et al.[81] determined that SAFT-VR was in good agreement with *Gibbs* ensemble simulation data for the vapor-liquid coexistence densities of square-well monomer fluids with potential

ranges $1.1 \le \lambda \le 1.8$. In order to examine the effect of λ on the phase behavior of dipolar fluids, and further test the SAFT-VR+D approach, we have studied the *PVT* behavior of the dipolar square-well monomer fluid with $\lambda = 1.8$ and $\sigma^* = 1.0$, $\varepsilon^* = 1.0$ $\mu^{*2} = 1.0$ (system 4) to compare to the results for system 2, for which $\lambda = 1.5$ with all other parameters the same. The results are presented in Figure 5. Compared to the results for system 2 (Figure 3b), we note that as λ increases, the density of the system increases at a given pressure and temperature. Good agreement is observed between the theoretical predictions and simulation data; the new SAFT-VR+D approach is seen to capture the effect of the potential range on the phase behavior.

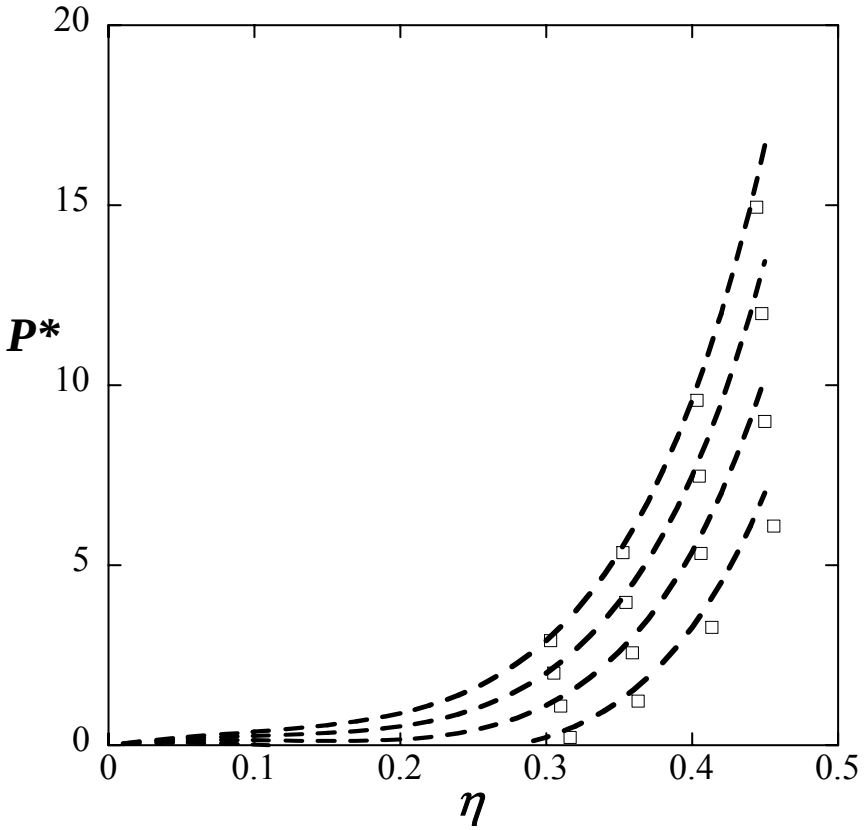

Figure 6: Isotherms for dipolar square-well monomer fluids with $\varepsilon^* = 1.0$, $\lambda = 1.8$, $\sigma^* = 1.0$ and dipole moment $\mu^{*2} = 1.0$ at T*=1.6, 2.0, 2.4 and 2.8 (from bottom to top). The squares represent *NPT* MC simulation results and the dashed lines predictions from the SAFT-VR+D equation with the GMSA approximation.

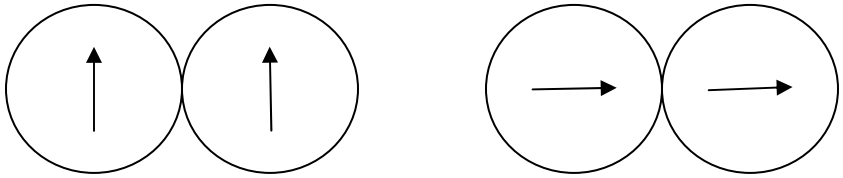

Figure 7: Schematic model for diatomic dipolar fluids with dipole moments embedded in every segment (a) perpendicular and (b) parallel to the vector joining the centers of the monomer segments.

Having seen that SAFT-VR+D equation can accurately describe the fluid phase behavior of dipolar square-well monomer fluids, we now turn to dipolar chain molecules. We first focus on diatomic molecules with a dipole moment in the center of both segments. In the SAFT-VR+D approach, the relative orientation of each dipole moment can be specifically determined by the azimuthal θ and polar ϕ angles of the inter-segment axis (Figure 1). Here we consider two specific diatomic molecules in which the dipole moments are both oriented perpendicular or parallel to the vector joining the centers of the monomers, as illustrated in Figure 6a and Figure 6b. Since the radial distribution function is dependent on the relative orientation of the dipole moments, here we are examining the ability of the theory to capture the effect of dipole orientation on the phase behavior of dipolar chain molecules. In Figure 7 we present the *PVT* behavior for dipolar square well diatomic fluids which have the same model parameters ($\varepsilon^* = 1.0$, $\lambda = 1.5$, $\sigma^* = 1.0$, $\mu^{*2} = 0.5$) in each segment but in figure a the dipole moments are aligned perpendicularly and figure b they are aligned in parallel. The corresponding phase envelopes are presented in Figure 8. From the Figures, we find that the fluids with the dipole moments aligned parallel exhibit a slightly higher density at a given pressure and temperature, and a slightly lower critical temperature, than the fluids in which the

dipoles are perpendicularly aligned. We find that the SAFT-VR+D EOS with the GMSA provides good agreement with the simulation data for the isotherms studied and the coexisting densities of the dipolar diatomic fluid with dipole moments in the perpendicular (system 6) arrangement. However, for the dipolar diatomic fluid in which the dipole moments are aligned parallel (system 5), the SAFT-VR+D EOS with the GMSA approximation under-predicts the density at a given pressure and temperature compared with the *NPT* ensemble simulations, particularly at low densities, and underestimates the saturated liquid density compared with the GEMC simulations. We believe that the main reason for the observed deviation is that, as stated earlier, Wertheim's solution for dipolar hard spheres with the MSA closure underestimates the radial distribution function for dipolar fluids at contact. If the GMSA is replaced by the LEXP approximation in the SAFT-VR+D EOS, a significant improvement in the theoretical predictions in comparison with the simulation data is seen (Figure 7 and 8) for both the *PVT* and phase behavior. This result confirms that an accurate description of the fluids structure is very important in determining the thermodynamic properties of chain fluids. We have also studied the *PVT* behavior of the parallel and perpendicularly aligned dipolar diatomic fluids with $\lambda = 1.8$ (Systems 7 and 8), the results of which are presented in Figure 9. Again we observe that the SAFT-VR+D EOS with the LEXP approximation provides good agreement with the simulation data for fluids with the dipole moments arranged perpendicular and parallel, while the use of the GMSA results in significant deviations for the fluids in which the dipolar segments are aligned in parallel. The SAFT-VR+D equation is therefore able to capture both the effect of potential range and orientation of the dipolar interactions on the phase behavior.

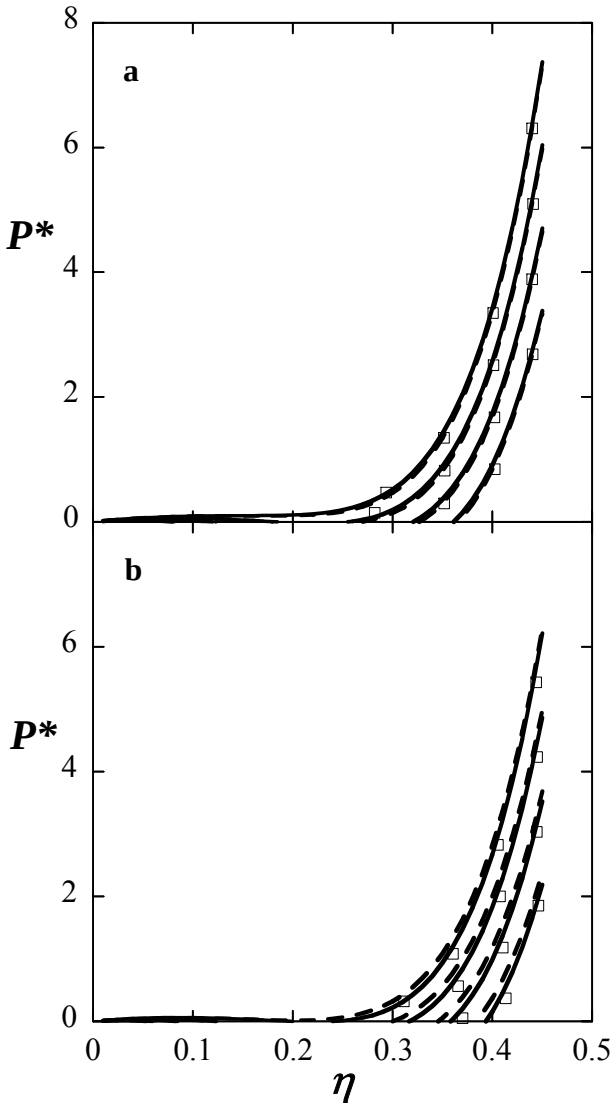

Figure 8: Isotherms for dipolar square well diatomic fluids with $\varepsilon^* = 1.0$, $\lambda = 1.5$, $\sigma^* = 1.0$ and dipole moments $\mu^{*2} = 0.5$ (a) perpendicular at T*=1.2, 1.4, 1.6 and 1.8 (from bottom to top), and (b) parallel at T*=1.0, 1.2, 1.4, and 1.6. The squares represent MC simulation results, the solid lines predictions from the SAFT-VR+D equation with the LEXP approximation and the dashed lines from SAFT-VR+D approach with the GMSA approximation.

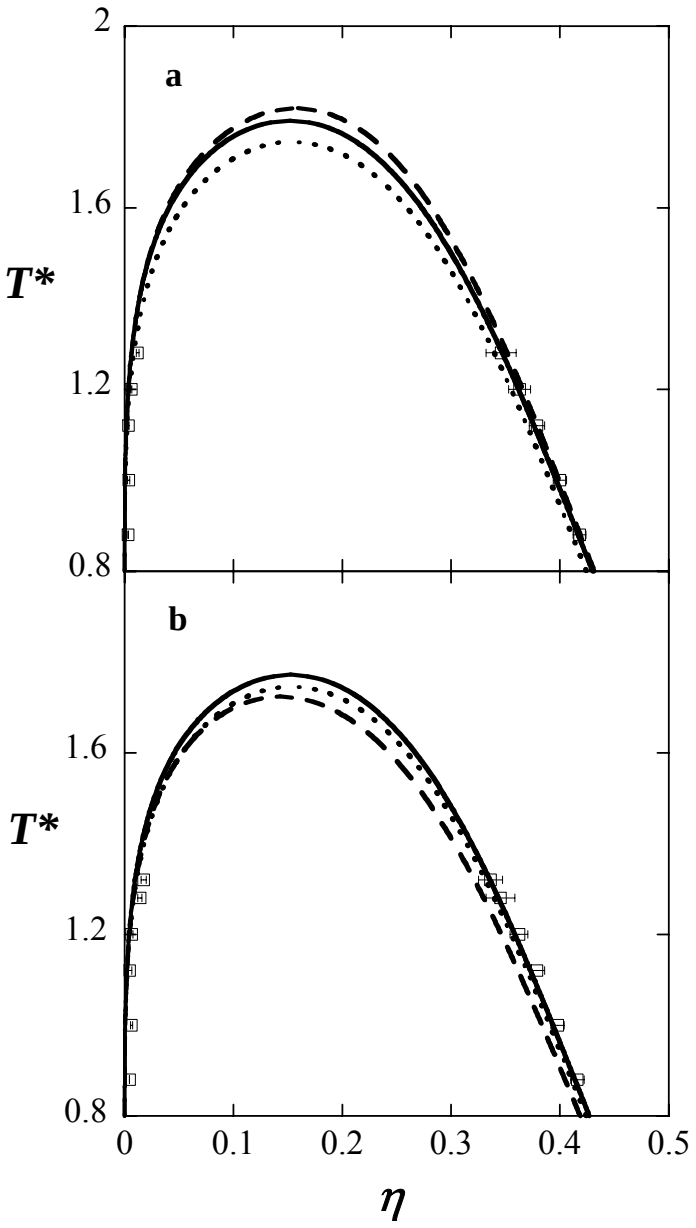

Figure 9: Coexisting densities of dipolar square-well diatomic fluids with $\varepsilon^* = 1.0$, $\lambda = 1.5$, $\sigma^* = 1.0$ and dipole moments $\mu^{*2} = 0.5$ (a) perpendicular and (b) parallel. The squares represent MC simulation results, the solid lines predictions from the SAFT-VR+D equation with the LEXP approximation, the dashed lines from the SAFT-VR+D equation with the GMSA approximation and approximation and the dotted lines predictions from the SAFT-VR+D equation for $\mu^{*2} = 0$.

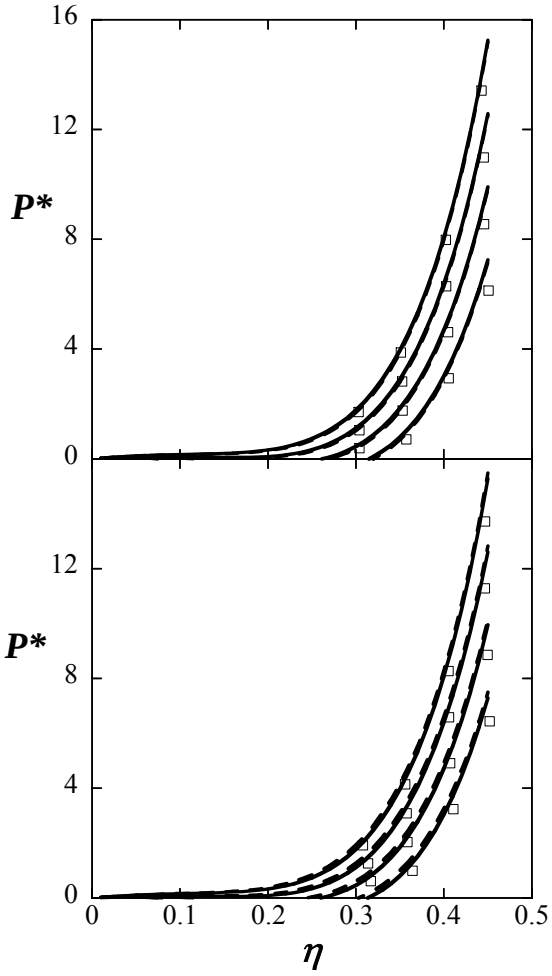

Figure 10: Isotherms for dipolar SW diatomic fluids with $\varepsilon^* = 1.0$, $\lambda = 1.8$, $\sigma^* = 1.0$ and dipole moments $\mu^{*2} = 0.5$ (a) perpendicular at T*=2.0, 2.4, 2.8 and 3.2 (from bottom to top), and (b) parallel at T*=2.0, 2.4, 2.8 and 3.2. The squares represent MC simulation results, the solid lines predictions from the SAFT-VR+D equation with the LEXP approximation and the dashed lines from the SAFT-VR+D equation with the GMSA approximation.

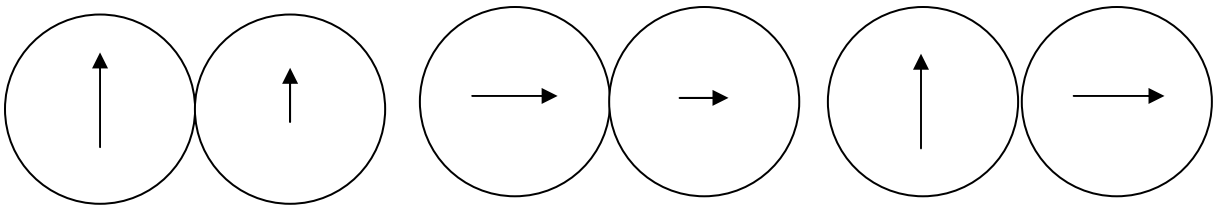

Figure 11: Schematic showing the diatomic molecular models used to describe a chain fluid with different magnitude and orientation of dipole moments embedded in the center of each segment.

Since real fluids, such as ketones, alcohols and many polymers, are typically composed of a mixture of polar and non-polar groups, it is desirable to be able to model chain molecules comprised of segments that have different magnitudes and orientations of dipole moments. To this end, we have studied the *PVT* behavior of dipolar diatomic fluids with different dipole moments in each segment (system 9, 10); in particular we have studied diatomics in which the magnitude of the dipole in one segment is twice that of the other segment (Figure 10). The results of which for perpendicular and parallel orientations of the dipoles are shown in Figures 11a and 11b respectively. We again find that, the SAFT-VR+D approach with the LEXP approximation provides good agreement with the simulation data for diatomic fluids with different magnitude of dipole moments arranged both perpendicular and in parallel. However, again, the SAFT-VR+D approach with the GMSA approximation underestimates the densities at a given pressure and temperature for the molecule with the dipole moments arranged perpendicularly. We have also studied the *PVT* behavior of diatomic dipolar fluids with different orientation of dipole moments in each segment (system 11, 12), as shown in Figure 10c. In these fluids, the pair distribution function due to the dipolar interaction will vanish since the angle-related functions $\Delta\left(\mathbf{n}_1\mathbf{n}_2\right)$ and $D\left(\mathbf{n}_1\mathbf{n}_2\mathbf{r}\right)$ in equation (2.14) are zero for the 90˚ relative orientation of the two dipoles (Figure 10c). In this case, the predictions from the SAFT-VR+D approach with the LEXP approximation and the GMSA approximation are the same. From Figure 12, we note that in all cases, good agreement is observed between the predictions from the SAFT-VR+D approach and simulation data, indicating that the theory can accurately describe the thermodynamic and phase behavior of fluids composed of segments with differing dipole moments.

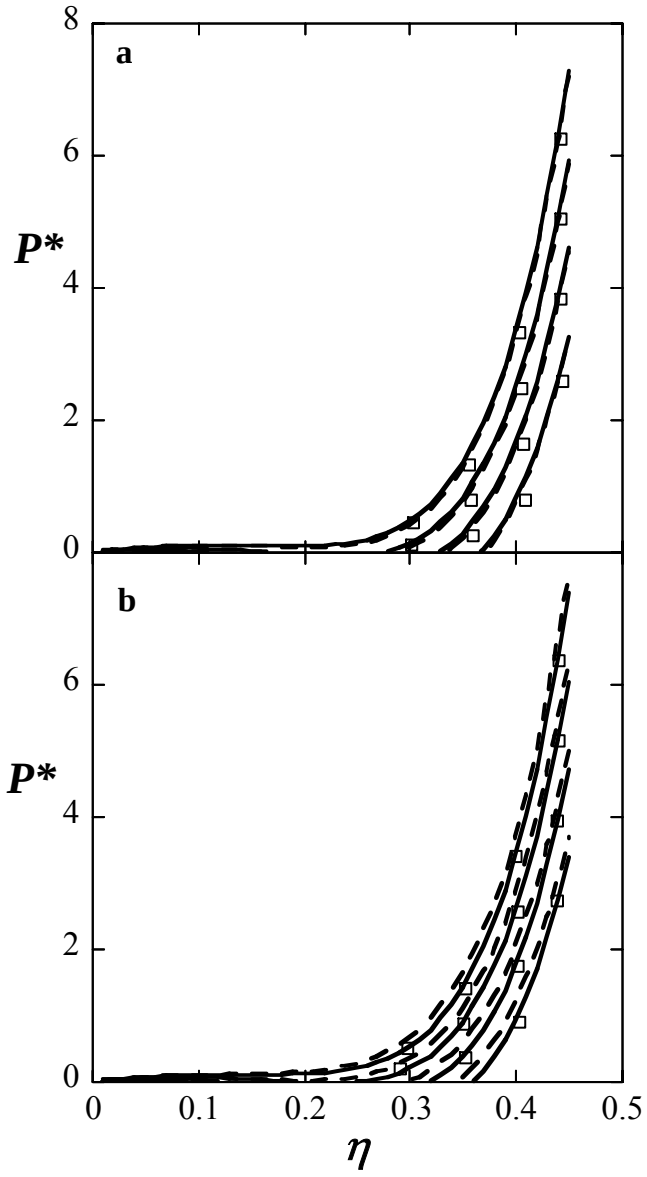

Figure 12: Isotherms for dipolar square well diatomic fluids with $\varepsilon^* = 1.0$, $\lambda = 1.5$, $\sigma^* = 1.0$ at T*=1.0, 1.2, 1.4, and 1.6. with (a) perpendicular dipole moments of μ^{*2}_1= 1.0 and μ^{*2}_2=0.5 and (b) parallel dipole moments of μ^{*2}_1= 1.0 and μ^{*2}_2=0.5. The squares represent MC simulation results, the solid lines predictions from the SAFT-VR+D equation with the LEXP approximation and the dashed lines from the SAFT-VR+D equation with the GMSA approximation.

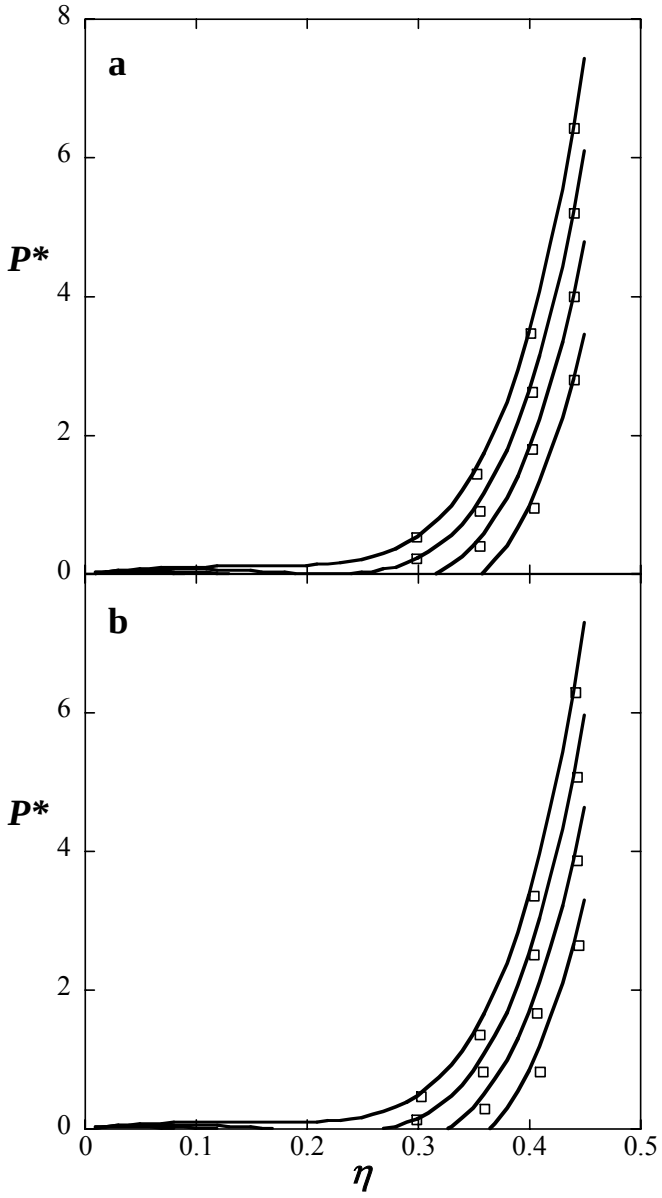

Figure 13: Isotherms for dipolar square *well* diatomic fluids with $\varepsilon^* = 1.0$, $\lambda = 1.5$, $\sigma^* = 1.0$ and (a) a perpendicular dipole moments of $\mu_1^{*2} = 0.5$ and parallel dipole moment of $\mu_2^{*2} = 0.5$ at T*=1.0, 1.2, 1.4, and 1.6. (b) perpendicular dipole moment of $\mu_1^{*2} = 1.0$ and parallel dipole moment of $\mu_2^{*2} = 1.0$ at T*=1.0, 1.2, 1.4, and 1.6. The squares represent MC simulation results and the solid lines predictions from the SAFT-VR+D equation with the LEXP approximation.

To illustrate the generality of this approach, we have also studied a model triatomic fluid in which the dipole moments are arranged perpendicularly or in parallel in the first two segments with the third segment having no dipole moment. Within the solution of Adelman and Deutch [65] for polar mixtures with the MSA closure, the SAFT-VR+D EOS describes a molecule consisting of a mixture of non-dipolar and dipolar segments with an effective dipole moment and density for the dipolar interaction. As mentioned before, due to the linearity in the MSA approximation, the anisotropic contribution to the pair distribution function due to the dipolar interaction between dipolar segments and non-dipolar segments equals zero. In the SAFT-VR+D approach, the pair distribution function between dipolar square-well segments and non-dipolar square-well segments is therefore equivalent to that between non-dipolar square-well segments. In the case of the triatomic molecules shown in Figure 13, the pair distribution function between segments 1 and 2 is $g^{DSW}\left(\mathbf{r}\boldsymbol{\omega}_1\boldsymbol{\omega}_2\right)$and the pair distribution function between segments 2 and 3 is $g_{23}^{SW}\left(\mathbf{r}\right)$. The Helmholtz free energy due to chain formation is therefore given by equation (2.31), in which the total number of segments is 3 and the number of pairs of dipolar segments is 1. This approach therefore describes a heteronuclear fluid, as the chain is composed of unlike segments, and can be modeled as in our previous work[82]. In Figure 14 we present isotherms predicted from the SAFT-VR+D approach compared to *NPT* MC simulation data to for two triatomic fluids (systems 13 and 14) with $\varepsilon^* = 1.0$, $\lambda = 1.5$, $\sigma^* = 1.0$ and reduced dipole moments of $\mu^{*2} =$ 1.0 in both segments and arranged in parallel (system 13) and perpendicular (system 14). We find that the fluid with the dipole moments in the parallel arrangement has a slightly higher pressure than the fluid with dipole moments arranged perpendicular

at given density and temperature, when all other parameters are the same. Good agreement is observed between the predictions from the SAFT-VR+D approach with the GMSA approximation and simulation data for system 14 in which the dipole moments are aligned perpendicular, while the SAFT-VR+D EOS with the LEXP approximation again provides excellent predictions for both fluids. Hence the solution of Adelman and Deutch when combined with the hetero-SAFT-VR approach is able to produce satisfactory thermodynamic properties for dipolar square well chain fluids consisting of dipolar and non-dipolar segments.

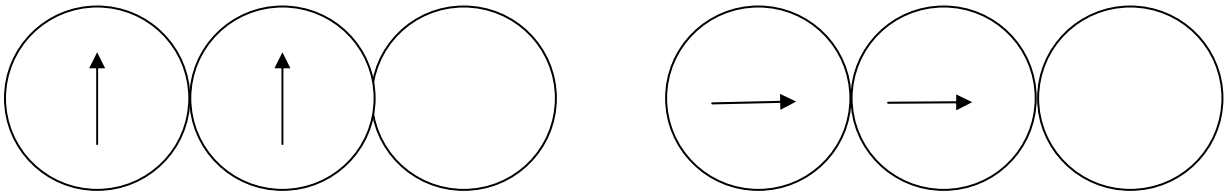

Figure 14: Schematic illustrating the triatomic molecular model used to describe a chain fluid with dipole moments embedded in the center of the first two segments. Segments are labeled 1 – 3 from left to right.

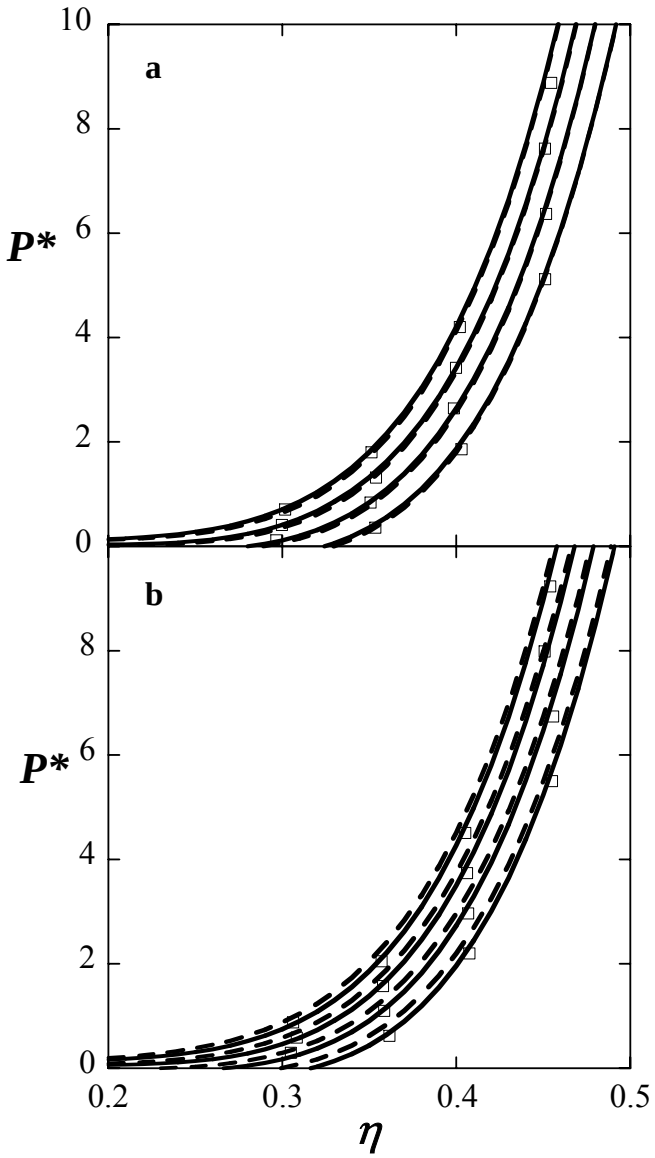

Figure 15: Isotherms for dipolar square well triatomic fluids with $\varepsilon^* = 1.0$, $\lambda = 1.5$, $\sigma^* = 1.0$ and dipole moments $\mu^{*2} = 1.0$ (a) perpendicular and (b) parallel at T*=1.6, 1.8, 2.0 and 2.2 (from bottom to top). The squares represent MC simulation results, the solid lines predictions from the SAFT-VR+D equation with the LEXP approximation and the dashed lines from the SAFT-VR+D equation with the GMSA approximation.

2.5 Conclusions

In this work, a SAFT-VR like equation of state, SAFT-VR+D, has been developed to study dipolar chain fluids which takes the dipolar square well fluid as the reference state. In this way, the SAFT-VR+D approach explicitly takes into account the magnitude and orientation of dipole moments, all of which are found to affect the thermodynamics and phase behavior of dipolar square well monomer and chain fluids. In order to gain a comprehensive understanding of the thermodynamic properties of the systems studied, and validate the SAFT-VR+D approach, both *NPT* MC and GEMC simulations were performed to obtain simulation data to compare to the theoretical predictions. We found that the SAFT-VR+D equation with the GMSA approximation provides good predictions for the phase behavior of the dipolar monomer fluids studied, and chain fluids with a perpendicular arrangement of the dipole moments. A more accurate approximation for the radial distribution function of dipolar square well fluids (LEXP approximation) was implemented to improve the performance of the SAFT-VR+D EOS for dipolar chain fluids in which the dipole moments are parallel to the vector joining the centers of the monomers. It is found that the SAFT-VR+D with the LEXP approximation is suitable for fluids with both vertical and horizontal arrangements of the dipole moments. Furthermore, using the solution of Adelman and Deutch for polar mixtures, the SAFT-VR+D with LEXP approximation gives a good description of the thermodynamic properties of dipolar chain fluids consisting of non-dipolar segments and dipolar segments.

CHAPTER III

PHASE BEHAVIOR OF DIPOLAR ASSOCIATING FLUIDS FROM THE SAFT-VR+D EQUATION OF STATE

3.1 Introduction

Fluids with anisotropic interactions, such as polar or hydrogen bonding interactions, are important not only to the traditional oil and chemical industries, but also in energy production and biological systems; water for example is essential to all known forms of life and can be considered the universal solvent. An accurate description of the phase behavior and thermodynamic properties of polar and associating fluids is therefore important to a diverse range of fields and applications.

Conventional engineering equations of state such as cubic equation of state, which provide a good description of the phase behavior of non-associating and/or non-polar components and their mixtures, cannot easily be used to describe the phase equilibrium of associating and/or polar components. For example, such models cannot be used to study the simultaneous vapor-liquid equilibria (VLE) and liquid-liquid equilibria (LLE) of alcohol-hydrocarbon mixtures with the same interaction parameters [83]. Increasingly both industrial and academic interest is switching to the development and application of more advanced thermodynamic models that explicitly account for anisotropic interactions and so more accurately describe the physical nature of complex fluid systems.

Perhaps the simplest approach to modeling polar and/or associating fluids is the cubic-plus-association (CPA) equation of state [84], which combines the Soave-Redlich-Kwong (SRK) equation of state with Werthieim's first order thermodynamic perturbation

theory to describe different type of hydrogen-bonding interactions. The CPA equation of state has been successfully applied to study a wide range of systems, including the VLE of alcohol-water-aliphatic hydrocarbon ternary system using single interaction parameters per binary system obtained from binary mixtures [85, 86]. However, to describe fluids such as acetone, which are both polar and associating, self-association is used to mimic the strong interactions within the fluid, since the theory does not explicitly account for polar effects [87].

An alternative approach to modeling associating and/or polar components is to use a true molecular based equation of state such as the associated perturbed anisotropic chain theory (APACT) developed by Donohue et al. [88, 89]. APACT treats pure fluids that associate through hydrogen bonding interactions and takes into account interactions due to dipole and/or quadrupole moments [90], however, for systems involving mulitpolar associating components, such as binary system ethanol and pentanol, an analytical solution cannot be determined and the chemical and material equilibria must be solved numerically. Though some simpler versions of the approach have been developed [91], they are still complicated.

Several versions of the SAFT equation of state have been developed for polar fluids in which dipolar and/or quadrupolar interactions are generally incorporated through the addition of the corresponding terms to equation 1. For the dipolar term, both the μ-expansion proposed by Gubbins and Gray [52] (which describes the interaction of dipolar hard sphere fluids using an angular pair correlation function), and the more rapidly converging Padé approximation of Stell and coworkers [53], have been widely adopted. For example, Muller and Gubbins [50] applied the μ-expansion to describe water as a

hard, spherical, associating, dipolar fluid within Wertheim's TPT theory, achieving good agreement with simulation and experimental data; Kraska et al. [48, 49] later extended the Lennard-Jones-SAFT theory of Muller and Gubbins using the multipolar μ-expansion for the dipolar-dipolar interaction to study the phase behavior of alcohols and water and their mixtures with *n*-alkanes. In the equation of state for alkanols and water Xu et al. [51] applied a Padé approximation to describe dipolar contribution. However, a common feature of these equations of state is to treat non-spherical dipolar molecules as spherical dipolar fluids. As a result, the orientation of the dipolar interaction and the possibility of multiple polar sites within a molecule cannot be taken into account.

In contrast, Jog et al. [54, 55] developed a SAFT EOS for tangent hard sphere chains with dipoles on alternate segments. In this work, although the position of the dipole moment is considered, the hard sphere pair correlation function is used to describe the pair correlation function between non-dipolar and dipolar hard spheres at contact, and so neglects the effect of the dipole and its orientation. Using the same approach to describe dipolar interactions, Tumakaka and Sadowski [56] have extended the PC-SAFT EOS to describe mixtures of non-dipolar and polar molecules and Dominik et al. [57] have modeled the phase equilbria and thermodynamic properties of ethers and esters with PC-SAFT + dipolar contribution due to Jog , Saggar and Fischer [58, 59]; the two approaches were found to yield similar results for the systems studied. More recently, Gross and Vrabec [60] developed a contribution for dipolar interactions based on third order perturbation theory which uses simulation data for the vapor-liquid equilibria of the two-center Lennard-Jones plus point dipole fluid to determine the model constants. The proposed term has been incorporated into the PC-SAFT equation of state and has been

shown to improve the description of pure component and mixture phase equilibria for dipolar fluids over the original PC-SAFT approach.

In chapter II, within the SAFT-VR framework, we developed a rigorous approach with which to describe the phase behavior and thermodynamic properties of dipolar fluids. Through a combination of the SAFT-VR approach, which is a recent extension of the SAFT approach to model dispersion interactions through a potential of variable range, and the generalized mean spherical approximation (GMSA), we presented the SAFT-VR+D approach. In the approach, the reference fluid is chosen as dipolar square well fluid, not square well fluid as used in the SAFT-VR EOS, so that the approach can explicitly describe the position and orientation of dipole moment in the dipolar monomer and chain fluids.

In this chapter, we extend the SAFT-VR+D approach to model dipolar associating fluids. Constant NPT and Gibbs ensemble Monte Carlo simulations were performed to test and validate the approach for dipolar associating fluids with one, two and four association sites. The remainder of the chapter is organized as follows: in section 3.2 we present the SAFT-VR+D model and theory for dipolar associating fluids. In section 3.3, details of the molecular simulations performed are presented. Results for the phase behavior of pure dipolar associating fluids are presented and compared with simulation results and the new approach applied to study the phase behavior of water are presented in section 3.4. Finally, concluding remarks are made and future work discussed in section 3.5.

3.2 Model and Theory

In this section we extend the SAFT-VR+D approach to study dipolar associating fluids. The molecules are modeled as hard spheres of diameter σ that can interact through a dipole moment μ embedded in the center of the sphere, a square well interaction to describe the dispersion interactions, and one, two or four short-range attractive square-well sites to describe association interactions that mimic hydrogen bonding (Figure 16). Hence the pair potential for the dipolar associating fluids studied is defined by

$$u\left(\mathbf{r}\boldsymbol{\omega}_1\boldsymbol{\omega}_2\Omega_1\Omega_2\right) = u^{SW}\left(r;\sigma\right) + u^{DIPOLE}\left(\mathbf{r}\boldsymbol{\omega}_1\boldsymbol{\omega}_2\right) + \sum_A \sum_B u_{AB}\left(\mathbf{r}\Omega_1\Omega_2\right) \qquad (3.1)$$

where, $\mathbf{r}$ is the vector between the center of the two monomers, $r = |\mathbf{r}|$ and $\boldsymbol{\omega}_i = \left(\theta_i, \phi_i\right)$ the set of angles defining the orientation of the dipole in monomer *i,* and Ω_i is the orientation of associating site *i* relative to vector ***r***. $u^{SW}\left(r;\sigma\right)$ and $u^{DIPOLE}\left(\mathbf{r}\boldsymbol{\omega}_1\boldsymbol{\omega}_2\right)$ represent the square-well potential and potential of dipolar interaction, and the definitions of $u^{SW}\left(r;\sigma\right)$ and $u^{DIPOLE}\left(\mathbf{r}\boldsymbol{\omega}_1\boldsymbol{\omega}_2\right)$ are referenced to our previous work. The u_{AB} represents the association potential, which is modeled by an anisotropic short-ranged square well interaction, where *A* and *B* represent interacting associating sites. As can be seen from Figure 16 the association sites are situated at a distance r_d from the center of the sphere. Sites of type *A* can bond to sites of type *B* on different molecules with attractive deep but narrow square well like energy ε^{HB} when the two sites are closer than the distance r_c. Sites of the same kind do not interact with each other.

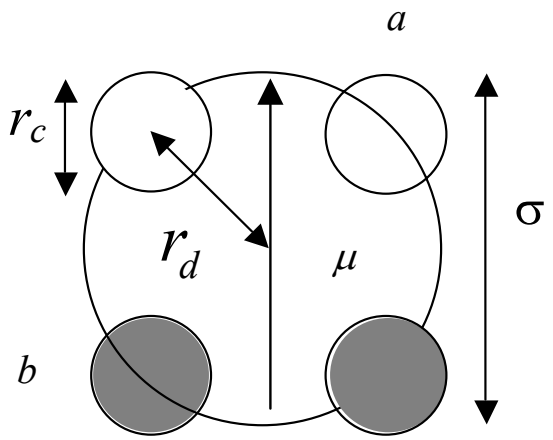

Figure 16: Schematic representation of the model used to describe associating fluids with four association sites.

Within the SAFT framework, the Helmholtz free energy *A* can be written as a sum of separate contributions:

$$\frac{A}{Nk_BT} = \frac{A^{IDEAL}}{Nk_BT} + \frac{A^{MONO}}{Nk_BT} + \frac{A^{ASSOC}}{Nk_BT} \tag{3.2}$$

Since in this work, we do not consider chain fluids, there is not chain term in the equation (3.2). The ideal and association contributions to equation 3.2 are given by equations (1.3) and (1.17) in section 2 of Chapter I, while the monomer term is as presented in Section 2.2.1.2 of Chapter II for the SAFT-VR+D equation.

3.3 Computer Simulations

We have performed Monte Carlo (MC) simulations in the isothermal-isobaric *(NPT)* and Gibbs ensembles (GEMC) to determine the *PVT* and phase behavior of several model dipolar associating fluids in order to compare with the theoretical results from the SAFT-VR+D equation for associating fluids. Molecular simulation studies of associating fluids can be challenging due to the strong association interactions between the molecules,

which can lead to the formation of stable clusters and poor sampling of phase space. As a result, several biasing schemes have been proposed to ensure efficient sampling of phase space in MC simulations of associating systems [92-96]. In particular, Tsangaris and De Pablo [96] proposed the bond-bias MC method and compared results from regular GEMC simulations with those from GEMC simulations using the bond biased move for associating Lennard-Jones monomer fluids with various association strengths. They concluded that regular GEMC simulations would fail for systems in which the association energy is ten times or larger than the dispersion energy. In our work, we focus on systems with low association energy compared to the dispersion interactions (i.e. $\varepsilon_{hb} < 10\varepsilon$) and therefore we do not employ any biasing techniques in the simulations.

The reaction field method, which has been used previously to calculate the vapor-liquid phase behavior of systems with long-range dipolar potential is applied to deal with the long-range dipolar interactions. The reaction field approach replaces the molecules beyond a cut-off distance by a dielectric continuum, the effect of which is taken into account by including a new term into the dipolar potential, viz

$$u^{dipole} = \begin{cases} -\left(\frac{\mu_1\mu_2}{r^3}\right) D - \frac{2(\varepsilon_{RF}-1)}{2\varepsilon_{RF}+1}\frac{\mu_1\mu_2}{r_c^3} & r < r_c \\ 0 & r \geq r_c \end{cases} \qquad (3.3)$$

where r_c is the cut-off distance beyond which the pair potential vanishes and ε_{RF} the dielectric constant of the continuum. In the simulations, the value of r_c is set to 2.5σ, and ε_{RF} to ∞.

In the *NPT* ensemble simulations, one cycle consists of three kinds of trial moves: *N* trial displacements of randomly chosen molecules, *N* trial rotations and one volume change. The extent of each trial move is adjusted to give an individual acceptance

probability of 30 - 40%. In the GEMC simulations, particle exchanges between two phases are performed in addition to the three trial moves described above. The traditional Widom particle insertion method is used to achieve particle exchanges [97]. Each simulation was started from an initial configuration in which 256 molecules are placed on a lattice in the simulation box. An initial simulation of 100,000 - 500,000 cycles was performed to equilibrate the system, before averaging for between 1,000,000 and 4,000,000 cycles. The thermodynamic properties of the system were obtained as ensemble averages and the errors estimated by determining the standard deviation.

Before studying the dipolar associating fluids of interest in this work, to check the accuracy of our simulation code, we performed NPT simulations for several hard associating fluids and obtained good agreement with the results of Jackson et. al. [39] for fluids with one and two association sites and Ghonasgi et. al. [98] for fluids with four association sites.

3.4 Results and discussion

3.4.1 Model fluids

We have applied the SAFT-VR+D approach to study the *PVT* and phase behavior of dipolar associating fluids. In order to validate and test the predictive ability of the SAFT-VR+D EOS for associating fluids, *NPT* and Gibbs ensemble Monte Carlo simulations have been performed for several dipolar associating fluids with one associating site (system 1), two associating sites (system 2), and four associating sites with different strengths of the association energy (systems 3 - 5), association volume (systems 6 and 7)

and dipole moment (systems 8 and 9). The details of each system studied are given in Table 7. The results of the *NPT* simulations are reported in Tables 8 – 10 and those of the GEMC simulations are given in Table 11.

Table 7: Model parameters for dipolar associating fluids studied. μ^{*2} is the reduced dipole moment, λ the range of the potential, r_c^* the reduced cutoff radius, ε^* the reduced depth of square well potential, ε_{ab}^* the reduced association energy.

System	Sites	μ^{*2}	λ	r_c^*	ε^*	ε_{ab}^*
1	1	1.0	1.5	1.05	1	5
2	2	1.0	1.5	1.05	1	5
3	4	1.0	1.5	1.05	1	2
4	4	1.0	1.5	1.05	1	5
5	4	1.0	1.5	1.05	1	7
6	4	1.0	1.5	1.1	1	5
7	4	1.0	1.5	1.1	1	3
8	4	0.5	1.5	1.05	1	5
9	4	2.0	1.5	1.05	1	5

Table 8: *NPT* MC simulation results for Systems 1 - 2. The reduced temperature is given by $T^* = k_B T / \varepsilon$, the reduced pressure is given by $P^* = P\sigma^3 / \varepsilon$ and the reduced energy is given by $E^* = E / N\varepsilon$.

System	T*	P*	η	Error	-E*	Error	System	T*	P*	η	Error	-E*	Error
1	1.2	0.1003	0.315	±0.011	5.42	±0.19	**2**	1.2	0.0262	0.346	±0.012	7.66	±0.31
		0.6731	0.360	±0.008	6.13	±0.14			0.5231	0.378	±0.008	8.38	±0.25
		2.0315	0.401	±0.006	6.80	±0.12			1.7509	0.415	±0.006	9.24	±0.23
		4.7581	0.449	±0.005	7.48	±0.10			4.2774	0.456	±0.005	10.12	±0.21
	1.4	0.5651	0.310	±0.010	5.16	±0.18		1.4	0.5113	0.328	±0.010	6.46	±0.25
		1.3937	0.358	±0.007	5.95	±0.14			1.2845	0.368	±0.008	7.30	±0.23
		3.1441	0.403	±0.005	6.65	±0.10			2.9360	0.410	±0.006	8.19	±0.21
		6.4672	0.450	±0.005	7.31	±0.10			6.0980	0.456	±0.005	9.10	±0.20
	1.6	1.0254	0.306	±0.009	4.97	±0.16		1.6	0.9835	0.316	±0.009	5.77	±0.21
		2.1035	0.355	±0.006	5.78	±0.13			2.0188	0.362	±0.007	6.67	±0.20
		4.2359	0.402	±0.005	6.50	±0.11			4.0733	0.406	±0.006	7.54	±0.20
		8.1455	0.450	±0.005	7.17	±0.10			7.8511	0.452	±0.008	8.40	±0.22
	1.8	1.4835	0.308	±0.009	4.90	±0.17		1.8	1.4492	0.310	±0.009	5.37	±0.20
		2.8076	0.355	±0.006	5.68	±0.12			2.7385	0.359	±0.007	6.29	±0.19
		5.3157	0.401	±0.005	6.39	±0.11			5.1827	0.404	±0.006	7.13	±0.17
		9.8034	0.449	±0.005	7.06	±0.10			9.5597	0.452	±0.007	7.96	±0.19
	2.0	1.9405	0.306	±0.008	4.79	±0.15		2.0	1.9112	0.308	±0.008	5.13	±0.18
		3.5087	0.354	±0.007	5.57	±0.13			3.4500	0.357	±0.007	6.03	±0.18
		6.3885	0.403	±0.006	6.33	±0.12			6.2756	0.403	±0.005	6.86	±0.16
		11.4483	0.450	±0.005	6.98	±0.10			11.2401	0.452	±0.005	7.67	±0.16

Table 9: *NPT* MC simulation results for Systems 3 - 6. The reduced temperature is given by $T^* = k_B T / \varepsilon$, the reduced pressure is given by $P^* = P\sigma^3 / \varepsilon$ and the reduced energy is given by $E^* = E / N\varepsilon$.

Sys.	T*	P*	η	Err.	-E*	Err.
3	1.2	0.1257	0.328	±0.012	5.78	±0.21
		0.7180	0.367	±0.007	6.45	±0.15
		2.0974	0.408	±0.006	7.13	±0.13
		4.8272	0.453	±0.005	7.80	±0.11
	1.4	0.5748	0.317	±0.010	5.40	±0.19
		1.4097	0.361	±0.007	6.15	±0.14
		3.1642	0.405	±0.006	6.88	±0.12
		6.4770	0.452	±0.005	7.56	±0.11
	1.6	1.0261	0.313	±0.009	5.18	±0.17
		2.1027	0.359	±0.007	5.96	±0.15
		4.2283	0.405	±0.005	6.70	±0.12
		8.1153	0.451	±0.005	7.39	±0.11
	1.8	1.4789	0.309	±0.008	5.00	±0.16
		2.7969	0.356	±0.007	5.79	±0.14
		5.2910	0.403	±0.006	6.55	±0.12
		9.7472	0.450	±0.005	7.24	±0.11
	2	1.9325	0.306	±0.008	4.85	±0.16
		3.4917	0.355	±0.007	5.67	±0.14
		6.3529	0.402	±0.005	6.43	±0.12
		11.3749	0.451	±0.005	7.13	±0.11
4	1.2	0.5921	0.406	±0.006	10.06	±0.25
		2.4482	0.449	±0.005	11.22	±0.24
	1.4	0.2353	0.316	±0.013	6.80	±0.31
		0.7505	0.362	±0.009	7.83	±0.27
		1.9784	0.405	±0.006	8.89	±0.24
		4.5180	0.450	±0.005	10.03	±0.23
	1.6	0.7587	0.309	±0.010	6.03	±0.25
		1.5802	0.358	±0.008	7.08	±0.23
		3.2709	0.402	±0.007	8.10	±0.23
		6.4844	0.448	±0.005	9.17	±0.22
	1.8	1.2596	0.308	±0.009	5.63	±0.23
		2.3674	0.356	±0.007	6.62	±0.21
		4.4954	0.402	±0.005	7.60	±0.20
		8.3632	0.449	±0.005	8.60	±0.20
	2	1.7466	0.306	±0.009	5.33	±0.22
		3.1275	0.354	±0.007	6.28	±0.19
		5.6738	0.401	±0.006	7.24	±0.19
		10.1765	0.449	±0.005	8.21	±0.19
5	1.4	0.4133	0.404	±0.007	13.36	±0.35
		2.3741	0.449	±0.005	14.87	±0.32
	1.6	0.2593	0.315	±0.015	8.98	±0.47
		0.7120	0.356	±0.010	10.13	±0.40
		1.8903	0.402	±0.007	11.58	±0.35
		4.4842	0.448	±0.006	13.11	±0.33
	1.8	0.8579	0.306	±0.011	7.54	±0.38
		1.6498	0.355	±0.009	8.87	±0.37
		3.3105	0.402	±0.007	10.29	±0.34
		6.5658	0.448	±0.005	11.73	±0.31
	2	1.4198	0.306	±0.009	6.78	±0.31
		2.5321	0.354	±0.007	8.02	±0.30
		4.6624	0.402	±0.007	9.36	±0.31
		8.5854	0.448	±0.005	10.71	±0.30
6	1.4	0.3080	0.358	±0.010	8.86	±0.31
		1.2765	0.399	±0.006	9.91	±0.26
		3.5146	0.441	±0.006	11.02	±0.25
	1.6	0.5306	0.306	±0.014	6.71	±0.35
		1.1696	0.354	±0.009	0.79	±0.27
		2.5931	0.398	±0.007	8.92	±0.25
		5.4651	0.442	±0.005	9.99	±0.23
	1.8	1.0541	0.303	±0.009	6.12	±0.25
		1.9909	0.352	±0.007	7.21	±0.24
		3.8557	0.398	±0.006	8.30	±0.23
		7.3631	0.444	±0.005	9.35	±0.22
	2	1.5602	0.305	±0.009	5.79	±0.25
		2.7817	0.351	±0.007	6.79	±0.22
		5.0741	0.398	±0.006	7.84	±0.22
		9.2108	0.445	±0.005	8.88	±0.21
	2.2	2.0539	0.304	±0.008	5.52	±0.22
		3.5505	0.351	±0.007	6.50	±0.21
		6.2585	0.398	±0.006	7.51	±0.21
		11.0161	0.446	±0.005	8.50	±0.20

Table 10: *NPT* MC simulation results for Systems 8 - 9. The reduced temperature is given by $T^* = k_B T / \varepsilon$, the reduced pressure is given by $P^* = P\sigma^3 / \varepsilon$ and the reduced energy is given by $E^* = E / N\varepsilon$.

Sys	T*	P*	η	Err	-E*	Err	Sys	T*	P*	η	Err	-E*	Err
8	1.2	0.7245	0.400	±0.008	9.14	±0.28	**9**	1.8	1.0610	0.328	±0.010	7.69	±0.29
		2.6045	0.445	±0.005	10.34	±0.24			2.1208	0.369	±0.007	8.70	±0.26
	1.4	0.3146	0.306	±0.013	6.05	±0.31			4.2000	0.410	±0.006	9.76	±0.25
		0.8513	0.355	±0.008	7.08	±0.25			8.0186	0.456	±0.005	10.90	±0.24
		2.1018	0.399	±0.007	8.11	±0.24		2	1.5572	0.319	±0.009	7.07	±0.26
		4.6646	0.445	±0.005	9.22	±0.22			2.8910	0.365	±0.007	8.17	±0.24
	1.6	0.8318	0.306	±0.010	5.52	±0.25			5.3891	0.408	±0.005	9.22	±0.22
		1.6738	0.353	±0.007	6.48	±0.22			9.8429	0.454	±0.005	10.30	±0.22
		3.3861	0.400	±0.006	7.49	±0.21		2.2	2.0440	0.315	±0.008	6.66	±0.24
		6.6221	0.446	±0.006	8.49	±0.22			3.6431	0.361	±0.007	7.74	±0.24
	1.8	1.3273	0.303	±0.009	5.15	±0.21			6.5466	0.407	±0.005	8.81	±0.22
		2.4546	0.353	±0.008	6.11	±0.21			11.6197	0.453	±0.005	9.86	±0.22
		4.6033	0.399	±0.006	7.05	±0.19		2.4	2.5245	0.312	±0.008	6.36	±0.23
		8.4928	0.447	±0.005	8.00	±0.19			4.3831	0.359	±0.006	7.42	±0.22
	2	1.8097	0.302	±0.008	4.93	±0.19			7.6825	0.405	±0.005	8.47	±0.21
		3.2091	0.352	±0.007	5.85	±0.18			13.3622	0.453	±0.005	9.52	±0.21
		5.7752	0.400	±0.006	6.77	±0.18		2.6	3.0004	0.309	±0.008	6.11	±0.22
		10.2988	0.447	±0.005	7.67	±0.18			5.1145	0.357	±0.007	7.17	±0.22
9	1.2	0.2637	0.385	±0.007	8.78	±0.27			8.8029	0.406	±0.005	8.24	±0.20
		2.0708	0.435	±0.006	10.08	±0.25			15.0798	0.452	±0.005	9.22	±0.20
	1.4	0.0165	0.358	±0.013	9.94	±0.39		2.8	3.4731	0.309	±0.007	5.95	±0.22
		0.4825	0.386	±0.007	10.68	±0.28			5.8399	0.356	±0.006	6.98	±0.21
		1.6611	0.419	±0.005	11.64	±0.26			9.9122	0.405	±0.006	8.03	±0.21
		4.1513	0.458	±0.005	12.74	±0.26			16.7788	0.452	±0.005	9.00	±0.20
	1.6	0.5503	0.338	±0.009	8.53	±0.29							
		1.3231	0.377	±0.008	9.52	±0.29							
		2.9646	0.413	±0.006	10.50	±0.25							
		6.1288	0.457	±0.005	11.68	±0.25							

Table 11: GEMC simulation results for the dipolar associating fluids studied (systems 4 - 9). The fixed variables during the simulation are defined as for table 3 and 4. The densities η, number of molecules *N* and reduced energies E^* in the coexisting vapor and liquid phases are labeled *v* and *l*, respectively.

Sys	T^*	η_l	*Err*	η_v	*Err*	N_l	N_v	$-E_l^*$	*Err*	$-E_v^*$	*Err*
4	0.9	0.464	±0.004	0.001	±0.000	341	171	14.24	±0.19	0.25	±0.19
	1	0.446	±0.005	0.004	±0.000	350	162	13.01	±0.23	0.42	±0.12
	1.1	0.417	±0.005	0.004	±0.000	458	54	11.28	±0.21	0.28	±0.15
	1.2	0.381	±0.007	0.012	±0.001	452	60	9.45	±0.22	0.59	±0.19
	1.3	0.346	±0.009	0.030	±0.006	466	46	7.99	±0.24	1.19	±0.37
5	1	0.473	±0.004	0.002	±0.000	296	216	19.58	±0.18	14.05	±0.27
	1.1	0.460	±0.005	0.001	±0.000	331	181	18.21	±0.23	0.22	±0.09
	1.2	0.441	±0.005	0.002	±0.000	322	190	16.43	±0.26	0.43	±0.13
	1.3	0.417	±0.007	0.006	±0.000	365	147	14.68	±0.30	0.68	±0.17
	1.4	0.385	±0.007	0.014	±0.001	422	90	12.66	±0.30	1.07	±0.29
6	0.9	0.460	±0.004	0.000	±0.000	368	144	14.96	±0.16	0.11	±0.07
	1	0.445	±0.005	0.001	±0.000	375	137	13.99	±0.19	0.11	±0.07
	1.1	0.424	±0.005	0.002	±0.001	503	9	12.61	±0.19	0.21	±0.28
	1.2	0.398	±0.006	0.007	±0.000	365	147	11.03	±0.24	0.49	±0.13
	1.3	0.367	±0.008	0.016	±0.002	334	178	9.59	±0.26	0.85	±0.18
7	0.8	0.445	±0.004	0.000	±0.000	398	114	10.24	±0.13	0.04	±0.03
	0.9	0.423	±0.005	0.002	±0.000	451	61	9.23	±0.13	0.11	±0.06
	1	0.399	±0.006	0.004	±0.000	387	125	8.43	±0.15	0.20	±0.07
	1.1	0.372	±0.006	0.010	±0.001	438	74	7.52	±0.14	0.39	±0.13
	1.2	0.339	±0.009	0.022	±0.002	350	162	6.54	±0.18	0.75	±0.13
	1.3	0.288	±0.015	0.045	0.005	331	181	5.48	±0.25	1.35	±0.21
8	0.9	0.461	±0.004	0.002	±0.000	396	116	13.42	±0.19	0.19	±0.09
	1	0.435	±0.005	0.003	±0.000	430	82	11.70	±0.19	0.25	±0.11
	1.1	0.400	±0.006	0.007	±0.001	418	94	9.87	±0.23	0.36	±0.13
	1.2	0.364	±0.008	0.018	±0.002	355	157	8.25	±0.25	0.73	±0.17
	1.3	0.318	±0.012	0.046	±0.007	416	96	6.71	±0.27	1.50	±0.32
	1.35	0.278	±0.016	0.072	±0.012	354	158	5.76	±0.31	2.07	±0.40
9	0.9	0.474	±0.005	0.001	±0.000	287	225	16.18	±0.21	8.86	±0.45
	1	0.464	±0.003	0.001	±0.000	452	60	16.16	±0.17	0.26	±0.15
	1.1	0.442	±0.005	0.003	±0.003	503	9	14.57	±0.20	0.90	±1.91
	1.2	0.410	±0.006	0.003	±0.000	413	99	12.19	±0.23	0.34	±0.14
	1.3	0.380	±0.007	0.008	±0.001	460	52	10.72	±0.22	0.59	±0.26

In Figure 17 we present the *PVT* behavior for dipolar associating fluids with one associating site (system 1, Figure 17a) and two associating sites (system2, Figure 17b) with the same parameters: $\mu^{*2} = 1.0$, $\lambda = 1.5$, $r_c^* = 1.05$, $\varepsilon^* = 1.0$ and $\varepsilon_{ab}^* = 5.0$. From Figure 17, we find that the fluid with two association sites exhibits higher densities at a given temperature and pressure than the fluid with one association site, which would be expected given the greater cohesion energy between the molecules, and that good agreement is obtained between the simulation results and theoretical predictions for each of the systems studied.

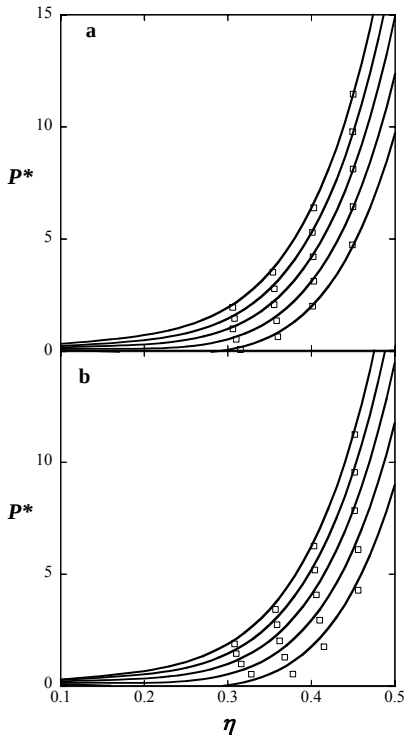

Figure 17: (a) Isotherms for dipolar square-well associating monomer fluids with one association site and (b) Isotherms for dipolar square-well associating monomer fluids with two association sites, with $\varepsilon^* = 1.0$, $\lambda = 1.5$, $\sigma^* = 1.0$, $\mu^{*2} = 1.0$, $r_c^* = 1.05$ and $\varepsilon_{ab}^* = 5.0$ at T* = 1.2, 1.4, 1.6, 1.8 and 2.0 (from bottom to top). The solid lines represent predictions from the SAFT-VR+D equation and the symbols the *NPT* Monte Carlo simulation data.

In figure 18 we present the *PVT* behavior for dipolar associating fluids with four association sites and different association energies (system 3 - 5). For each system studied the remaining SAFT-VR+D parameters are the same: $\mu^{*2} = 1.0$, $\lambda = 1.5$, $r_c^* = 1.05$, $\varepsilon^* = 1.0$. From figure 18, we find that the fluids with higher association energy exhibit higher densities at a given temperature and pressure than those with lower association energy. Similarly, when compared with the *PVT* behavior for dipolar associating fluids with one and two associating sites (system1 and 2), the fluids with four associating sites remaining all other parameters the same (system 4) exhibits higher densities at a given temperature and pressure. Again, good agreement is observed between the simulation results and theoretical predictions for each of the systems studied over a wide range of temperatures and pressures.

We have also determined the fluid phase diagram for systems 4 and 5 in order to further test the SAFT-VR+D approach. From the results presented in Figure 19, and as would be expected, we find that the fluid with higher association energy $\varepsilon_{ab}^* = 7$, system 5) has a higher critical temperature and wider phase envelope than the fluid with a lower association energy ($\varepsilon_{ab}^* = 5.0$, system 4). Additionally good agreement is obtained between the simulation results and theoretical predictions for both systems studied. From these results, we can conclude that the SAFT-VR+D approach provides a good description of the thermodynamic properties of dipolar association fluid with one, two or four association sites as a function of association energy (i.e. from $\varepsilon_{ab}^* = 2$ to $\varepsilon_{ab}^* = 7$).

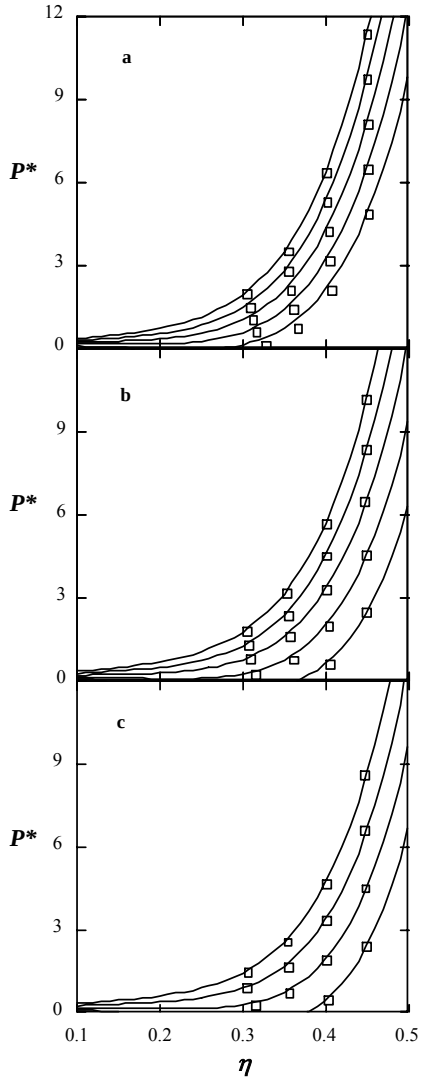

Figure 18: Isotherms for dipolar square-well associating monomer fluids with four association sites with $\varepsilon^* = 1.0$, $\lambda = 1.5$, $\sigma^* = 1.0$, $\mu^{*2} = 1.0$, $r_c^* = 1.05$ and (a) $\varepsilon_{ab}^* = 2.0$ at T* = 1.2, 1.4, 1.6, 1.8 and 2.0 (from bottom to top), (b) $\varepsilon_{ab}^* = 5.0$ at T* = 1.2, 1.4, 1.6, 1.8 and 2.0 (from bottom to top), (c) $\varepsilon_{ab}^* = 7.0$ at T* = 1.4, 1.6, 1.8 and 2.0 (from bottom to top), The solid lines represent predictions from the SAFT-VR+D equation and the symbols the *NPT* Monte Carlo simulation data.

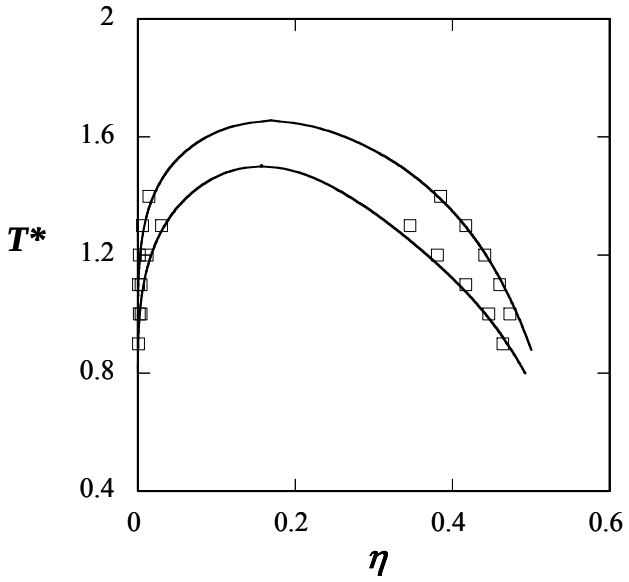

Figure 19: Coexisting densities for dipolar square-well associating monomer fluids with four association sites (a) system 4: $\mu^{*2} = 1.0$, $\lambda = 1.5$, $r_c^* = 1.05$, $\varepsilon^* = 1.0$,and $\varepsilon_{ab}^* = 5.0$ (bottom one) (b) system 5: $\mu^{*2} = 1.0$, $\lambda = 1.5$, $r_c^* = 1.05$, $\varepsilon^* = 1.0$,and $\varepsilon_{ab}^* = 7.0$ (top one). The symbols represent the GEMC simulation data and the solid lines predictions from the SAFT-VR+D equation.

Since a square-well potential is applied to mimic the hydrogen bonding interaction in the dipolar association fluids, the cutoff distance r_c^* plays an important role in the thermodynamics properties of dipolar associating fluids. In order to examine the effect of r_c^* on the phase behavior of dipolar associating fluids and further test the SAFT-VR+D approach, we have studied the *PVT* behavior of the dipolar square-well associating fluid with $\lambda = 1.5$ and $\sigma^* = 1.0$, $\varepsilon^* = 1.0$ $\mu^{*2} = 1.0$ $\varepsilon_{ab}^* = 5.0$ $r_c^* = 1.1$ (system 6) to compare to the results for system 4, for which $r_c^* = 1.05$ with all other parameters the same. The results are presented in Figure 20 and compared to those for system 4 (Figure 18b), we

note that as r_c^* increases, the pressure of the system decreases at a given density and temperature, which reflects the weaker intermolecular interactions between the molecules for smaller values of r_c^*. Good agreement is again observed between the theoretical predictions and the simulation data. We have also studied the phase diagram for systems 6, the results of which are presented in Figure 21. From a comparison of Figures 21 and 19 (bottom line, system 4) we see that as the cutoff distance is increased the critical temperature of the dipolar associating fluid increases, due to the increase in the attractive association interaction. Good agreement is seen between the theoretical phase diagram from the SAFT-VR+D approach and the GEMC simulation data, though we note slight deviations are observed at low temperature (T^*<1.1). The observed deviations could be due to the association interactions prohibiting efficient sampling of phase space or a shortcoming in the theory. We note that good agreement is obtained at low temperatures for system 4 which has shorter association range and therefore overall weaker association interactions. Furthermore, if we compare the results for system 6 with those for system 7 (figure 22), which has a lower association energy ($\varepsilon_{ab}^* = 3.0$) with the other parameters the same, we again see that the SAFT-VR+D approach provides good agreement with the simulation data at low temperatures. We therefore believe, since the under-prediction is only observed in the liquid density at low temperatures for system 6 in which the association energy is at its strongest, that the association interactions are preventing the efficient sampling of the system.

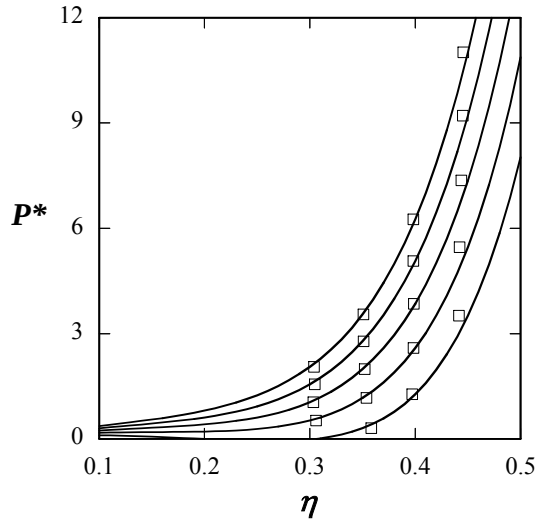

Figure 20: Isotherms for dipolar square-well associating monomer fluids with four association sites for system 4: $\mu^{*2} = 1.0$, $\lambda = 1.5$, $r_c^* = 1.05$, $\varepsilon^* = 1.0$, and $\varepsilon_{ab}^* = 5.0$ at T^* = 1.2, 1.4, 1.6, 1.8, 2.0 (from bottom to top). The solid lines represent predictions from the SAFT-VR+D equation and the symbols the *NPT*-MC simulation data.

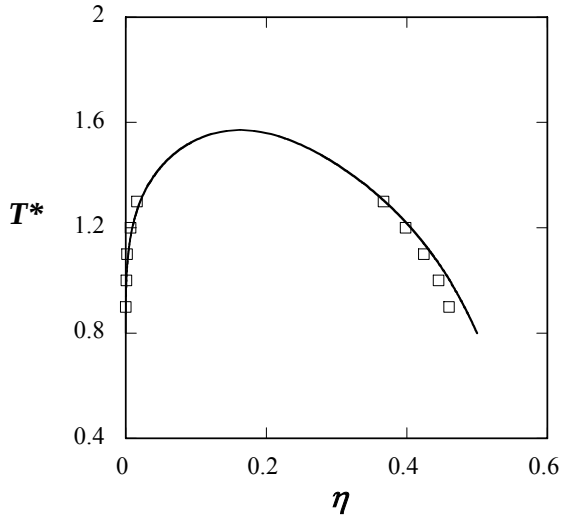

Figure 21: Coexisting densities for dipolar square-well associating monomer fluids with four association sites and $\mu^{*2} = 1.0$, $\lambda = 1.5$, $r_c^* = 1.1$, $\varepsilon^* = 1.0$, and $\varepsilon_{ab}^* = 5.0$ (system 6). The circles represent the GEMC simulation data and the solid lines predictions from the SAFT-VR+D equation.

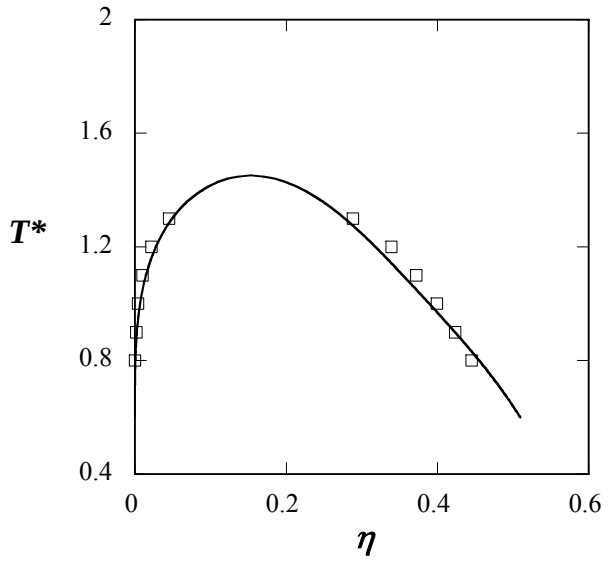

Figure 22: Coexisting densities for dipolar square-well associating monomer fluids with four association sites and $\mu^{*2} = 1.0$, $\lambda = 1.5$, $r_c^* = 1.1$, $\varepsilon^* = 1.0$, and $\varepsilon_{ab}^* = 3.0$ (system 7). The circles represent the GEMC simulation data and the solid lines predictions from the SAFT-VR+D equation.

We now turn to the effect of the strength of the dipole moment on the *PVT* and phase behavior of dipolar associating fluids. In figure 23 we present the *PVT* behavior of the dipolar associating fluids with four association sites with different dipole moments, namely systems 8 and 9, which have different dipole moments, $\mu^{*2} = 0.5$ and $\mu^{*2} = 2.0$ respectively, with other same parameters ($\lambda = 1.5$, $r_c^* = 1.05$, $\varepsilon^* = 1.0$, and $\varepsilon_{ab}^* = 5.0$). From figure 23(a), we note that, excellent agreement is observed between the predictions from the SAFT-VR+D approach and simulation data. However, the SAFT-VR+D approach slightly under-predicts the pressure at a given temperature and density for high dipole moment ($\mu^{*2} = 2.0$) as shown in Figure 23(b). In figure 24, the *PVT* behavior of

the dipolar associating fluid with four association sites of system 9 was presented at higher temperature (T^*=2.2, 2.4, 2.6, 2.8). From the figure, better agreement between simulation results and theoretical prediction is seen than that of the same system at low temperature. We have also studied the phase equilibria of the dipolar associating fluid with different dipole moments, system 8 and 9 shown in figure 25. For system 8, obtain excellent agreement between simulation results and theoretical prediction from the SAFT-VR+D approach, however we see a slight deviation between the theoretical predictions and simulation data for system 9 with the higher dipole moment.

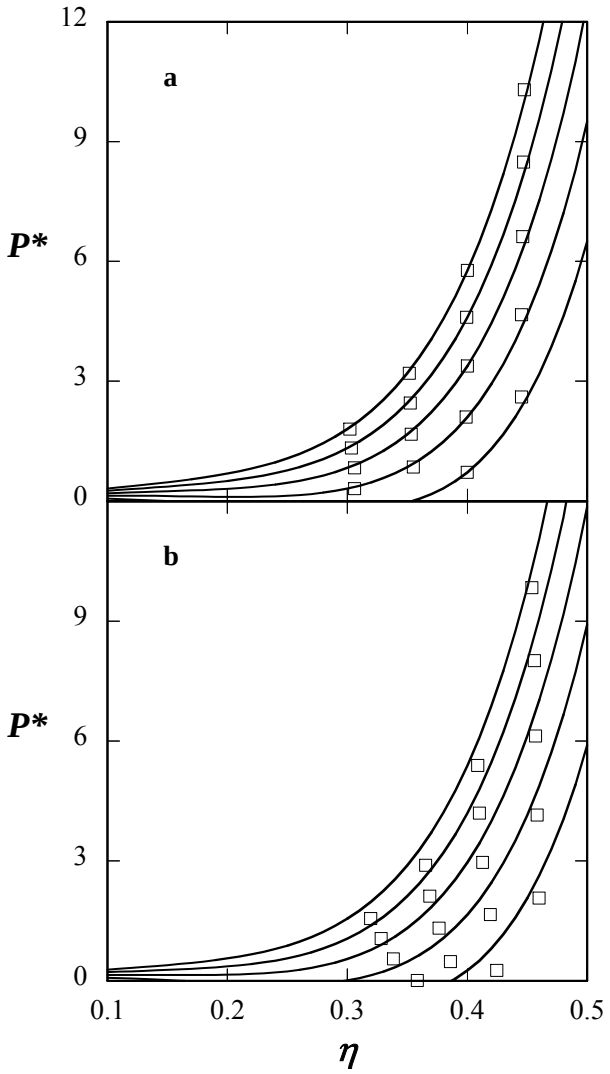

Figure 23: Isotherms for dipolar square-well associating monomer fluids with four association sites for (a) $\mu^{*2} = 0.5$ and (b) $\mu^{*2} = 2.0$, $\lambda = 1.5$, $r_c^* = 1.05$, $\varepsilon^* = 1.0$, and $\varepsilon_{ab}^* = 5.0$ at T*= 1.2, 1.4, 1.6, 1.8, and 2.0 (from bottom to top). The solid lines represent predictions from the SAFT-VR+D equation and the symbols the *NPT*-MC simulation data.

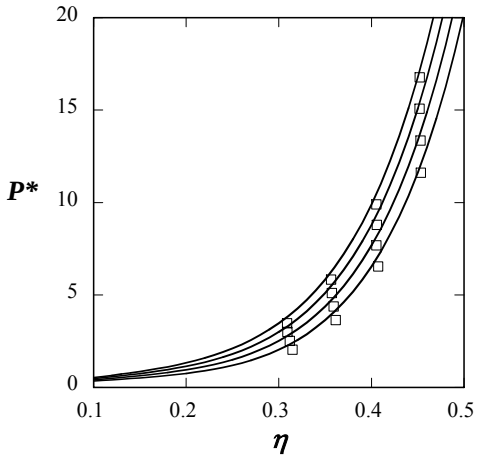

Figure 24: Isotherms for dipolar square-well associating monomer fluids with four association sites of system 8: $\mu^{*2} = 2.0$, $\lambda = 1.5$, $r_c^* = 1.05$, $\varepsilon^* = 1.0$, and $\varepsilon_{ab}^* = 5.0$ at T*= 2.2, 2.4, 2.6, 2.8 (from bottom to top) The solid lines represent predictions from the SAFT-VR+D equation and the cycles the *NPT*-MC simulation data.

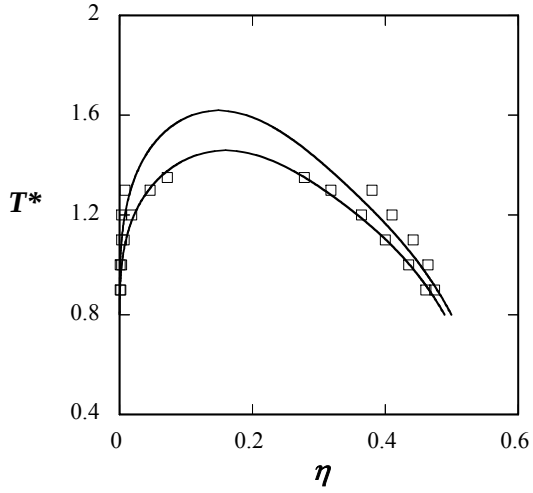

Figure 25: Coexisting densities for dipolar square-well associating monomer fluids with four association sites for (a) system 5: $\mu^{*2} = 0.5$, $\lambda = 1.5$, $r_c^* = 1.05$, $\varepsilon^* = 1.0$, and $\varepsilon_{ab}^* = 5.0$ and (b) system 6 $\mu^{*2} = 2.0$, $\lambda = 1.5$, $r_c^* = 1.05$, $\varepsilon^* = 1.0$, and $\varepsilon_{ab}^* = 5.0$. The symbols represent the GEMC simulation data and the solid lines predictions from the SAFT-VR+D equation.

3.4.2 Water

Having seen that SAFT-VR+D equation can accurately describe the fluid phase behavior of dipolar square-well associating fluids with one, two and four association sites, we now turn to the study of real fluids, and specifically water. The experimental dipole moment for water is used in the calculations and the remaining parameters determined by fitting to experimental vapor pressure and saturated liquid density data [99]. We compare the results obtained with those from the original SAFT-VR approach in Figure 26. From the figure, we can see that the critical temperature from the SAFT-VR+D approach is slightly lower than that of the SAFT-VR EOS though both methods over-predict the critical point due to the analytic nature of the equations of state [13, 14]. Although from a visual inspection the agreement with experimental data from the two approaches is comparable, the SAFT-VR+D approach provides a more accurate correlation of both the vapor pressure and saturated liquid density of water than the SAFT-VR approach when the absolute average deviations (AAD) are calculated: the AAD over the whole phase diagram is 0.92% for the vapor pressures and 2.87% for saturated liquid densities for the SAFT-VR+D approach, compared with 1.18% and 3.06% respectively for the SAFT-VR equation. We also note from Figure 26 that both the SAFT-VR and SAFT-VR+D equations cannot capture the experimentally observed density maximum at lower temperature. We find that in order to capture this behavior a temperature-dependent segment diameter is needed as shown in Figure 27. A similar result is obtained using the SAFT1 equation, which uses temperature-dependent parameters in it's description of the water phase diagram.

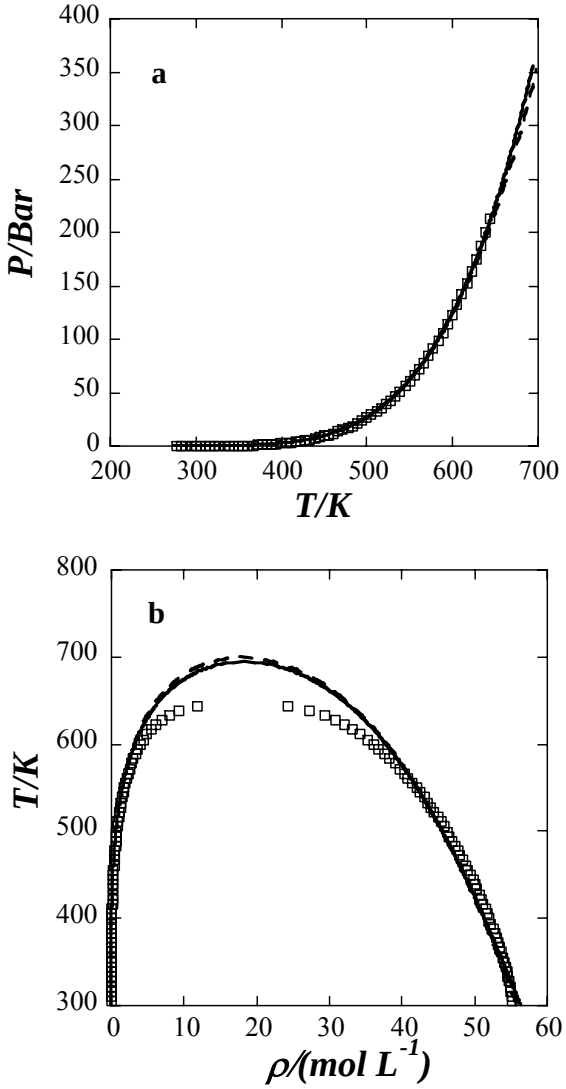

Figure 26: Vapor pressures (a) and vapor - liquid coexistence densities (b) for water compared with theoretical predictions. The results obtained from the SAFT-VR EOS are represented as dashed lines and those from the SAFT-VR+D as solid lines. The squares represent experimental data.

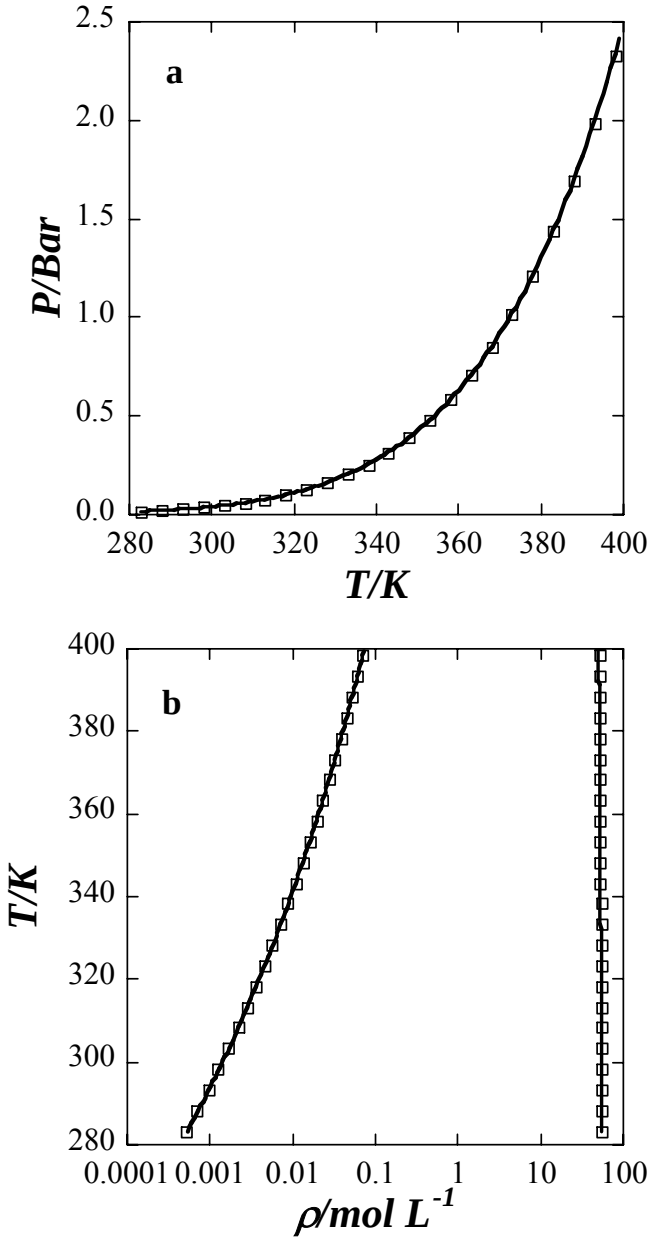

Figure 27: Vapor pressures (a) and vapor and liquid coexistence densities (b) for water compared with theoretical predictions from 283.15K to 400K. The squares represent the experimental data. The results obtained from the SAFT-VR+D EOS correspond to solid lines.

3.5 Conclusion

In this chapter, a SAFT-VR+D approach for associating fluids has been presented and *NPT* MC and GEMC simulations performed to obtain simulation data with which to compare and validate the SAFT-VR+D approach for associating fluids. For the systems studied the theoretical predictions are in good agreement with simulation data. The effect of the range of association energy and association volume has been studied and good agreement is obtained, though slight deviations were seen between the theoretical predictions and simulation data for the saturated liquid densities at low pressure for the strongest association system studied. This is believed to be due to poor sampling in the GEMC simulations due to the formation of clusters of associating molecules. The comparison between the theoretical predictions and simulation data illustrates that the SAFT-VR+D approach can accurately describe the thermodynamic properties of dipolar associating fluids. Additionally, we have applied the SAFT-VR+D approach to water. Although the improvement seen in the description of the fluid phase diagram is minimal compared to the original SAFT-VR approach, the dipolar model for water allows us to explicitly study the effect of the dipolar interactions on solvent properties.

CHAPTER IV

PHASE BEHAVIOR OF ELECTROLYTE FLUIDS FROM THE SAFT-VR+DE EQUATION OF STATE

4.1 Introduction

Electrolyte solutions, and in particular, aqueous electrolyte solutions, are central to chemical, biological and environmental processes. The thermodynamic properties of electrolyte solutions are therefore crucial to the design and operation of, for example, aqueous protein separations, in addition to the more traditional processes in the chemical and petroleum industries. The importance of understanding the thermodynamics of electrolyte solutions is reflected by the significant body of work devoted to developing theoretical tools to predict their thermodynamic and physical properties.

One of the key barriers to the development of predictive approaches for electrolyte solutions is the complexity of the interactions and how to describe the long-range charge-charge and charge-polar interactions. Several theoretical models have been developed to specifically deal with these interactions in electrolyte solutions. In particular, the Debye-Huckle theory was the first theory for electrolyte solutions and considers the ions to be point charges, and so does not include the effect of the volume of the ions and treats the solvent as a dielectric continuum. The Debye-Huckle approach provides a good description of low concentration electrolyte solutions and has been used to develop many semi-empirical equations of state (EOSs) for electrolyte systems such as the Pitzer [100] equations and the electrolytic NRTL [101, 102] model.

Perturbation theory was first applied to model electrolyte solutions by Stell and Lebowitz [103] using the hard sphere as a reference state and Debye-Huckle theory to deduce the perturbation term of the Helmholtz free energy for ion-ion interaction. Henderson later [104] proposed a restricted perturbation theory in which the ion-ion interaction is treated as a perturbation term. Both approaches treat the solvent as a continuous medium and hence are McMillan-Mayer (MM) level of models (as opposed to Born-Oppenheimer (BO) models that explicitly include the solvent). MM models, in which the ions are hard spheres, are referred to as primitive models. Subsequently, Henderson and coworkers [105] extended their approach to ion-dipole mixtures and Chan [106] later applied this model to simple chloride solutions and found that the non-primitive model, which explicitly models the solvent as dipolar molecules, did not give better results than the primitive model, despite the more realistic nature of the model. The apparent failure was attributed to inaccurate predicts of the reference hard-sphere fluid properties. In an alternative approach Jin and Donohue [107-109] combined the perturbed-anisotropic-chain theory [110] for short – range interactions between molecules with Henderson's primitive model for the long range Coulombic interactions and studied a range of single and multiple electrolyte solutions.

As an alternative to perturbation theory, a number of theories for electrolyte solutions have been proposed based on integral-equation theory. Within integral equation theory, two important approximations, the hypernetted chain (HNC) and the mean spherical approximation (MSA), have been used to solve the Ornstein-Zernike equation for electrolyte fluids. However, while the HNC [111, 112] approximation is accurate it is

mathematically complex and does not provide analytical solutions. For example, an important HNC theory is the reference interaction site model (RISM), developed by Chandler [113] and Hirata [114, 115] which takes into account the molecular shape of the ions and solvent; however, it yields a trivial dielectric constant for the solvent in BO models and the solution is not analytic, requiring numerical methods. In contrast, the MSA allows for analytical solutions to be developed for a wide range of model fluids [116]. Independently Waisman and Lebowitz [117, 118] and Blum [119] obtained analytical expressions for the thermodynamic properties of the restricted and unrestricted primitive MSA models respectively (restricted refers to primitive models in which the hard spheres are of equal diameter and opposite sign).The primitive MSA (PMSA) clearly accounts for the effect of the volume of the ions explicitly; when the diameters of the ions vanish the MSA expression reduces to the D-H equation. The PMSA model has been applied to develop equations of state for electrolyte fluids by several authors. For example, Ball [120] established an EOS for electrolyte solutions that used the PMSA to describe the long-range interactions, and Lu [121] et al. have used the PMSA to calculate the activity coefficients of single and mixed aqueous electrolyte solutions using ionic-strength-dependant effective diameters for the cation.

To explicitly account for the effect of the solvent, Blum [122, 123] and Adelman and Deutch [124] developed analytic non-primitive MSA (NPMSA) expressions for the thermodynamic properties of a mixture of equal sized ions and dipolar hard-spheres. Blum and Wei [125] later extended the solutions to the system of arbitrary sizes of charged and dipolar hard spheres. The solution of the NPMSA includes three types of

interaction: ion-ion, ion-dipole and dipole-dipole interactions. Hoye and Stell [126, 127] have used the approach of Blum and Wei to yield explicit forms for the ion-ion, ion-dipole and dipole-dipole pair distribution functions. Li et al. [128] subsequently tested the NPMSA against Monte Carlo simulation data and found that it provides a good description of the ion-ion interaction but underestimates the ion-dipole interaction. Lvov and Wood [129] applied the restricted NPMSA, which considers the ions and solvent to be the same size, to correlate the density of aqueous NaCl systems and give reasonable accuracy over a wide range of temperatures and pressures using 12 empirically adjustable parameters. For a comprehensive review of theories developed for aqueous electrolyte fluids the reader is directed to the excellent reviews of Loehe and Donohue [130] and Anderko and coworkers [131].

In this chapter we propose a new equation of state for electrolyte fluids that combines the analytical results of the MSA with an accurate model for the short-range dispersion and association interactions, which also play an important role in determining the thermodynamic properties of electrolyte systems. Through a combination of integral equation theory and perturbation theory, within the framework of the statistical associating fluid theory, we can develop a statistical mechanics based model that accurately captures the key molecular level interactions. Within the SAFT framework, many extensions of the original equations have been proposed and several variations have been specifically developed to describe electrolyte solutions. For example, Liu [132] et al. established an EOS for aqueous electrolyte fluids based on Wertheim's theory for association interactions and the semi-restricted NPMSA (i.e., equal sized hard spheres

were used to model the cations and anions and a different sized hard sphere used for the solvent); Wu and Prausnitz [133] calculated the phase equilibria for systems containing hydrocarbons, water and salt by combining the Peng-Robinson EOS with the SAFT term for association interactions and the MSA to describe the ion-ion interactions; Tan and Radosz [134] have coupled SAFT1 with the restricted primitive model (RPM) to represent aqueous strong electrolytes and Cameretti and coworkers [135] have extended the PC-SAFT equation to model aqueous electrolyte solutions through the addition of a Debye-Huckle theory ion-ion interaction term. Of particular relevance to the current work Galindo et al. [35, 36] who first extended the SAFT-VR EOS to model electrolyte solutions using an additive electrostatic term from the RPM with the MSA closure. The SAFT-VRE approach has been used to predict the vapor pressures of electrolyte solutions in good agreement with experimental data; however, deviations from the experimental data are observed at high ion concentration (> 10 molar), which may be due to the ion-solvent interactions not being adequately represented by the dielectric constant of the solvent. The SAFT-VRE approach has also been used to successfully study the salting out of n-alkanes in water by strong electrolytes [37] using the experimental dielectric constant for water as input to the calculations.

A common feature of these equations of state is that a McMillan-Mayer level of theory is applied to describe the Coulombic interactions and therefore the effect of the solvent is not been explicitly taken into account and values for the dielectric constant must be obtained.

Here, we present the SAFT-VR+D approach which is a BO level equation of state that models electrolyte solutions through a combination of the MSA for the non-primitive model and the statistical associating fluid theory for potentials of variable range (SAFT-VR); the non-primitive model is used in order to explicitly take into account the effect of the solvent. *NPT* Monte Carlo simulations have been performed and used to validate the new approach. Additionally, to demonstrate the advantage of the use of the non-primitive model, we compare results from the SAFT-VR approach and the non-primitive model with those from the restricted non-primitive model, which constrains the size of the cation, anion and solvent to be equal and the semi non-primitive model, in which only the ions and solvent are of different sizes with the size of the cation and anion being equal.

The remainder of the chapter is organized as follows: in section 4.2 we present the SAFT-VR+DE model and theory for electrolyte solutions. In section 4.3, details of the molecular simulations performed are presented. Results for the phase behavior of electrolyte solutions with different non-primitive models are presented and compared with simulation results in section 4.4. Finally, concluding remarks are made and future work discussed in section 4.5.

4.2 Model and Theory

In this chapter we extend the SAFT-VR approach to study the thermodynamic properties of electrolyte solutions in which the solvent is explicitly taken into account as a dipolar fluid. The electrolyte solutions are represented as a mixture of ions and solvent molecules as shown in Figure 28. The ions are described as hard spheres, half with charge $+q$ and diameter σ^+, and half with charge $-q$ and diameter σ^-. The solvent is

described as dipolar associating square-well molecules of diameter σ_d with dipole moment μ embedded in the center of the molecule and four association sites to mimic the hydrogen bonding. As shown in Figure 16 in Chapter III, the four association sites, two of type a and two of type b, are situated off-center at a distance r_d in a tetrahedral arrangement on the hard sphere. Two sites interact through a square-well potential when they are closer than a distance r_c apart. In the dipolar association model, there are two types of association sites, type *a* and type *b* with interactions between sites of different type only. In our model for electrolyte solutions, in addition to the dispersion and association interactions between solvent molecules, electrostatic charge-charge, charge-dipole and dipole-dipole interactions describe the interaction of the ions, the ions within the solvent, and dipolar solvent-solvent interactions respectively.

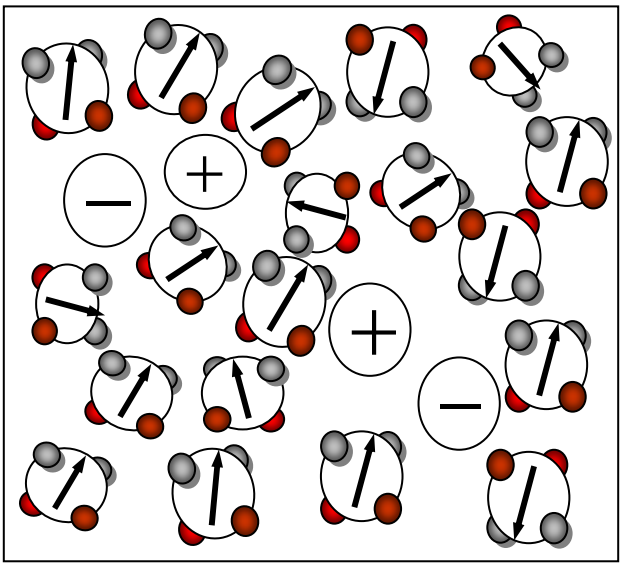

Figure 28: Schematic showing the model used to describe electrolyte solutions in which solvent molecules are explicitly described as dipolar association molecule with four association sites.

Hence, the pair potential for the reference fluid is defined by

$$u(\mathbf{r}) = u^{SW}(r) + u^{CC}(r) + u^{CD}(r) + u^{DD}(r) \tag{4.1}$$

where, $u^{SW}(r)$ represents the square-well potential, $u^{CC}(r)$ the Coulombic charge-charge interaction, $u^{CD}(r)$the charge-dipole interaction, and $u^{DD}(r)$the dipole-dipole interaction. As in the original SAFT-VR equation the square-well potential is given by

$$u_{ij}^{SW}(r) = \begin{cases} +\infty & \text{if} \quad r < \sigma_{ij} \\ -\varepsilon_{ij} & \text{if} \quad \sigma_{ij} \le r < \lambda_{ij}\sigma_{ij} \\ 0 & \text{if} \quad r \ge \lambda_{ij}\sigma_{ij} \end{cases} \tag{4.2}$$

where σ_{ij} is the diameter of the interaction, λ_{ij} the range and ε_{ij} the depth of the square-well potential and the inter- and intra-molecular cross interactions between segments are obtained from standard combining rules, *viz*

$$\sigma_{ij} = \frac{\sigma_{ii} + \sigma_{jj}}{2} \tag{4.3}$$

$$\varepsilon_{ij} = \left(1 - k_{ij}\right)\left(\varepsilon_{ii}\varepsilon_{jj}\right)^{1/2} \tag{4.4}$$

$$\lambda_{ij} = \left(\frac{\lambda_{ii}\sigma_{ii} + \lambda_{jj}\sigma_{jj}}{\sigma_{ii} + \sigma_{jj}}\right) \tag{4.5}$$

The Coulombic charge-charge potential between ions can be represented by

$$u_{ij}^{CC}(r) = \begin{cases} +\infty & \text{if} \quad r \le \sigma_{ij} \\ \dfrac{z_i z_j e^2}{4\pi\varepsilon r} & \text{if} \quad r > \sigma_{ij} \end{cases} \tag{4.6}$$

where r is the center-to-center distance, $e = 1.602 \times 10^{-19} C$ is the elementary charge, and ε is the permittivity of the continuous dielectric medium. The charge-dipole potential can be defined by

$$u_{ij}^{CD}(r) = \begin{cases} +\infty \quad \text{if} & r \le \sigma_{ij} \\ \dfrac{z_i e \mu}{4\pi\varepsilon r^2}(\hat{r}.\hat{n}) \quad \text{if} & r > \sigma_{ij} \end{cases} \tag{4.7}$$

and the dipole-dipole potential as

$$u_{ij}^{DD}(r) = \begin{cases} +\infty \quad \text{if} & r \le \sigma_{ij} \\ -\dfrac{\mu^2}{4\pi\varepsilon r^3} D(\mathbf{n}_1 \mathbf{n}_2 \hat{\mathbf{r}}) \quad \text{if} & r > \sigma_{ij} \end{cases} \tag{4.8}$$

where

$$D(\mathbf{n}_1 \mathbf{n}_2 \hat{\mathbf{r}}) = 3(\mathbf{n}_1 \cdot \hat{\mathbf{r}})(\mathbf{n}_2 \cdot \hat{\mathbf{r}}) - \mathbf{n}_1 \cdot \mathbf{n}_2 \tag{4.9}$$

Here $\hat{\mathbf{r}}$ is the unit vector in the direction of $\mathbf{r}$ joining the center of the segments and $\mathbf{n}_i$ is a unit vector parallel to the dipole moment of segment i.

Within the SAFT framework, the Helmholtz free energy A for the electrolyte solutions studied in this work can be written in the form

$$\frac{A}{Nk_BT} = \frac{A^{ideal}}{Nk_BT} + \frac{A^{mono.}}{Nk_BT} + \frac{A^{assoc.}}{Nk_BT} \tag{4.10}$$

where A^{ideal} is the free energy of the ideal fluid, $A^{mono.}$ is the contribution due to the reference monomer fluid, and $A^{assoc.}$ represents the free energy due to association interactions. We have not included the contribution due to chain formation, as only charged/dipolar monomer molecules are considered in this study. Here we present the general expressions for each term in equation (4.10) in turn for the ternary mixture of cations (component 1), anions (component 2) and solvent molecules (component 3).

4.2.1 Ideal Contribution

The ideal contribution to the free energy is expressed as:

$$\begin{aligned}\frac{A^{ideal}}{NkT} &= \sum_{i=1}^{n} x_i \ln(\rho_i \Lambda_i{}^3) - 1 \\ &= x_1 \ln(\rho_1 \Lambda_1{}^3) + x_2 \ln(\rho_2 \Lambda_2{}^3) + x_3 \ln(\rho_3 \Lambda_3{}^3) - 1\end{aligned} \tag{4.11}$$

where $\rho_i = N_i / V$ the number density, Λ_i the thermal de Broglie wavelength of species i and x_i the mole fraction of component i.

4.2.2 Monomer Contribution

The monomer free energy is given by,

$$\frac{A^{mono.}}{NkT} = \left(\sum_{x=1}^{n} x_i m_i \right) \frac{A^{mono.}}{N_s kT} = \left(\sum_{x=1}^{n} x_i m_i \right) a^{mono.} \tag{4.12}$$

where N_s is the total number of segments, determined from the product of the total number of molecules N and the number of segments per molecule m_i, which in this work is always equal to 1. a^{mono} is the free energy per monomer segment of the reference fluid which is a mixture of charged and dipolar hard spheres that interact through square-well, and Coulombic charge-charge, charge-dipole and dipole-dipole interactions. $a^{mono.}$ can be separated into two terms, a^M due to the square-well potential, and a^{MSA} due to the anisotropic long-range interactions, *viz.*

$$a^{mono} = a^M + a^{MSA} \tag{4.13}$$

4.2.2.1 Square-Well Attractive contribution

In the SAFT-VR equation a^M is approximated by a second order high temperature expansion using Barker and Henderson's perturbation theory for mixtures [136], *viz*

$$a^M = a^{HS} + \beta a_1 + \beta^2 a_2 \tag{4.14}$$

where $\beta = 1/kT$, a^{HS} is the free energy of the hard sphere reference fluid and a_1 and a_2 are the first and second perturbation terms respectively. The hard sphere reference term a^{HS} is determined from the expression of Boublik [137] and Mansoori and co-workers [138] for multicomponent hard sphere systems,

$$a^{HS} = \frac{6}{\pi\rho_s}\left[\left(\frac{\zeta_2^3}{\zeta_3^2} - \zeta_0\right)\ln(1-\zeta_3) + \frac{3\zeta_1\zeta_2}{1-\zeta_3} + \frac{\zeta_2^3}{\zeta_3(1-\zeta_3)^2}\right] \tag{4.15}$$

where ρ_s is the number density of segments, which is defined as the total number of segments divided by the total volume N_s/V and ζ_l is the reduced density given by a sum over all segments i,

$$\begin{aligned}\zeta_l &= \frac{\pi}{6}\rho_s\left[\sum_{i=1}^{n} x_{s,i}(\sigma_i)^l\right] \\ &= \frac{\pi}{6}\rho_s[x_{s,1}(\sigma_1)^l + x_{s,2}(\sigma_2)^l + x_{s,3}(\sigma_3)^l]\end{aligned} \tag{4.16}$$

where σ_i is diameter of segments of type i and $x_{s,i}$ is the mole fraction of segments in the mixture, and is given by

$$x_{s,i} = \frac{m_i x_i}{\sum_{k=1}^{n} m_k x_k} = \frac{m_i x_i}{m_1 x_1 + m_2 x_2 + m_3 x_3} = x_i \tag{4.17}$$

The first perturbation term a_1 describing the mean-attractive energy is obtained from the sum of all pair interactions,

$$\begin{aligned} a_1 &= \sum_{i=1}^{n}\sum_{j=1}^{n} x_{s,i}x_{s,j}\left(a_1\right)_{ij} \\ &= x_{s,1}^2\left(a_1\right)_{11} + 2x_{s,1}x_{s,2}\left(a_1\right)_{12} + 2x_{s,1}x_{s,3}\left(a_1\right)_{13} + x_{s,2}^2\left(a_1\right)_{22} + 2x_{s,2}x_{s,3}\left(a_1\right)_{23} + x_{s,3}^2\left(a_1\right)_{33} \end{aligned} \tag{4.18}$$

where $\left(a_1\right)_{ij}$ is obtained from the mean-value theorem as proposed by Gil-Villegas *et al.* [9],

$$\begin{aligned} \left(a_1\right)_{ij} &= -2\pi\rho_s\varepsilon_{ij}\int_{\sigma_{ij}}^{\infty} r_{ij}^2 g_{ij}^{HS}(r_{ij})dr_{ij} \\ &= -\rho_s\alpha_{ij}^{VDW} g_{ij}^{HS}(\sigma_{ij};\zeta_3^{eff}) \end{aligned} \tag{4.19}$$

and

$$\alpha_{ij}^{VDW} = \frac{2\pi}{3}\sigma_{ij}^3\varepsilon_{ij}\left(\lambda_{ij}^3 - 1\right) \tag{4.20}$$

In this work we use mixing rule MX3b as defined in reference [10] since we are concerned with the phase behavior of electrolyte solutions and will not consider the critical region [ref mccabe paper showing problems). Therefore $g_{ij}^{HS}(\sigma_{ij};\zeta_3^{eff})$ is given by

$$g_{ij}^{HS}\left[\sigma_{ij};\zeta_3^{eff}\left(\lambda_{ij}\right)\right] = \frac{1}{\left(1-\zeta_3^{eff}\right)} + \frac{3D_{ij}\zeta_3^{eff}}{\left(1-\zeta_3^{eff}\right)^2} + 2\frac{\left(D_{ij}\zeta_3^{eff}\right)^2}{\left(1-\zeta_3^{eff}\right)^3} \tag{4.21}$$

where D_{ij} is given by

$$D_{ij} = \frac{\sigma_{ii}\sigma_{jj}}{\sigma_{ii}+\sigma_{jj}}\frac{\sum_{i=1}^{n} x_i\sigma_{ii}^2}{\sum_{i=1}^{n} x_i\sigma_{ii}^3} \tag{4.22}$$

The effective packing fraction $\zeta_3^{eff}\left(\lambda_{ij}\right)$can be written as,

$$\zeta_3^{eff}\left(\zeta_3,\lambda_{ij}\right)=c_1\left(\lambda_{ij}\right)\zeta_3+c_2\left(\lambda_{ij}\right)\zeta_3^2+c_3\left(\lambda_{ij}\right)\zeta_3^3 \tag{4.23}$$

and following the original SAFT-VR approach [10]

$$\begin{pmatrix}c_1\\c_2\\c_3\end{pmatrix}=\begin{pmatrix}2.25855 & -1.50349 & 0.249434\\ -0.669270 & 1.40049 & -0.827739\\ 10.1576 & -15.0427 & 5.30827\end{pmatrix}\begin{pmatrix}1\\ \lambda_{ij}\\ \lambda_{ij}^{\,2}\end{pmatrix} \tag{4.24}$$

The second order perturbation term for the monomer excess free energy a_2 is expressed as:

$$\begin{aligned}a_2&=\sum_{i=1}^{n}\sum_{j=1}^{n}x_{s,i}x_{s,j}\left(a_2\right)_{ij}\\&=x_{s,1}^2\left(a_2\right)_{11}+2x_{s,1}x_{s,2}\left(a_2\right)_{12}+2x_{s,1}x_{s,3}\left(a_2\right)_{13}\\&\quad+x_{s,2}^2\left(a_2\right)_{22}+2x_{s,2}x_{s,3}\left(a_2\right)_{23}+x_{s,3}^2\left(a_2\right)_{33}\end{aligned} \tag{4.25}$$

where $\left(a_2\right)_{ij}$ is obtained through the local compressibility approximation:

$$\left(a_2\right)_{ij}=\frac{1}{2}K^{HS}\varepsilon_{ij}\rho_s\frac{\partial\left(a_1\right)_{ij}}{\partial\rho_s} \tag{4.26}$$

and K^{HS} is the Percus-Yevick expression for the hard-sphere isothermal compressibility,

$$K^{HS}=\frac{\zeta_0(1-\zeta_3)^4}{\zeta_0(1-\zeta_3)^2+6\zeta_1\zeta_2(1-\zeta_3)+9\zeta_2^3} \tag{4.27}$$

4.2.2.2 MSA contribution

The non-primitive model is used in our description of electrolyte solutions in order to explicitly take into account the effect of the solvent. Here we briefly summarize the expressions of Blum's solution for the non-primitive model within the mean spherical

approximation [139]; the expressions for the other models considered for comparison are listed in the appendix. In the MSA, the properties for the non-primitive model are expressible with three parameters Γ, B^{10} and b_2, which correspond to the ion-ion, ion-dipole and dipole-dipole interactions respectively, and are given by the solution of three algebraic equations, *viz.*

$$\sum_{i=1}^{n-1} \rho_i \left(a_i^0\right)^2 + \rho_n \left(a_n^1\right)^2 = \alpha_0^2 \tag{4.28}$$

$$-\sum_{i=1}^{n-1} \rho_i a_i^0 k_{ni}^{10} + a_n^1 \left(1 - \rho_n k_{nm}^{11}\right) = \alpha_0 \alpha_2 \tag{4.29}$$

$$\left(1 - \rho_n k_{nm}^{11}\right)^2 + \rho_n \sum_{i=1}^{n-1} \rho_i \left(k_{ni}^{10}\right)^2 = y_1^2 + \rho_n \alpha_2^2 \tag{4.30}$$

where the quantities in equations (4.28) - (4.30) are defined as

$$\alpha_0^2 = 4\pi\beta e^2, \qquad \alpha_2^2 = \frac{4\pi\beta\mu^2}{3}$$

$$\beta_3 = 1 + \frac{1}{3}b_2, \qquad \beta_6 = 1 - \frac{1}{6}b_2$$

$$\lambda = \frac{\beta_3}{\beta_6}, \qquad y_1 = \frac{4}{\beta_6(1+\lambda)^2}$$

$$w_1 = \sum_{i=1}^{n-1} \frac{\rho_i z_i^2}{\beta_6(\sigma_n + \lambda\sigma_i)(1+\Gamma\sigma_i)},$$

$$w_2 = \frac{1}{2}\rho_n\sigma_n^2 B_{10} \sum_{i=1}^{n-1} \frac{\rho_i z_i^2 \sigma_i^2}{\left[2\beta_6(\sigma_n + \lambda\sigma_i)(1+\Gamma\sigma_i)\right]^2}$$

(4.31)

$$\upsilon_\eta = \frac{-\frac{w_1}{2} + \sqrt{\left(\frac{w_1}{2}\right)^2 + \frac{2B_{10}w_2}{\beta_6^2}}}{w_2}, \qquad \Delta\Gamma_i = \frac{\upsilon_\eta\rho_n\sigma_n^2\sigma_i^2 B_{10}}{8\beta_6(\sigma_n + \lambda\sigma_i)}$$

$$D_i^F = \frac{z_i\beta_6}{2(1+\sigma_i\Gamma - \Delta\Gamma_i)}, \qquad m_i = \frac{\upsilon_\eta D_i^F}{(\sigma_n + \lambda\sigma_i)}$$

$$D = 1 + \upsilon_\eta^2\rho_n\sigma_n^2 \sum_{i=1}^{n-1} \frac{\rho_i\sigma_i^2 (D_i^F)^2}{\left[2\beta_6(\sigma_n + \lambda\sigma_i)\right]^2}, \qquad D_{ac} = \sum_{i=1}^{n-1} \rho_i (D_i^F)^2$$

$$\Gamma_i^s = \frac{(1+\Gamma\sigma_i - \Delta\Gamma_i)D - 1}{\sigma_i}$$

$$\Omega_{10} = \upsilon_\eta \sum_{i=1}^{n-1} \frac{\rho_i \sigma_i \left(D_i^F\right)^2}{\left(\sigma_n + \lambda \sigma_i\right)},$$

$$N_i = \frac{2D_i^F}{\beta_6 \sigma_i}\left[1 + \frac{\upsilon_\eta \rho_n \sigma_n^3 B_{10} \sigma_i}{24\left(\sigma_n + \lambda \sigma_i\right)}\right] - \frac{z_i}{\sigma_i},$$

$$a_i^0 = \frac{\beta_6 \Gamma_i^s D_i^F}{D_{ac}}, \qquad a_n^1 = \frac{D\beta_6}{2D_{ac}}\left[\frac{\sigma_n B_{10}}{2} + \frac{\Omega_{10}\lambda}{D\beta_6}\right] \tag{4.32}$$

$$-k_{ni}^{10} = \frac{\sigma_n^2 D_i^F}{2D\beta_6^2}\left[\frac{\upsilon_\eta}{\left(\sigma_n + \lambda \sigma_i\right)} + \frac{\Omega_{10}\Gamma_i^s}{D_{ac}}\right] + \frac{\sigma_n^3 B_{10} a_i^0}{12\beta_6}$$

$$1 - \rho_n k_{nm}^{11} = \frac{1}{D\beta_6}\left[\lambda + \frac{\rho_n \sigma_n^2 \Omega_{10} a_n^1}{2\beta_6^2}\right] + \frac{\rho_n \sigma_n^3 B_{10} a_n^1}{12\beta_6}$$

In the mean spherical approximation, the internal energy is given by

$$\frac{\beta E}{V} = \frac{1}{4\pi}\left\{\alpha_0^2 \sum_{i=1}^{n-1} \frac{\rho_i z_i^2 \left(D - 1 - \sigma_i \Gamma_i^s\right)}{\sigma_i\left(1 + \sigma_i \Gamma_i^s\right)} - \rho_n \alpha_0 B_{10}\left(\frac{-B_{10}\sigma_n^3 \alpha_0}{12\beta_6} + 2\alpha_2\right) - \frac{2\alpha_2^2 \rho_n b_2}{\sigma_n^3}\right\} \tag{4.33}$$

and the ionic excess chemical potentials as:

$$\beta\mu_i = \frac{z_i\left(\alpha_0^2 N_i - \alpha_0 \alpha_2 \rho_n m_i\right)}{4\pi} \tag{4.34}$$

The chemical potential of dipole molecule is given by:

$$\beta\mu_n = \frac{\left(-\alpha_0 \alpha_2 B_{10} - 2\alpha_2^2 b_2 / \sigma_n^3\right)}{4\pi} \tag{4.35}$$

Following Adelman [140] the dielectric constant can be written as

$$\varepsilon_A = 1 + \frac{\rho_n \alpha_2^2 \beta_6^2 \left(1 + \lambda\right)^4}{16} \tag{4.36}$$

The Helmholtz free energy is presented by

$$\frac{\beta A}{V}=\frac{1}{12\pi}\left\{-2\alpha_0^2\sum_{i=1}^{n-1}\frac{\rho_i z_i^2\left(D-1-\sigma_i\Gamma_i^s\right)}{\sigma_i\left(1+\sigma_i\Gamma_i^s\right)}+\rho_n\alpha_0 B_{10}\left(\frac{-B_{10}\sigma_n^3\alpha_0}{12\beta_6}+2\alpha_2\right)\right\}+J' \quad (4.37)$$

where

$$\begin{aligned}
&J'=\frac{1}{3\pi}\sum_{mnl}\sum_{ij}\rho_i\rho_j\sigma_{ij}^3(2l+1)^{-1}\left[h_{ij}^{mnl}\left(r=\sigma_{ij}\right)\right]^2,\\
&h_{ij}^{000}\left(\sigma_{ij}\right)=\frac{Q_{ij}^{'00}}{3\pi\sigma_{ij}}\\
&h_{in}^{011}\left(\sigma_{in}\right)=\frac{\sqrt{3}Q_{in}^{'01}}{3\pi\sigma_{in}}\\
&h_{nn}^{110}\left(\sigma_n\right)=\frac{Q_{nn}^{'11}+2q'}{2\sqrt{3}\pi\sigma_n}\\
&h_{nn}^{112}\left(\sigma_n\right)=\frac{\sqrt{10}\left(Q_{nn}^{'11}-q'\right)}{2\sqrt{3}\pi\sigma_n}
\end{aligned} \quad (4.38)$$

where

$$\begin{aligned}
&q'=\frac{-b_2(\lambda+3)}{(1+\lambda)^2}\\
&Q_{ij}^{'00}=\frac{2\pi}{\Delta}\left(\sigma_{ij}+\frac{\pi\sigma_i\sigma_j\xi_2}{4\Delta}\right)-\frac{1}{2}D_i^F D_j^F\left(\frac{\rho_n\sigma_n^2\upsilon_\eta^2}{D\beta_6^2\left(\sigma_n+\lambda\sigma_i\right)\left(\sigma_n+\lambda\sigma_j\right)}+\frac{4\Gamma_i^s\Gamma_j^s}{DD_{ac}}\right)\\
&Q_{in}^{'00}=Q_{ni}^{'00}=\frac{2\pi}{\Delta}\left(\sigma_{in}+\frac{\pi\sigma_i\sigma_n\xi_2}{4\Delta}\right)\\
&Q_{in}^{'01}=-\frac{D_i^F}{D\beta_6}\left(\frac{\lambda\upsilon_\eta}{\sigma_n+\lambda\sigma_i}+2\Gamma_i^s a_n^1\right)\\
&Q_{ni}^{'10}=\frac{D_i^F}{D\beta_6}\left(\frac{\lambda\upsilon_\eta}{\sigma_n+\lambda\sigma_i}+2\Gamma_i^s a_n^1\right)\\
&Q_{nn}^{'11}=\frac{2\lambda}{D\rho_n\sigma_n^2}\left(\lambda+\frac{\rho_n\sigma_n^2\Omega^{10}a_n^1}{2\beta_6^2}\right)+\frac{\sigma_n B^{10}a_n^1}{2\beta_6}-\frac{2}{\rho_n\sigma_n^2}
\end{aligned} \quad (4.39)$$

Since in the MSA, the excess Gibbs free energy equals the excess internal energy, then the pressure is given by

$$\beta P = \frac{\beta(E - A)}{V} \tag{4.40}$$

4.2.3 Association contribution

Based on the theory of Wertheim, the contribution due to association of s_i sites on species *i* is obtained as [7]:

$$\frac{A^{ASSOC}}{NkT} = \sum_{i=1}^{n} x_i \left[\sum_{a=1}^{s_i} (\ln X_{a,i} - \frac{X_{a,i}}{2}) + \frac{s_i}{2} \right] \tag{4.41}$$

where the first sum is over the number of species *i* and the second sum is over all s_i sites of type *a* on species *i*, and $X_{a,i}$ is the fraction of molecules of type *i* not bonded at site *a,* which is obtained from the numerical solution of the mass action equations :

$$X_{a,i} = \frac{1}{1 + \sum_{j=1}^{n} \sum_{b=1}^{s_i} \rho x_j X_{b,j} \Delta_{a,b,i.j}} \tag{4.42}$$

The function $\Delta_{a,b,i.j}$, which characterizes the association between site *a* on molecule *i*, and site *b* on molecules *j*, can be written as

$$\Delta_{a,b,i.j} = K_{a,b,i,j} f_{a,b,i,j} g^M(\sigma_{ij}; \zeta_3) \tag{4.43}$$

where, $g^M(\sigma_{ij}; \zeta_3)$ is the contact value of the monomer-monomer radial distribution function, $f_{a,b,i,j} = \exp\left(-\psi_{a,b,i,j} / kT\right) - 1$ is the Mayer *f* function of the *a*-*b* site-site bonding interaction $\psi_{a,b,i,j}$, and $K_{a,b,i,j}$ is the volume available for bonding [47]. The radial distribution function is obtained from a temperature expansion as

$$g^{M}\left(\sigma_{ij};\zeta_{3}\right)=g_{0}^{HS}\left(\sigma_{ij};\zeta_{3}\right)+\beta\varepsilon_{ij}g_{1}\left(\sigma_{ij};\zeta_{3}\right) \tag{4.44}$$

where the hard-sphere radial distribution function is given by the Boublik hard-sphere contact value

$$g_{0}^{HS}\left(\sigma_{ij};\zeta_{3}\right)=\frac{1}{\left(1-\zeta_{3}\right)}+\frac{3D_{ij}\zeta_{3}}{\left(1-\zeta_{3}\right)^{2}}+2\frac{\left(D_{ij}\zeta_{3}\right)^{2}}{\left(1-\zeta_{3}\right)^{3}} \tag{4.45}$$

In our model for electrolyte solutions only the solvent molecules are modeled as associating molecules with four association sites. Therefore, the association contribution to the free energy for a fluid with a four-site associating component can be simplified from equation (4.41) to

$$\frac{A^{ASSOC}}{NkT}=x_{3}\left[4\left(\ln X_{3}-\frac{X_{3}}{2}\right)+2\right] \tag{4.46}$$

Since all four sites are equivalent the fraction of solvent molecules not bonded is given by

$$X_{3}=\frac{1}{1+2\rho x_{3}X_{3}\Delta_{33}} \tag{4.47}$$

where Δ_{33} defined by equation (4.43).

4.3 Computer Simulations

Monte Carlo simulations have been performed to study the thermodynamic properties of several model electrolyte solutions and provide data with which to test the new theoretical approach. The simulations were performed in the isothermal-isobaric (*NPT*) ensemble. And the reaction field method, which truncates the potential at a finite distance

from each ion and dipolar molecule is used to describe the long-range charge-charge, charge-dipole and dipole-dipole interactions [74, 141]. The reaction field approach replaces the molecules beyond a cut-off distance by a dielectric continuum, the effect of which is taken into account by including an additional term into the long-range charge-charge, charge-dipole and dipole-dipole interactions, viz

$$u^{CC} = \begin{cases} q_i q_j \left[\frac{1}{r} + \frac{\left(\varepsilon_{RF} - 1\right)}{\left(2\varepsilon_{RF} + 1\right)} \frac{r^2}{r_c^3} \right] & r < r_c \\ 0 & r \geq r_c \end{cases} \tag{4.48}$$

$$u^{CD} = \begin{cases} -\frac{2\left(\varepsilon_{RF} - 1\right)}{\left(2\varepsilon_{RF} + 1\right)} \frac{\mathbf{r}}{r^3} q.\mu & r < r_c \\ 0 & r \geq r_c \end{cases} \tag{4.49}$$

$$u^{DD} = \begin{cases} -\left(\frac{\mu_1 \mu_2}{r^3} \right) D - \frac{2\left(\varepsilon_{RF} - 1\right)}{2\varepsilon_{RF} + 1} \frac{\mu_1 \mu_2}{r_c^3} & r < r_c \\ 0 & r \geq r_c \end{cases} \tag{4.50}$$

where r_c is the cut-off distance beyond which the pair potential vanishes and ε_{RF} the dielectric constant of the continuum. In our simulations, the value of r_c is set to 3.0σ, and ε_{RF} to ∞. The usual periodic boundary conditions and minimum image convention are used. One simulation cycle consists of three kinds of trial moves: *N* trial displacements of randomly chosen molecules, *N* trial rotations and one volume change. The extent of each trial move is adjusted to give an individual acceptance probability of 30 - 40%. Each simulation was started from an initial configuration in which 256 molecules are placed on a lattice in the simulation box. An initial simulation of 100,000 - 500,000 cycles was performed to equilibrate the system, before averaging for between 500,000 and 1,000,000 cycles. The thermodynamic properties of the system were

obtained as ensemble averages and the errors estimated by determining the standard deviation.

Due to the simplicity and the speed of the reaction field method, several comparisons have been performed in the literature to the Ewald summation technique [73, 142, 143]. For dipolar fluids, the reaction field method has been shown to be provide results in agreement with the Ewald summation [[77], [142]. Additionally, several authors have applied the reaction field method to study ionic fluids, for example, Cummings et al. [144] performed molecular dynamics simulations to determine the equilibrium structure and properties of supercritical water and supercritical aqueous solutions and Zhu and Robbinson [145] applied have studied the solvation structure in a moderately concentrated salt solution. The reaction field method has also been used to simulate mixtures of ions and dipoles. For example, Bandura et .al [146] performed MC simulations to determine ion solvation thermodynamics and the structure of ion-dipole systems and confirmed that the reaction field method is accurate for mixtures of ions and dipolar solvents with moderate values of dipole moments and charges.

4.4 Results and discussion

We have studied the phase behavior of several model electrolyte solutions. In particular comparisons are made between theoretical predictions and *NPT* ensemble Monte Carlo simulation data for several model systems in order to test the new SAFT-VR+DE approach. The model systems studied are detailed in Table 12 and the results of the *NPT* MC simulations are reported in Table 13 and 14. Systems 1-4 are so-called symmetric

electrolyte solutions, in that they have equal sized ions and solvent molecules, system 5 represents a semi-symmetric electrolyte solution in which the ions are of equal size, but differ from the size of the solvent, and system 6 describes an asymmetric electrolyte solution with different sized cation, anion and solvent molecules.

Table 12: Model parameters for electrolyte fluids studied. σ_d^*, σ^{+*} and σ^{-*} are the reduced diameter of solvent molecule, cation and anion, μ^{*2} the reduced dipole moment, ε^* the reduced depth of square well potential , λ the range of the potential, ψ^* the reduced association energy, r_c^* the reduced cutoff radius, N^{ION} number of ions and $N^{Solvent}$ number of solvent molecules .

System	σ_d^*	σ^{+*}	σ^{-*}	μ^{*2}	ε^*	λ	ψ^*	r_c^*	N^{ION}	$N^{Solvent}$
1	1	1	1	0.5	1	1.5	5	1.05	8	248
2	1	1	1	1.0	1	1.5	5	1.05	8	248
3	1	1	1	0.5	1	1.5	5	1.05	4	252
4	1	1	1	0.5	1	1.5	5	1.05	16	240
5	1	0.5	0.5	1.0	1	1.5	5	1.05	8	248
6	1	1/3	2/3	1.0	1	1.5	5	1.05	8	248

Table 13: *NPT* MC simulation results for Systems 1 - 4. The reduced temperature is given by $T^* = k_B T / \varepsilon$, the reduced pressure is given by $P^* = P\sigma^3 / \varepsilon$ and the reduced energy is given by $E^* = E / N\varepsilon$.

SYS.	*T**	*P**	*eta*	*ERR.*	*-E**	*ERR.*	SYS.	*T**	*P**	*eta*	*ERR.*	*-E**	*ERR.*
1	1.2	0.3208	0.402	0.008	17.47	0.28	**3**	1.2	0.4947	0.3982	0.0059	12.15	0.24
		2.1922	0.451	0.005	19.20	0.23			2.3668	0.4458	0.0064	13.40	0.25
	1.4	0.4548	0.357	0.008	15.26	0.25		1.4	0.6295	0.3508	0.0068	10.06	0.23
		1.6788	0.402	0.007	16.31	0.33			1.8628	0.3996	0.0061	11.19	0.22
		4.2295	0.447	0.006	17.11	0.23			4.4158	0.4472	0.0048	12.33	0.22
	1.6	1.2669	0.353	0.007	14.70	0.22		1.6	0.6315	0.3068	0.0080	8.59	0.21
		2.9478	0.401	0.005	15.33	0.20			1.4475	0.3513	0.0067	9.48	0.21
		6.1674	0.451	0.006	16.46	0.22			3.1401	0.4012	0.0061	10.57	0.21
	1.8	0.9596	0.294	0.008	13.37	0.50			6.3641	0.4464	0.0049	11.58	0.21
		2.0401	0.352	0.014	13.92	0.80		1.8	1.1258	0.3041	0.0078	8.19	0.20
		4.1532	0.398	0.012	14.64	0.70			2.2254	0.3503	0.0066	9.08	0.19
		8.0221	0.450	0.015	16.57	0.73			4.3522	0.4002	0.0054	10.11	0.19
2	1.2	0.1859	0.411	0.008	18.96	0.42			8.2274	0.4470	0.0039	11.08	0.18
		2.0379	0.452	0.004	19.93	0.22	**4**	1.2	0.5878	0.419	0.005	29.77	0.22
	1.4	0.3421	0.359	0.007	16.48	0.24			1.8917	0.456	0.003	30.40	0.20
		1.5471	0.406	0.006	17.82	0.27		1.4	0.1432	0.348	0.004	25.35	0.19
		4.0785	0.454	0.004	18.80	0.22			1.3541	0.405	0.004	28.39	0.21
	1.6	0.3773	0.295	0.009	14.03	0.23			3.9055	0.457	0.004	30.47	0.21
		1.1570	0.353	0.008	15.19	0.24		1.6	0.1738	0.318	0.011	22.61	0.80
		2.8190	0.408	0.005	17.34	0.21			0.9429	0.350	0.009	24.70	0.35
		6.0196	0.452	0.005	17.94	0.23			2.6061	0.406	0.005	27.74	0.20
	1.8	0.8709	0.299	0.007	13.64	0.20			5.8224	0.458	0.004	29.72	0.20
		1.9329	0.357	0.007	14.81	0.22		1.8	0.6583	0.292	0.009	21.44	0.73
		4.0273	0.405	0.006	16.50	0.32			1.7062	0.357	0.01	25.99	1.59
		7.8772	0.453	0.005	17.39	0.21			3.7977	0.404	0.005	27.23	0.20
									7.6592	0.457	0.006	28.19	0.46

Table 14: *NPT* MC simulation results for Systems 5 - 6. The reduced temperature is given by $T^* = k_B T / \varepsilon$, the reduced pressure is given by $P^* = P\sigma^3 / \varepsilon$ and the reduced energy is given by $E^* = E / N\varepsilon$.

SYSTEM	*T**	*P**	*eta*	*ERROR*	*-E**	*ERROR*
5	1.4	0.0724	0.334	0.010	18.95	0.29
		1.1905	0.395	0.005	20.40	0.30
		3.6384	0.446	0.006	21.12	0.24
	1.6	0.2337	0.279	0.005	16.68	0.19
		0.9472	0.338	0.005	18.67	0.20
		2.5400	0.396	0.006	19.54	0.23
		5.6772	0.448	0.006	20.30	0.23
	1.8	0.7658	0.285	0.005	16.17	0.29
		1.7745	0.347	0.005	18.01	0.19
		3.8157	0.397	0.005	19.09	0.20
		7.6213	0.450	0.005	19.73	0.21
6	1.4	0.0656	0.350	0.003	19.65	0.20
		1.1802	0.391	0.007	19.82	0.25
		3.6225	0.442	0.005	20.35	0.42
	1.6	0.2289	0.306	0.015	17.26	0.33
		0.9399	0.343	0.007	17.30	0.29
		2.5288	0.399	0.006	19.24	0.22
		5.6596	0.444	0.005	19.59	0.33
	1.8	0.7607	0.302	0.007	16.29	0.40
		1.7666	0.356	0.005	17.31	0.66
		3.8033	0.398	0.006	18.68	0.21
		7.6018	0.446	0.006	18.91	0.36

In figure 29, we present a comparison between predictions from the SAFT-VR+DE approach with the *NPT* ensemble simulation results for the *PVT* behavior of the model restricted electrolyte solution in which the cation, anion and solvent molecules are all of the same size (i.e., systems 1 and 2). Two different dipolar solvents are considered; system 1 with $\mu^{*2} = 0.5$ and system 2 with $\mu^{*2} = 1.0$. From the Figure 29 we see that the system with the highest reduced dipole moment (system 2) exhibits the highest density at a given pressure and temperature, as would be expected due to the increase in attractive interactions between the solvent molecules. We observe good agreement between the simulation results and theoretical predictions over a wide range of temperatures and

pressures, though the proposed approach is seen to slightly under-predict the simulation data at high densities. This could be due to inadequate sampling in the Monte Carlo simulations at high densities due to the strong association interactions. A similar trend was observed in a recent study of dipolar associating systems.

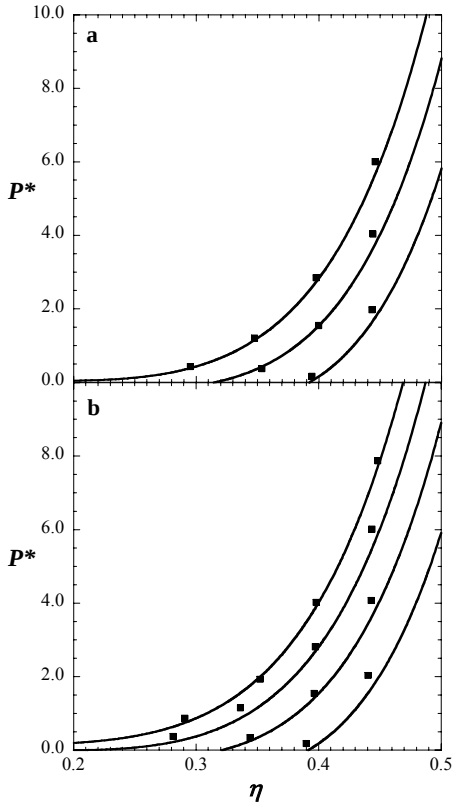

Figure 29: Symmetric electrolyte solution with $\varepsilon^* = 1.0$, $\lambda = 1.5$, $\sigma^{+*} = \sigma^{-*} = \sigma_d^* = 1.0$, $\psi^* = 5.0$, $r_c^* = 1.05$, charge $q = 1$, ions concentration 8/256 and (a) dipole moment $\mu^{*2} = 0.5$, at T* = 1.2, 1.4 and 1.6 (from bottom to top), (b) dipole moment $\mu^{*2} = 1.0$, T* = 1.2, 1.4, 1.6 and 1.8 (from bottom to top). The solid lines represent predictions from the SAFT-VR+DE equation and the squares the *NPT*-MC simulation data.

Since the concentration of ions in electrolyte solutions plays an important role in determining their thermodynamic properties, we have studied the *PVT* behavior of electrolyte solution with differing ion concentrations; namely 0.79%, 1.59% and 3.2% which correspond to systems 1, 3 and 4 respectively. The concentrations reported are in the form of mol % of salt; for comparison, a 1 M NaCl solution corresponds to 1.77 mol %. The results for systems 3 and 4 are presented in Figure 30. From Figures 29 and 30 we note that as the concentration of the ions increases the density at a given pressure and temperature increases, since the attractive ion-ion interaction is stronger than the dipole-dipole interaction. Good agreement is obtained in all cases between the simulation data and theoretical predictions for the systems. We have not examined more concentrated solutions in this work, since we have used the reaction field method to describe the Coulombic interactions; such systems will be the focus of a more detailed study to test the SAFT-VR+DE approach in future work. We note however that Wei and Blum [139] have demonstrated that their non-primitive model solution is valid for moderate sized differences in ion diameters and for moderate to low concentrated solutions.

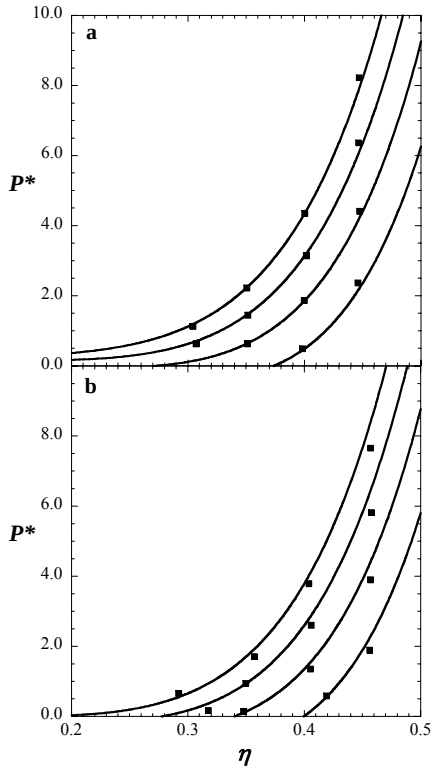

Figure 30: Symmetric electrolyte solution with $\varepsilon^* = 1.0$, $\lambda = 1.5$, $\sigma^{+*} = \sigma^{-*} = \sigma_d^* = 1.0$, $\psi^* = 5.0$, $r_c^* = 1.05$, charge $q = 1$, dipole moment $\mu^{*2} = 0.5$ and (a) 4/256, at T* = 1.2, 1.4 and 1.6 (from bottom to top), (b) 16/256, T* = 1.2, 1.4, 1.6 and 1.8 (from bottom to top). The solid lines represent predictions from the SAFT-VR+DE equation and the squares the *NPT*-MC simulation data.

In order to obtain a more comprehensive understanding of the thermodynamic properties of the systems studied we have also examined different models for the long-range interactions, namely the Debye-Huckel theory, and the primitive and non-primitive models. In Figure 31, we present a comparison of the theoretical predictions from these different electrolyte models, with the results from the SAFT-VR+DE approach and the *NPT* ensemble MC simulation data for system 2 at T* = 1.8. As mentioned previously, for the Debye-Huckel theory and the primitive models, we need to pre-determine the

dielectric constant of the dipolar solvent, which depends on the dipole moment, temperature and the composition of the electrolyte solution. In applications of the primitive model the determination of the dielectric constant can be problematic and often introduces additional approximations. For example in the SAFT-VRE approach [35], the experimental value of the dielectric constant of pure water at each temperature is used in the study of aqueous electrolyte solutions instead of that of the mixture, while Wu and Prausnitz [133] proposed a correlation for the dielectric constant of mixtures of hydrocarbons and aqueous salt solution based on the dielectric constant of water, the composition of the mixture and an adjustable constant for each hydrocarbon. In the SAFT-VR+DE approach the dielectric constant is not required as an input to the calculations. However, we must determine the dielectric constant for the Debye-Huckel and primitive models studied for comparison purposes only. Since dielectric constant data is not available for model solutions, we calculate the dielectric constant Adelman's formula for the dielectric constant from the non-primitive model. We note from the figure that, the theoretical prediction from the Debye-Huckel theory (dash-dot line) under-predicts the density at given pressure and temperature; the theoretical prediction from the SAFT-VR approach with the primitive models under-predicts the density at a given pressure and temperature (RPM and PM provide the exact same theoretical prediction for the symmetric system studied). The prediction from the SAFT-VR+DE approach (i.e. non-primitive model) is in good agreement with the simulation data illustrating the need for an accurate dielectric constant. As expected for the symmetric system studied the

restricted non-primitive model and the semi non-primitive model provide the same solutions.

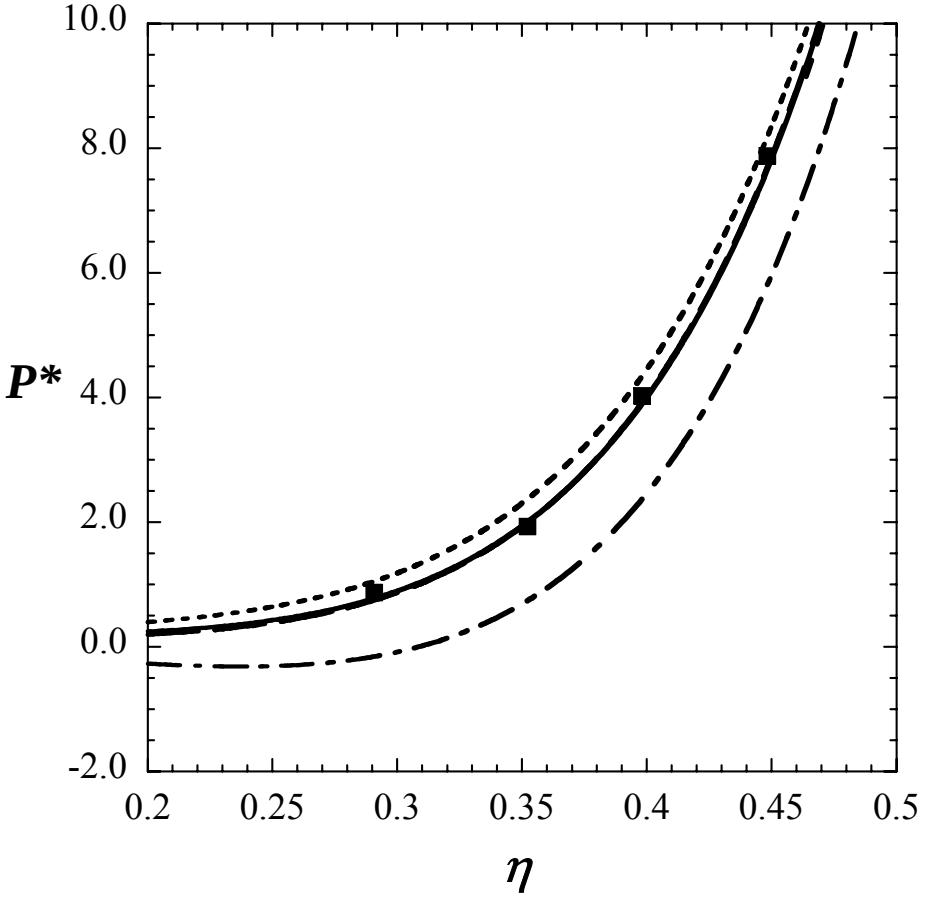

Figure 31: Symmetric electrolyte solution with $\varepsilon^* = 1.0$, $\lambda = 1.5$, $\sigma^{+*} = \sigma^{-*} = \sigma_d^* = 1.0$, $\psi^* = 5.0$, $r_c^* = 1.05$, charge $q = 1$, ions concentration 8/256 and dipole moment $\mu^{*2} = 1.0$ at T^*=1.8 from different models The solid line represents the non-primitive model, the dash-point line the Debye-Huckel theory, the point line the restricted primitive model, the small dash the primitive model, the long dash line the restricted non-primitive model, the middle dash line the semi non-primitive model.

Having seen that the SAFT-VR+DE equation with the non-primitive model to describe the long-range interactions can accurately describe the *PVT* behavior of symmetric electrolyte solutions, we now turn to semi-symmetric electrolyte solutions, which have ions of the same size but different sized solvent molecules. In Figure 32 we present the *PVT* behavior for a semi-symmetric electrolyte solution (system 5), which has the same model parameters as system 2 but the size of the ions are now half that of the solvent. From the figures (Figure 32 and 29b), we find that the semi-symmetric electrolyte solution exhibits a slightly higher density at a given pressure and temperature than the symmetric electrolyte solution (figure 29b) and that the SAFT-VR+DE EOS provides good agreement with the simulation data for the isotherms studied.

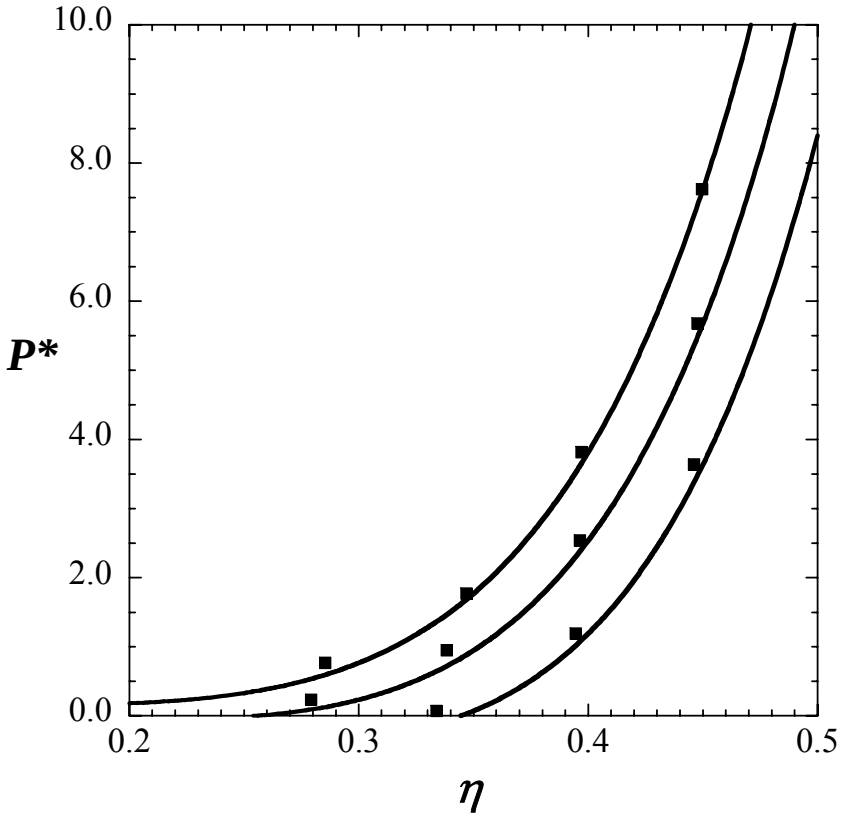

Figure 32: Semi-asymmetric model electrolyte solution with $\varepsilon^* = 1.0$, $\lambda = 1.5$, $\sigma_d^* = 1.0$, $\sigma^{+*} = \sigma^{-*} = 0.5$, $\psi^* = 5.0$, $r_c^* = 1.05$, charge $q = 1$, ions concentration 8/256 and dipole moment $\mu^{*2} = 1.0$, at T^* = 1.4, 1.6 and 1.8 (from bottom to top), The solid lines represent predictions from the SAFT-VR+DE equation and the squares the NPT-MC simulation data.

In order to demonstrate the advantages and accuracy of the SAFT-VR+DE approach and the difference between the non-primitive model and other MSA models for the long-range electrostatic interactions we have again compared the isotherms predicted from the SAFT-VR+DE approach with predictions from the SAFT-VR approach combined with the Debye-Huckel theory and the primitive model (RPM and PM). The results from the different models studied for system 5 at T*=1.8.are shown in Figure 33,

along with the to *NPT* ensemble MC simulation data for comparison. It can be seen from the figure that the predictions using Debye-Huckle theory and the restricted non-primitive model (RNPM), in which the same effective diameters are used for the ions and solvent, show the greatest deviations from the simulation data, which illustrates the importance of correctly accounting for the effect of the size of the ions and solvent in the non-primitive model. The results using the RPM and PM model both under-predict the density at a given temperature and pressure, and result in identical predictions since both models do not explicitly take into account the solvent but mimic the solvent as a dielectric continuum. Again the prediction from the SAFT-VR+DE EOS is in good agreement with the simulation data for the studied system, illustrating the need for both an accurate value of the dielectric constant and accurate representation of the size asymmetry between the solvent and ions.

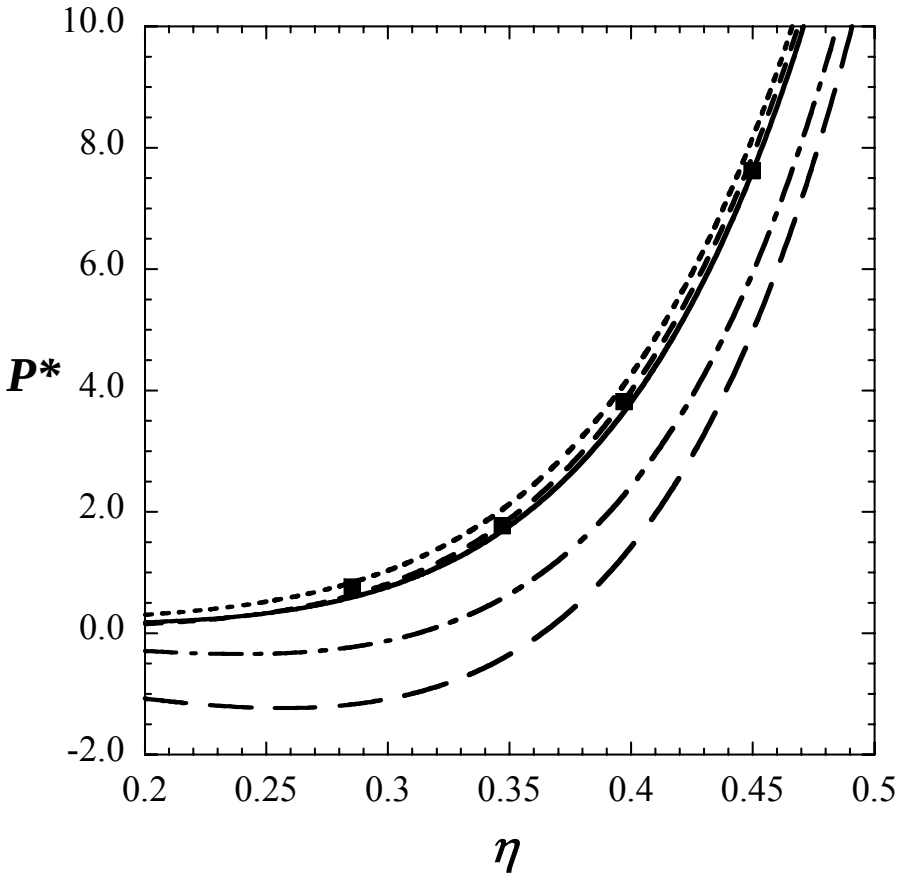

Figure 33: Semi-symmetric model electrolyte solution with $\varepsilon^* = 1.0$, $\lambda = 1.5$, $\sigma_d^* = 1.0$, $\sigma^{+*} = \sigma^{-*} = 0.5$, $\psi^* = 5.0$, $r_c^* = 1.05$, charge $q = 1$, ions concentration 8/256 and dipole moment $\mu^{*2} = 1.0$ at T^*=1.8 from different models. The solid line represents the non-primitive model, the dash-point line the Debye-Huckel theory, the point line the restricted primitive model, the small dash the primitive model, the long dash line the restricted non-primitive model, the middle dash line the semi non-primitive model.

Since real electrolyte solutions, such aqueous solutions of NaCl, are typically composed of ions of different size, it is desirable to be able to model asymmetric electrolyte solutions that are comprised of ions and solvent of different diameters. To test the ability of the SAFT-VR+DE equation in this respect we have studied the *PVT* behavior of an asymmetric electrolyte solution in which the solvent, cation, and anion

diameters are in the ratio 3:1:2 (system 6). The results are presented in Figure 34, where again we see that the SAFT-VR+DE approach provides good agreement with the simulation data. From Figure 29b, Figure 32 and Figure 34, we note that the asymmetric system exhibits the highest density at a given pressure and temperature, while the symmetric system has the lowest density. We again compare the theoretical predictions obtained from the SAFT-VR+DE equation with different MSA models for the system 6 at T* = 1.8 with the *NPT* MC simulation data in Figure 35. From the figure we note similar trends to those observed for the semi-asymmetric system studied: namely, the predictions from the Debye-Huckel and the restricted non-primitive model exhibit the poorest agreement with the *NPT* MC simulation data, indicating that the effect of the size of the ions and solvent plays an important role in determining the thermodynamic properties of electrolyte solutions; a slight difference is observed between the theoretical predictions obtained with the primitive model and the restricted primitive model, in which an effective diameter for the ions is used, and the dielectric constant, which has to be pre-determined for the primitive models, is calculated from the MSA theory of the dielectric constant for dipolar hard spheres. From the comparison, it can also be seen that the predictions using the semi non-primitive model, in which the effective size of ions is used, only slightly under-predicts the density at a given pressure and temperature in comparison with the simulation data and SAFT-VR+DE approach.

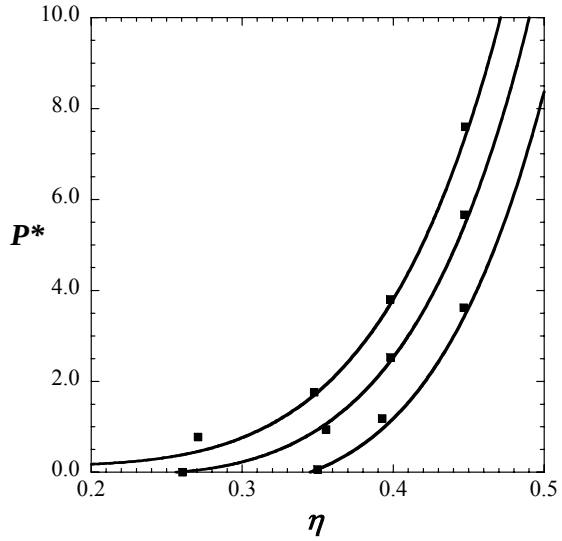

Figure 34: Asymmetric model electrolyte solution with $\varepsilon^* = 1.0$, $\lambda = 1.5$, $\sigma_d^* = 1.0$, $\sigma^{+*} = 1/3$, $\sigma^{-*} = 2/3$, $\psi^* = 5.0$, $r_c^* = 1.05$, charge $q = 1$, ions concentration 8/256 and dipole moment $\mu^{*2} = 1.0$, at T* = 1.4, 1.6 and 1.8 (from bottom to top), The solid lines represent predictions from the SAFT-VR+DE equation and the squares the *NPT*-MC simulation data.

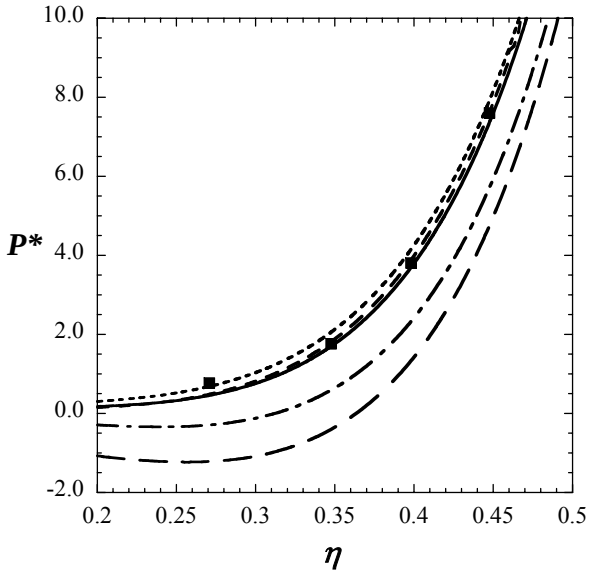

Figure 35: Aymmetric model electrolyte solution with $\varepsilon^* = 1.0$, $\lambda = 1.5$, $\sigma_d^* = 1.0$, $\sigma^{+*} = 1/3$, $\sigma^{-*} = 2/3$, $\psi^* = 5.0$, $r_c^* = 1.05$, charge $q = 1$, ions concentration 8/256 and dipole moment $\mu^{*2} = 1.0$ at T*=1.8 from different models. The solid line represents the non-primitive model, the dash-dot line the Debye-Huckel theory, the dotted line the restricted primitive model, the small dash the primitive model, the long dash line the restricted non-primitive model, the middle dash line the semi non-primitive model.

4.5 Conclusion

In this work, the SAFT-VR+DE approach has been developed through a combination of the SAFT-VR equation and the MSA solution of the non-primitive model, in which the solvent molecules are explicitly described. The theoretical expressions needed to study the ion-ion, ion-dipole and dipole-dipole interactions have been presented. *NPT* MC simulations were performed to obtain simulation data with which to compare to the theoretical predictions and test the new theoretical approach. We find that the SAFT-VR+DE equation provides a good description of the *PVT* behavior of the electrolyte systems studied. We have also compared the non-primitive model with five other models for the long-range interactions; namely the Debye-Huckel theory, the primitive model (RPM and PM) in which the dielectric constant is obtained from the MSA theory for dipolar hard spheres, the restricted non-primitive model and the semi-restricted-non-primitive model. We find that the restricted non-primitive model shows the largest deviations from the Monte Carlo simulation data, indicating the importance of properly accounting for the differences in size of the ions and solvent if the thermodynamics of real electrolyte solutions are to be accurately described. We have also shown the importance of an accurate description of the dielectric constant and how the predictive capability of the primitive model and the Debye-Huckel theory strongly depends on the value of dielectric constant. By using the non-primitive model in the SAFT-VR+DE approach we avoid the need to find experimental data for the dielectric constant or develop correlations in mixed solvent electrolyte systems, and so expand the flexibility of the theory considerably over other SAFT based approaches for electrolytes solutions. We

also find that the predictions obtained from the semi-restricted non-primitive model are very similar to those from the non-primitive model, indicating that the assumption of equal sized ions is reasonable. Given the relative simplicity of the semi-restricted non-primitive model, it may be advantageous to use this approximation when developing engineering equations of state for electrolyte solutions. Although we have only tested the proposed SAFT-VR+DE approach for relatively dilute electrolyte solutions and monomer ions and solvent, our approach is generally applicable and can easily be applied to more concentrated electrolyte solutions with the consideration of ion-ion association and chain-like ions and/or solvent through the addition of a chain term in which the pair distribution function can be derived from the mean spherical approximation.

4.6 Appendix

Due to the complexity of the Wei and Blum's solution of the MSA, discrepancies in the implementation of the solution of the NPM can be found in the literature. In order to verify our implementation of the solutions of the non-primitive model, we reproduce the results presented in Figures 1 and 2 of reference [129]. For the system studied, $\sigma_+ = 0.19$ nm, $\sigma_- = 0.365$ nm , $\sigma_n = 0.276$ nm, $\mu = 2.21$ D, $T = 298.15$ K and the density of water is set to $1.0 g/cm^3$. The results are presented in Figure 36. From Figure 36a, we can see the value of b2 agrees well with that in the literature, however the values of Γ and B_{10} are bigger than those in the literature. The values of Γ and B_{10} in the literature are less than 1.0 which we think it is unreasonable low, especially for the Γ. In Figure 36b, the dielectric constants as function of molality are compared with the value in

the paper of Wei and Blum. From the comparison, they match each other very well. Based on these comparisons, we believe that our implementation of the solution is correct and the discrepancy between the restricted NPM and semi NPM and NPM may come from the approximation introduced during the extension of the MSA solution.

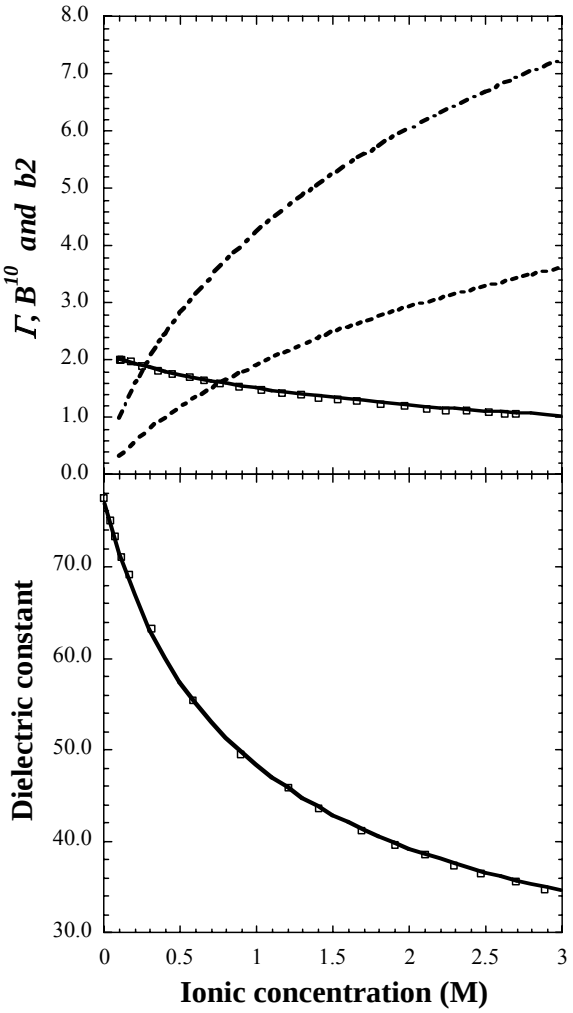

Figure 36: Comparison to the results in Wei and Blum's paper for aqueous NaCl with $\sigma^{+} = 0.19nm$, $\sigma^{-} = 0.365nm$, $\sigma_n = 0.276nm$, $\mu = 2.21D$, and the density of water is set to $1.0g/cm^3$ at $T = 298.15K$ (a), the value of three parameters as function of ionic concentration, and (b) the dielectric constant as a function of ionic concentration.

Other models except the non-primitive model studied in this chapter:

1. Debye-Huckel

The Helmholtz free energy is given by

$$\frac{A^{DH}}{NKT} = -\frac{\kappa^3}{12\pi\rho}$$

where κ is the inverse Debye screening length

$$\kappa^2 = \frac{4\pi z^2 e^2 \rho\beta}{\varepsilon}$$

1. RPM of MSA

The Helmholtz free energy is given by

$$\frac{A^{RPM}}{NKT} = -\frac{3x^2 + 6x + 2 - 2(1+2x)^{3/2}}{12\pi\rho\sigma^3}$$

with $x = \kappa\sigma$

2. The primitive model of MSA

The Helmholtz free energy can be expressed by

$$\frac{A^{PM}}{NKT} = -\frac{1}{\rho}\left[\frac{\beta e^2}{4\pi\varepsilon}\sum_k \frac{\rho_k z_k}{1+\Gamma\sigma_k}\left(\Gamma z_k + \frac{\pi P_n \sigma_k}{2\Delta}\right) - \frac{\Gamma^3}{3\pi}\right]$$

where $\Delta = 1 - \xi_3$ and Γ is the scaling parameter that can be calculated from

$$\Gamma^2 = \frac{\beta e^2}{4\varepsilon}\sum_k \frac{\rho_k z_k}{(1+\Gamma\sigma_k)^2}\left(z_k - \frac{\pi P_n \sigma_k^2}{2\Delta}\right)^2$$

with

$$P_n = \frac{\sum_k \frac{\rho_k \sigma_k z_k}{1+\Gamma\sigma_k}}{1+\frac{\pi}{2\Delta}\sum_k \frac{\rho_k \sigma_k^3}{1+\Gamma\sigma_k}}$$

3. Semi non-primitive model (SNPM) of MSA

The electrolyte solution is modeled as a mixture of ions and dipoles. The ions are hard spheres of diameter of σ_i, half with charge +q and half with charge –q. The dipoles are hard spheres of diameter σ_d, with a central point dipole of magnitude μ. The ration between the diameter of dipoles and diameter of ions is defined

$$p = \sigma_d \big/ \sigma_i$$

The solution is decided by two independent variables, which represent the intensity of the ions and the dipoles, respectively

$$d_0^{\,2} = \frac{4\pi q^2 \rho_i \sigma_i^{\,2}}{kT}$$
$$d_2^{\,2} = \frac{4\pi \mu^2 \rho_d}{3kT} = y$$

The solution of MSA is given in terms of the three energy parameters b_0 (ion-ion), b_1 (ion-dipole) and b_2 (dipole-dipole), and the three parameters satisfy the following set of equations

$$a_1^{\,2} + a_2^{\,2} = d_0^{\,2}$$
$$a_1 K_{10} - a_2[1-K_{11}] = d_0 d_2$$
$$K_{10}^{\,2} + [1-K_{11}]^2 - y_1^{\,2} = d_2^{\,2}$$

where

$$a_1 = \frac{\Delta - 2\beta_6 D_F}{2{D_F}^2}$$

$$a_2 = \frac{-b_1}{2\beta_6 {D_F}^2}\left[\frac{\Delta}{2} + \frac{\beta_3 D_F}{p}\right]$$

$$K_{10} = p\frac{b_1}{2\Delta}\left[1 + a_1\Lambda\right]$$

$$1 - K_{11} = \frac{\beta_3 - \frac{p}{2}a_2 b_1 \Lambda}{\Delta}$$

$$y_1 = \frac{\beta_6}{{\beta_{12}}^2}$$

$$D_F = \frac{1}{2}\left[\beta_6(1 + b_0) - \frac{b_1 p}{12}\right]$$

$$\Delta = {b_1}^2 / 4 + {\beta_6}^2$$

$$\Lambda = \frac{1 + b_0}{2} + \frac{p}{6}\beta_6$$

$$\beta_3 = 1 + b_2 / 3$$

$$\beta_6 = 1 - b_2 / 6$$

$$\beta_{12} = 1 + b_2 / 12$$

$$\beta_{24} = 1 - b_2 / 24$$

The excess Helmholtz free energy is given by

$$\frac{A^{MSA}}{NKT} = \frac{1}{12\pi\rho{\sigma_d}^3}\left[p^3{d_0}^2 b_0 - 2p^2 d_0 d_2 b_1 - J'\right]$$

$$J' = p^3{Q_{ii}}^2 + p(p+1){Q_{id}}^2 + {Q_{dd}}^2 + 2{q'}^2$$

where

$$Q_{ii} = -a_1 + 2 + \frac{\beta_6}{D_F}$$

$$Q_{id} = \frac{b_1}{\Delta}\left[\beta_3 + + a_1(3\Lambda - 2D_F)\right]$$

$$Q_{dd} = \frac{1}{\Delta}\left[2{\beta_3}^2 - p b_1 a_2(3\Lambda - 2D_F)\right] - 2$$

$$q' = b_2\beta_{24} / {\beta_{12}}^2$$

The excess chemical potential for ion and dipole are expressed as

$$\frac{\mu_i^{MSA}}{KT} = (q^*)^2\left(b_0 - \frac{d_2 b_1}{d_0 p}\right)$$

$$\frac{\mu_d^{MSA}}{KT} = -\frac{(\mu^*)^2}{3}\left(2b_2 + \frac{d_0 b_1 p^2}{d_2}\right)$$

The excess internal energy of the system is

$$\frac{U^{MSA}}{NKT} = \frac{1}{4\pi\rho\sigma_d^{\,3}}\left[p^3 d_0^{\,2} b_0 - 2p^2 d_0 d_2 b_1 - 2d_2^{\,2} b_2\right]$$

In MSA, the excess Gibbs free energy equals the excess internal energy, thus, the compressibility factor can be given as

$$Z^{MSA} = \frac{P^{MSA}}{\rho KT} = \frac{U^{MSA} - A^{MSA}}{NKT}$$

CHAPTER V

THERMODYNAMIC PROPERTIES OF IMIDAZOLIUM-BASED IONIC LIQUIDS FROM THE SAFT-VR EQUATION OF STATE

5.1 Introduction

Ionic liquids (IL_S) are liquids comprised entirely of ions with melting points around or below room temperature [147]. During the past decade ILs have received great attention as environmentally benign solvent replacements due to their negligible vapor pressure, low melting point and broad liquid range [147-149]. ILs typically consist of a large, organic cation with a weakly coordinating inorganic anion, which frustrates packing and lowers the melting point. The most common ILs are those composed of imidazolium or pyridinium cations with alkyl substitute groups and bulky inorganic anions such as $[PF_6]^-$, $[BF_4]^-$, $[NO_3]^-$ [150]. Since both the cation and anion can be varied, the term "designer solvent"[151] is often used to describe these chemicals since their properties, such as the melting point, viscosity, density, hydrophobicity and miscibility in water, can be adjusted through changes to the type and structure of the ions. Figure 37 shows some examples of typical cations and anions of ILs. ILs are widely used in electrochemistry [150], biochemistry [152] and as solvents in synthetic catalysis [153-155] and separations [156, 157]. However, one of the barriers preventing more widespread adoption of ILs by industry is that there is little data on their thermodynamic and thermophysical properties, despite the recent explosion of ILs studies reported in the literature. Experimental

measurements of fundamental properties which enable the characterization of ionic liquids are still quite scarce and knowledge of binary and ternary mixture data, invaluable in the design of industrial processes, is even more limited [158]. The main reason for this is the sheer number of ILs that can be synthesized through different cation and anion combinations.

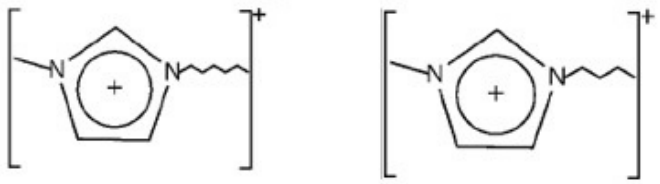

BF_4^- PF_6^-

Figure 37: Some examples of typical ionic liquid cations and anions.

An alternative approach to obtain information on the physical properties of ionic liquids is to use theoretical models, or equations of state. In the literature, there are few approaches with which to correlate or predict the thermodynamics properties of ILs. One of the approaches is the Tait equation which is an excellent model for high-pressure density correlation [159, 160]. Gu et. al [159] have applied the Tait equation to correlate the densities of ILs such as [bmim][PF6], [omim][PF6] and [omim][BF4] at different temperatures and pressures up to 206.94 MPa. Jacquemin et al. [161] used a linear equation based on the Tait equation to express the correlation of densities with temperature for six ILs. While such approaches can accurately correlate experimental data they cannot be used to predict the densities and other properties of ILs as the

parameters in the correlations depend strongly on the temperatures and pressures to which they were fitted.

Equations of state have only recently been applied in the literature to correlate and predict the thermodynamic properties of ILs. In perhaps the first application, Camper and coworkers [162-164] applied regular solution theory to model gas solubilities, such as CO_2 and light hydrocarbons in ILs containing imidazolium rings with the assumption that short-range forces dominate in room-temperature ILs. It was found that regular solution theory could be used to model gas solubility at low pressure with empirically determined constants that depend only on the gas. Also they observed that for hydrocarbons, the solubility increases as the number of carbon atoms increases and the number of double bond increases. Kato et al. [165] have measured vapor liquid equilibrium and excess for imidazolium-based ILs and predicted their thermodynamic behavior using the NRTL and UNIQUAC models. They [166] also applied group contribution methods such as the original and modified UNIFAC approaches to predict the vapor liquid equilibria and activity coefficients at infinite dilution for various solutes in the ILs studied. In their work, a modified COSMO approach, COSMO-RS(O1) was used to predict activity coefficients and the temperature dependence for systems containing ILs. They found that the modified UNIFAC method provided a reliable description of the vapor liquid equilibria, activity coefficients and excess enthalpies and qualitative agreement was obtained with experimental data using the COSMO-RS solvation model. Shariati et al [167] extended the Peng-Robinson equation of state to model the vapor liquid equilibria of binary systems of [emim][PF6] and fluoroform. Shiflett et. al [168] applied the

Redlich-Kwong equation of state to model CO_2 solublility in [bmim][BF4] and [bmim][PF6] at pressures under 2 MPa, but found that the approach cannot accurately predict the phase behavior of the systems studied at high pressure.

Approaches based on perturbation theory have also been applied to correlate and predict the thermodynamics properties of ILs. Qin et al [169] reported the correlation of Henry's constants for 20 solutes such as hydrocarbons in ionic liquids based on a perturbed-hard-sphere theory. In their approach, the solution is considered to be a dielectric continuum, which is perhaps reflected in the poor accuracy of the correlation obtained. Recently Kroon *et al.* [170] extended the truncated perturbed chain polar statistical associating fluid theory to predict the phase behavior of ionic liquid and CO_2 systems. In their approach, they assumed that the cation and the anion of the ILs form an ion pair due to Coulombic interactions; therefore, IL molecules were considered to be highly asymmetric neutral ion pairs with a large dipole moment. The equation was applied to model the phase behavior of several imidazolium-based IL + CO_2 systems using binary interaction parameters fitted to experimental data. However, one drawback of this approach is that they do not explicitly consider Coulomb interactions; by approximating the ionic nature of the fluid with multipolar interactions such as dipole-dipole, dipole-quadrupole, and quadrupole-quadrupole the complexity of the equation and the number of parameters in the equation is increased substantially.

In this work, we extend the SAFT-VR approach to study the densities of imidazolium-based ILs up to high pressure by using the heteronuclear SAFT-VR model. In our approach the charge-charge Coulombic interactions are taken into account through

the mean spherical approximation. The remainder of the chapter is organized as follows: in section 5.2 we present the SAFT-VR approach for ILs. In section 5.3, details of the parameterization of the equation are presented. Results for isotherms of several imidazolium-based ILs are presented in section 5.4. Finally, concluding remarks are made and future work discussed in section 5.5.

5.2 Model and Theory

In this work we extend the SAFT-VR approach to study ionic liquids. Within the framework of SAFT, the ionic liquids are represented by a flexible heteronuclear chain, which consists of two homonuclear chains with charged hard spheres/hard spheres, which tangibly bond together. As Figure 38 shows, the cation is represented as a homonuclear chain composed of $m_1 - 1$ hard spherical segments, with one segment carrying a single positive hard sphere charge of diameter σ_1. The anion is described by a homonuclear chain of $m_2 - 1$ hard spheres of diameter σ_2, again with one segment carrying a negative charge; these two chains bond together tangentially to form heteronuclear chain due to the high concentration of ion in the ILs system and relative strong attractive interaction between cation and anion. The number density and the carried charge are ρ_+ and z_+e for the positive segment, ρ_- and z_-e for the negative segment, and ρ_n and 0 for the uncharged segment. In terms of the charge neutrality condition, the relation $\rho_+ z_+ + \rho_- z_- = 0$ is always true. The total number of segment is given by $m = m_1 + m_2$ and the number density is given by

$$\rho = \frac{(\rho_+ + \rho_- + \rho_n)}{m} \tag{5.1}$$

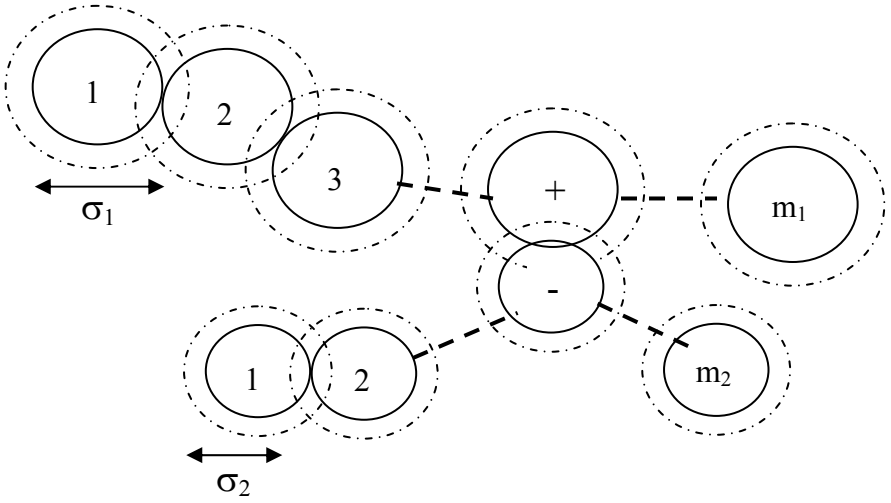

Figure 38: Schematic of the model for ionic liquids.

In our approach, the reference fluid is a mixture of square-well spheres and square-well charged spheres. Hence, the pair potential for the reference fluid is defined by

$$u(\mathbf{r}) = u^{SW}(r;\sigma) + u^{COULOMB}(r) \tag{5.2}$$

Here, $u^{SW}(r;\sigma)$ and $u^{COULOMB}(r)$ represent the square-well potential and Coulombic potential respectively. $u^{SW}(r;\sigma)$ is given by

$$u_{ij}^{SW}(r;\sigma) = \begin{cases} +\infty & \text{if} \quad r < \sigma_{ij} \\ -\varepsilon_{ij} & \text{if} \quad \sigma_{ij} \le r < \lambda_{ij}\sigma_{ij} \\ 0 & \text{if} \quad r \ge \lambda_{ij}\sigma_{ij} \end{cases} \tag{5.3}$$

where σ_{ij} is the diameter of the interaction, λ_{ij} the range and ε_{ij} the well depth of the SW potential. The inter- and intra-molecular cross interactions between segments are obtained from the standard Lorentz-Berthelot combining rules, *viz*

$$\sigma_{ij} = \frac{\sigma_{ii} + \sigma_{jj}}{2} \tag{5.4}$$

$$\varepsilon_{ij} = \left(1 - k_{ij}\right)\left(\varepsilon_{ii}\varepsilon_{jj}\right)^{1/2} \tag{5.5}$$

$$\lambda_{ij} = \left(\frac{\lambda_{ii}\sigma_{ii} + \lambda_{jj}\sigma_{jj}}{\sigma_{ii} + \sigma_{jj}}\right) \tag{5.6}$$

The Coulombic potential between two charges is represented by

$$u_{ij}^{Coulomb}(r) = \begin{cases} +\infty & \text{if} \quad r \le \sigma_{ij} \\ \dfrac{z_i z_j e^2}{4\pi\varepsilon r} & \text{if} \quad r > \sigma_{ij} \end{cases} \tag{5.7}$$

where r is the center-to-center distance, $e = 1.602 \times 10^{-19} C$ the elementary charge, and ε is the permittivity of the continuous dielectric medium, which is an adjustable parameter in the model. Within the framework of the SAFT-VR approach, the excess Helmholtz free energy can be divided into two contributions from, respectively, the charged/uncharged square-well spheres, and chain formation.

$$\frac{A^{excess}}{NKT} = \frac{A^{CSW}}{NKT} + \frac{A^{chain}}{NKT} \tag{5.8}$$

Since in this work, we do not consider associating fluids, there is not association term in the equation. We will summarize each contribution in turn.

5.2.1 Charged/uncharged square-well monomer contribution

Within the GMSA the excess Helmholtz free energy per monomer a^{CSW}, is given by

$$a^{CSW} = a^{SW} + a^{Columbic} \tag{5.9}$$

where a^{SW} describes the contribution to the free energy due to dispersion interactions and $a^{Columbic}$ the contribution due to Coulombic interactions. Within the high temperature perturbation theory of Barker and Henderson, in the inverse of the temperature $\beta = 1/k_B T$, the square-well term a^{SW} is given by,

$$a^{SW} = a^{HS} + \beta a_1 + \beta^2 a_2 \tag{5.10}$$

The hard sphere reference term a^{HS} is determined from the expression of Boublik [137] and Mansoori and co-workers [138] for multicomponent hard sphere systems, viz

$$a^{HS} = \frac{6}{\pi\rho_s}\left[\left(\frac{\zeta_2^3}{\zeta_3^2} - \zeta_0\right)\ln(1-\zeta_3) + \frac{3\zeta_1\zeta_2}{1-\zeta_3} + \frac{\zeta_2^3}{\zeta_3(1-\zeta_3)^2}\right] \tag{5.11}$$

where ρ_s is the number density of segments, which is defined as the total number of segments divided by the total volume N_s/V and ζ_l is the reduced density given by a sum over all segments i,

$$\begin{aligned}\zeta_l &= \frac{\pi}{6}\rho_s\left[\sum_{i=1}^{n} x_{s,i}(\sigma_i)^l\right] \\ &= \frac{\pi}{6}\rho_s[x_{s,1}(\sigma_1)^l + x_{s,2}(\sigma_2)^l]\end{aligned} \tag{5.12}$$

where σ_i is diameter of segments of type i and $x_{s,i}$ is the mole fraction of segments in the mixture given by

$$x_{s,i} = \frac{m_i}{m_1 + m_2} \tag{5.13}$$

The first perturbation term a_1 describing the mean-attractive energy is obtained from the sum of all pair interactions,

$$\begin{aligned} a_1 &= \sum_{i=1}^{n}\sum_{j=1}^{n} x_{s,i}x_{s,j}\left(a_1\right)_{ij} \\ &= x_{s,1}^2\left(a_1\right)_{11} + 2x_{s,1}x_{s,2}\left(a_1\right)_{12} + x_{s,2}^2\left(a_1\right)_{22} \end{aligned} \tag{5.14}$$

where $\left(a_1\right)_{ij}$ is obtained from the mean-value theorem as proposed by Gil-Villegas *et al.* [9],

$$\begin{aligned} \left(a_1\right)_{ij} &= -2\pi\rho_s\varepsilon_{ij}\int_{\sigma_{ij}}^{\infty} r_{ij}^2 g_{ij}^{HS}(r_{ij})dr_{ij} \\ &= -\rho_s\alpha_{ij}^{VDW} g_{ij}^{HS}(\sigma_{ij};\zeta_3^{eff}) \end{aligned} \tag{5.15}$$

where

$$\alpha_{ij}^{VDW} = \frac{2\pi}{3}\sigma_{ij}^3\varepsilon_{ij}\left(\lambda_{ij}^3 - 1\right) \tag{5.16}$$

Within the van der Waals one fluid theory the radial distribution function $g_{ij}^{HS}(\sigma_{ij};\zeta_3^{eff})$ is approximated by that for a pure fluid, *viz*

$$\left(a_1\right)_{ij} = -\rho_s\alpha_{ij}^{VDW} g_0^{HS}\left[\sigma_x;\zeta_x^{eff}\left(\lambda_{ij}\right)\right] \tag{5.17}$$

where $g_{ij}^{HS}(\sigma_{ij};\zeta_3^{eff})$ is obtained from the Carnahan and Starling equation of state,[171]

$$g_0^{HS}\left[\sigma_x;\zeta_x^{eff}\left(\lambda_{ij}\right)\right] = \frac{1-\zeta_x^{eff}/2}{\left(1-\zeta_x^{eff}\right)^3} \tag{5.18}$$

The effective packing fraction $\zeta_x^{eff}\left(\lambda_{ij}\right)$is obtained within the van der Waals one fluid theory from the corresponding packing fraction of the mixture ζ_x given by,

$$\zeta_x^{eff}\left(\zeta_x,\lambda_{ij}\right) = c_1\left(\lambda_{ij}\right)\zeta_x + c_2\left(\lambda_{ij}\right)\zeta_x^2 + c_3\left(\lambda_{ij}\right)\zeta_x^3 \tag{5.19}$$

where

$$\begin{pmatrix} c_1 \\ c_2 \\ c_3 \end{pmatrix} = \begin{pmatrix} 2.25855 & -1.50349 & 0.249434 \\ -0.669270 & 1.40049 & -0.827739 \\ 10.1576 & -15.0427 & 5.30827 \end{pmatrix} \begin{pmatrix} 1 \\ \lambda_{ij} \\ \lambda_{ij}^{\,2} \end{pmatrix} \tag{5.20}$$

and

$$\zeta_x = \frac{\pi}{6}\rho_s \sigma_x^3 \tag{5.21}$$

with

$$\begin{aligned} \sigma_x^3 &= \sum_{i=1}^{n}\sum_{j=1}^{n} x_{s,i} x_{s,i} \sigma_{ij}^3 \\ &= x_{s,1}^2 \sigma_{11}^3 + 2x_{s,1} x_{s,2} \sigma_{12}^3 + x_{s,2}^2 \sigma_{22}^3 \end{aligned} \tag{5.22}$$

This corresponds to mixing rule MX1b in the original SAFT-VR approach for mixtures.[10]

The second order perturbation term for the monomer excess free energy a_2 is expressed as:

$$\begin{aligned} a_2 &= \sum_{i=1}^{n}\sum_{j=1}^{n} x_{s,i} x_{s,j} \left(a_2\right)_{ij} \\ &= x_{s,1}^2 \left(a_2\right)_{11} + 2x_{s,1} x_{s,2} \left(a_2\right)_{12} + x_{s,2}^2 \left(a_2\right)_{22} \end{aligned} \tag{5.23}$$

where $\left(a_2\right)_{ij}$ is obtained through the local compressibility approximation:

$$\left(a_2\right)_{ij} = \frac{1}{2} K^{HS} \varepsilon_{ij} \rho_s \frac{\partial \left(a_1\right)_{ij}}{\partial \rho_s} \tag{5.24}$$

and K^{HS} is the Percus-Yevick expression for the hard-sphere isothermal compressibility,

$$K^{HS} = \frac{\zeta_0 (1-\zeta_3)^4}{\zeta_0 (1-\zeta_3)^2 + 6\zeta_1 \zeta_2 (1-\zeta_3) + 9\zeta_2^3} \tag{5.25}$$

In our work, Blum's primitive model is applied to represent the charged/uncharged hard sphere. The free energy due to the Coulomb interaction $a^{Columbic}$ is given by:

$$a^{Columbic} = -\frac{z^2 e^2 \beta \Gamma}{\varepsilon(1+\sigma_{12}\Gamma)} + \frac{\Gamma^3}{3\rho\pi} \tag{5.26}$$

with Γ calculated by

$$\Gamma = \frac{(1+2\sigma_{12}\kappa)^{1/2} - 1}{2\sigma_{12}} \tag{5.27}$$

5.2.2 Chain Contribution

The contribution to the free energy due to chain formation from *m* square-well charged/uncharged monomers is given by,

$$a^{Chain} = -\sum_{ij}(m_i - 1)\ln g^{CSW}(\sigma_{ij}) \tag{5.28}$$

where $g^{CSW}(\sigma_{ij})$ is represented by the LEXP approximation:

$$g_{ij}^{CSW}(\sigma_{ij}) = g_{ij}^{SW}(\sigma_{ij})\left(1 + \left(\frac{z_i z_j e^2 \beta}{\varepsilon\sigma_{ij}(1+\sigma_{ij}\Gamma)^2}\right)\right) \tag{5.29}$$

The radial distribution function for the square well monomers $g_{ij}^{SW}(\sigma_{ij})$ is approximated by a first-order high-temperature perturbation expansion:

$$g_{ij}^{SW}(\sigma_{ij};\zeta_3) = g_{ij}^{HS}(\sigma_{ij};\zeta_3) + \beta\varepsilon_{ij} g_1^{SW}(\sigma_{ij}) \tag{5.30}$$

where the contact value of the radial distribution function $g_{ij}^{HS}(\sigma_{ij};\zeta_3)$ at the actual packing fraction ζ_3 is obtained from the expression of Boublik [137],

$$g_{ij}^{HS}(\sigma_{ij};\zeta_3) = \frac{1}{1-\zeta_3} + 3\frac{D_{ij}\zeta_3}{(1-\zeta_3)^2} + 2\frac{(D_{ij}\zeta_3)^2}{(1-\zeta_3)^3} \tag{5.31}$$

and

$$\begin{aligned} D_{ij} &= \frac{\sigma_{ii}\sigma_{jj}\sum_{i=1}^{n} x_{s,i}\sigma_{ii}^2}{(\sigma_{ii}+\sigma_{jj})\sum_{i=1}^{n} x_{s,i}\sigma_{ii}^3} \\ &= \frac{\sigma_{ii}\sigma_{jj}(x_{s,1}\sigma_{11}^2 + x_{s,2}\sigma_{22}^2)}{(\sigma_{ii}+\sigma_{jj})(x_{s,1}\sigma_{11}^3 + x_{s,2}\sigma_{22}^3)} \end{aligned} \tag{5.32}$$

$g_1^{SW}(\sigma_{ij},\zeta_3)$ is determined using the Clausius virial theorem and the first derivative of the free energy with respect to the density [9] giving:

$$g_1^{SW}(\sigma_{ij}) = \frac{1}{2\pi\varepsilon_{ij}\sigma_{ij}^3}\left[3\left(\frac{\partial(a_1)_{ij}}{\partial\rho_s}\right) - \frac{\lambda_{ij}}{\rho_s}\frac{\partial(a_1)_{ij}}{\partial\lambda_{ij}}\right] \tag{5.33}$$

If we consider [bmim][BF_4] as an example, our model consists of $m-2$ uncharged segments, one positively charged segment and one negatively charged segment. The free energy due to the chain formation is therefore given by,

$$a^{chain} = -(m_1-1)\ln g^{SW}(\sigma_{11}) - (m_2-1)\ln g^{SW}(\sigma_{22}) - \ln g^{CSW}(\sigma_{12}) \tag{5.34}$$

5.3 Parameterization of the SAFT-VR EOS

In this work, the SAFT-VR approach is extended to correlate and predict isotherms of ILs through the combination of the SAFT-VR approach and the mean spherical approximation. The ILs studied are 1-butyl-3-methylimidazolium tetrafluoroborate ([bmim][BF4]), 1-butyl-3-methylimidazolium hexafluoroborate ([bmim][PF6]), 1-butyl-

3-methylimidazolium bis(trifluoromethylsulfonyl)amide ([bmim][NTf2]), 1-hexyl-3-methylimidazolium bis(trifluoromethylsulfonyl)amide ([hmim][NTf2]), 1-octyl-3-methylimidazolium tetrafluoroborate ([omim][BF4]) and 1-octyl-3-methylimidazolium hexafluoroborate ([omim][PF6]). In Figure 37, a schematic representation of these ILs is shown. In our approach, these ILs are modeled as heteronuclear charged chains, which consist of two homonuclear square-well chains to represent the cation and anions respectively. In the original SAFT-VR EOS four parameters are needed to model non-associating homonuclear chain molecules, i.e., the diameter of the segment σ, the number of segments m, the depth of the square-well potential ε and the range of the square-well potential λ. To describe ILs eight SAFT-VR parameters have to be determined, which are the size, shape and square-well potential parameters for the cations and the anions. Additionally in the primitive model of the mean spherical approximation the dielectric constant must be determined and is used as an adjustable parameter in this work. For the cations [bmim], [hmim] and [omim], the SAFT-VR parameters are obtained by fitting to experimental vapor pressures and saturated liquid density data for butylbenzene, hexylbenzene and octylbenzene respectively The vapor pressure curve and coexisting densities of butylbenzene, hexylbenzene and octylbenzene are shown in the Figure 39-41 and the parameters are listed in Table 15. Other SAFT-VR parameters involved in each ILs, that is the size, shape and depth and range of square well potential, and the dielectric constant, are determined by fitting to the isotherm of each ILs at the highest temperature available in the literature. Then the isotherms of the ILs at other temperatures are predicted using the parameters obtained for each ILs at the highest temperature.

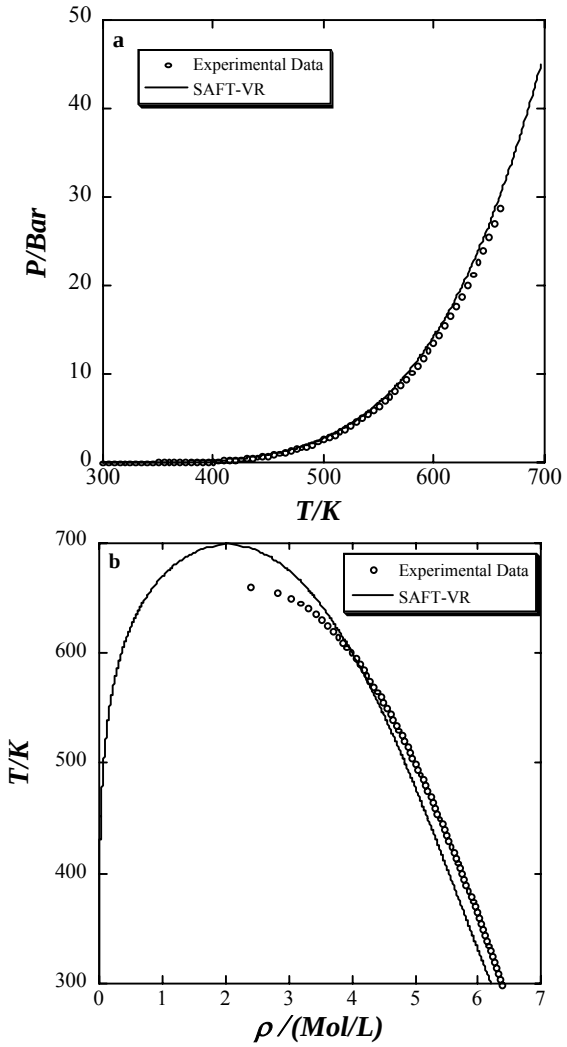

Figure 39: (a) Vapor pressure and (b) Coexisting densities for butylbenzene. Solid lines represent the results from the SAFT-VR approach and circles the experimental data taken from [172].

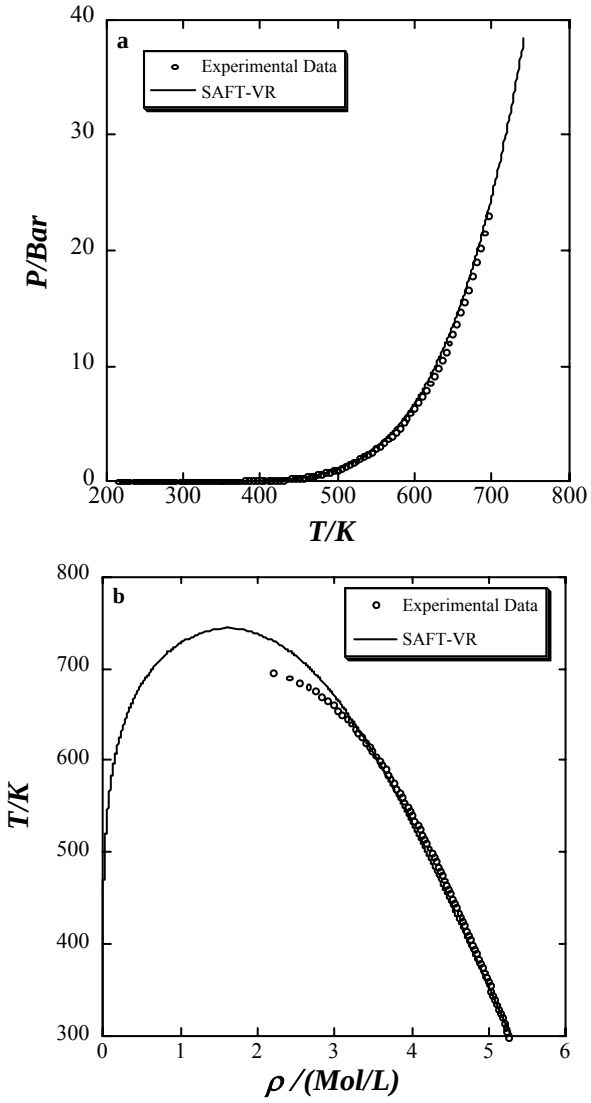

Figure 40: (a) Vapor pressure and (b) Coexisting densities for hexylbenzene. Solid lines represent the results from the SAFT-VR approach and circles experimental data taken from [172].

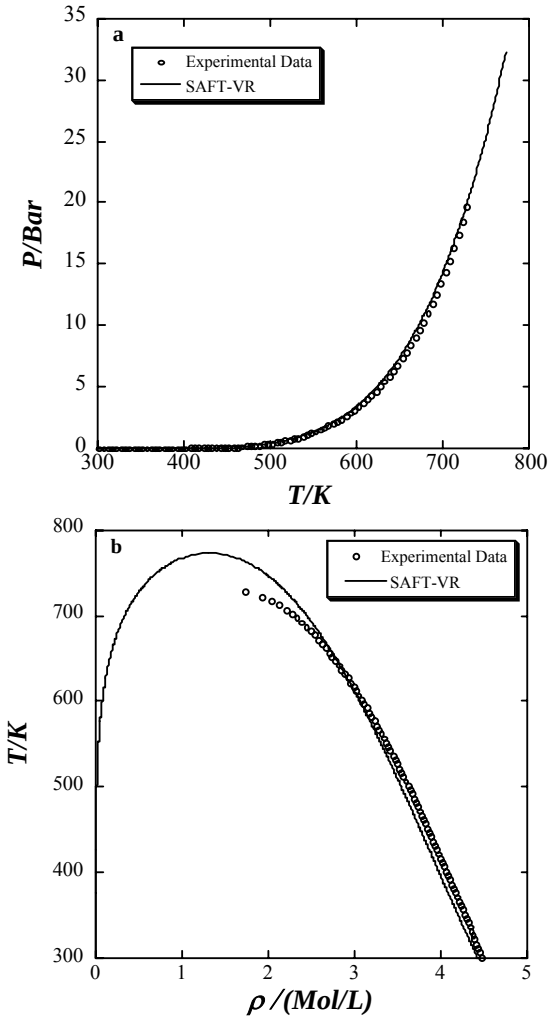

Figure 41: (a) Vapor pressure and (b) Coexisting densities for octylbenzene. Solid lines represent the results from the SAFT-VR approach and circles the experimental data taken from [172].

Table 15: SAFT-VR parameters for ionic liquids studied in this work

		Cation				Anion				
	M_w	σ	m	ε / k	λ	σ	m	ε / k	λ	ε_0
	(g/mol)	$\overset{0}{A}$	-	K	-	$\overset{0}{A}$	-	K	-	-
[bmim][BF4]	226.02	3.8452	3.59	250.47	1.6339	4.3787	1.0	564.86	1.6959	1.0
[bmim][PF6]	284.18	3.8452	3.59	250.47	1.6339	5.0717	1.0	787.69	1.157	1.0
[bmim][NTf2]	419.34	3.8452	3.59	250.47	1.6339	5.002	2.0	496.4	1.3784	1.0
[hmim][NTf2]	447.39	3.8	4.34	228.38	1.6883	5.186	2.0	471.88	1.1963	0.7
[omim][BF4]	282.13	3.8598	5.0	229.51	1.6803	3.6998	2.0	736.94	1.172	1.06
[omim][PF6]	340.29	3.8598	5.0	229.51	1.6803	4.0706	2.0	812.99	1.1697	1.06

5.4 Results

Isotherms for several alkylmethylimidazolium ILs have been studied using the SAFT-VR approach in combination with the primitive model of the mean spherical approximation. In Figure 42, isotherms for [bmim][BF_4] at temperatures of 332.73 K, 322.85 K, 313.01 K, 303.23K and 298.34 K are presented. The experimental isotherm at 332.73K was used to fit the SAFT-VR parameters for the $[BF_4]^-$ anion. The isotherms at other temperatures are then predicted using these parameters. From the figure, it is seen that good agreement between experimental data and the theoretical calculation from the model is obtained. The dielectric constant for the ionic liquid is 1.0. The value of the dielectric constant obtained from the theory is less than the experimental value, which is usually around 5-12. One possible reason for the lower value used in this work, is the simple way in which we take into account the long-range ion-ion interactions in the ionic liquids. Since ILs are highly asymmetric neutral ion pairs, the molecules are polarizable and as such will have dipole moments and/or quadrupolar moments as a result of the charge distribution over the ion pairs. It may be possible to obtain the dielectric constant closer to the experimental value if the ionic liquids are considered as charged polar chain molecules, with the polar interactions included through the SAFT-VR+D approach [173]. Figure 43 and 44 presents isotherms for [bmim][PF_6] and [bmim][NTf_2] at different temperatures and pressures up to 100 MPa. The SAFT-VR parameters used for the cation are the same as those used to decribe [bmim][BF4] since the parameters for the cation are transferable. Again, we see that the theoretical results are in good agreement with the experimental data.

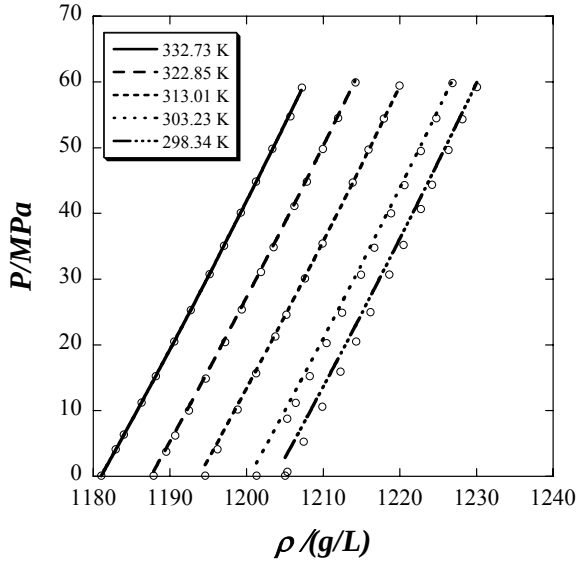

Figure 42: Isotherm of the density of [bmim][BF4] at temperature 332.73K, 322.85K, 313.01K, 303.23K and 298.34K. The circles represent the experimental data [160] and the curves from the SAFT-VR equation of state.

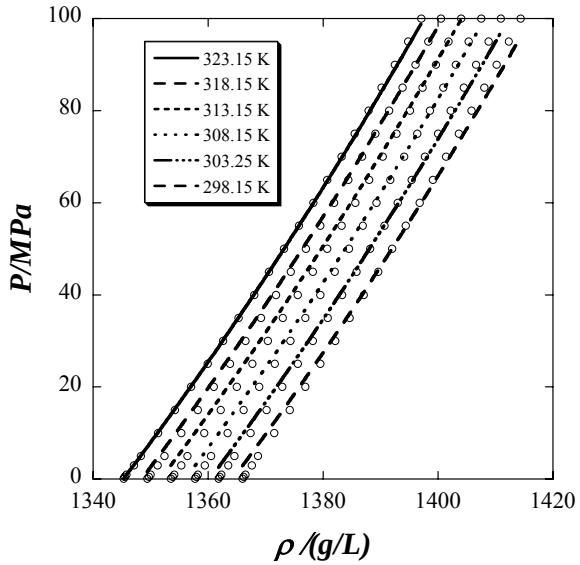

Figure 43: Isotherm of the density of [bmim][PF6] at temperature 323.15K, 318.15K, 313.15K, 308.15K, 303.15K and 298.15K. The circles represent the experimental data [160] and the curves from the SAFT-VR equation of state.

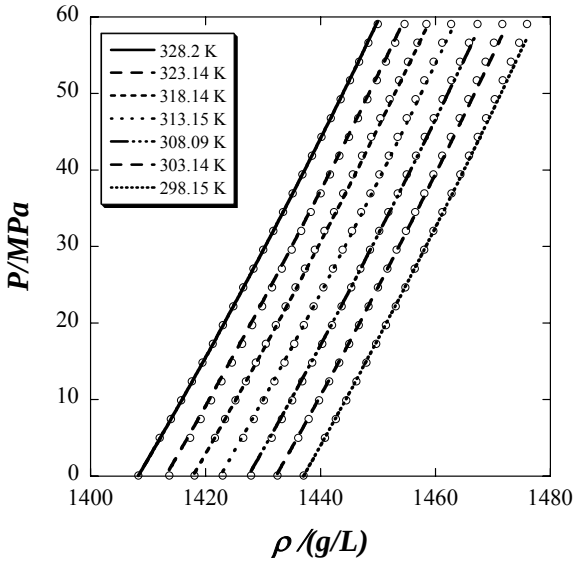

Figure 44: Isotherm of the density of [bmim][NTf2] at temperature 328.2K, 323.14K, 318.14K, 313.15K, 308.09K, 303.14K and 298.15K. The circles represent the experimental data [174] and the curves from the SAFT-VR equation of state.

In Figure 45, isotherms for [hmim][NTf_2] are presented at temperature 333.15K, 323.15K, 313.15K, 303.15K and 298.15K. Similarly, the SAFT-VR parameters for the anion were obtained by fitting to the experimental data of isotherm for [hmim][NTf_2] at 333.15 K. Isotherms at other temperatures are predicted using these parameters. We find that, the dielectric constant for this ionic liquid is less than 1.0 (0.7), which is obtained by fitting to experimental data, and good agreement is observed between the experimental data and theoretical results.

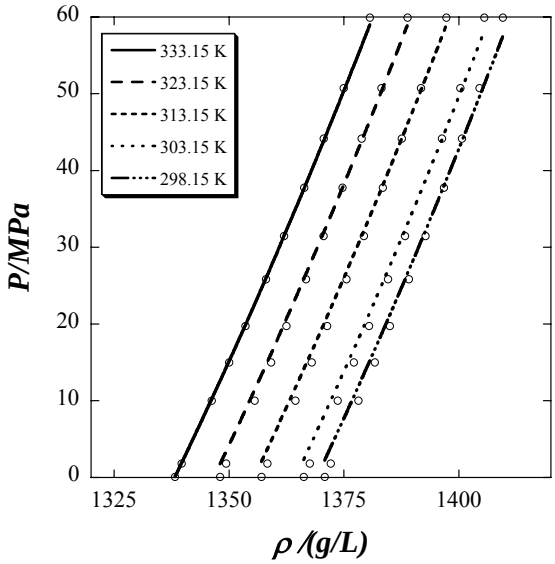

Figure 45: Isotherm of the density of [hmim][NTf2] at temperature 333.15K, 323.15K, 313.15K, 303.15K and 298.15K. The circles represent the experimental data [174] and the curves from the SAFT-VR equation of state.

We have also studied isotherms for ionic liquids [omim][BF_4] and [omim][PF_6] up to very high pressures (more than 200MPa). For these ionic liquids, the SAFT-VR parameters for the anions were obtained by fitting to the experimental data at 298.15K and 323.15K. The correlations for both [omim][BF_4] and [omim][PF_6] are presented in Figure 46 and 47. The same dielectric constant is used for both ILs. From the figures, it is seen that, the correlations from the SAFT-VR approach are in good agreement with the experimental data, especially for [omim][PF_6].

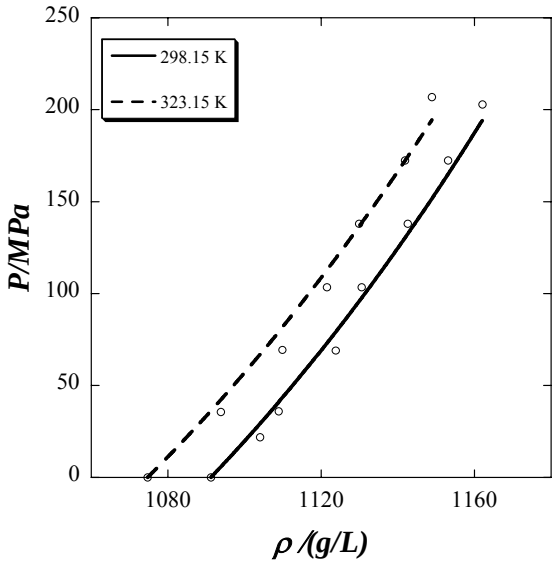

Figure 46: Isotherm of the density of [omim][BF4] at temperature 323.15K and 298.15K. The circles represent the experimental data [159] and the curves from the SAFT-VR equation of state.

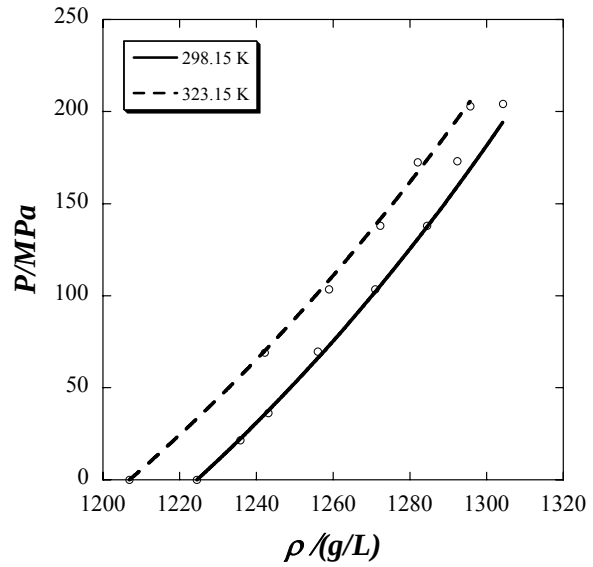

Figure 47: Isotherm of the density of [omim][PF6] at temperature 323.15K and 298.15K. The circles represent the experimental data [159] and the curves from the SAFT-VR equation of state.

5.5 Conclusion

In this work, the SAFT-VR approach is extended to model of the PVT behavior of several alkylmethylimidazolium ILs using the primitive model of mean spherical approximation to describe the Coulombic interactions. In the approach, ILs are modeled as heteronuclear charged chain molecules composed of two homonuclear chain with unit positive and negative charge respectively. Compared with experimental data, the approach provides a good way to correlate and predict the densities of the ILs studied in this work.

CHAPTER VI

CONCLUSION AND RECOMMENDATION

Understanding the thermodynamics and phase behavior of polar and electrolyte fluids is central to a wide range of processes in chemical, environmental and biological engineering. As a result, several groups have focused on the development of theoretical models for such systems. Within the family of SAFT equations of state, attention has primarily focused on the development of additional terms to describe the polar or/and electrostatic interactions that exist in polar and electrolyte fluids. When we started this project, our goal was to rigorously incorporate the effect of anisotropic interactions such as polar and electrostatic interactions on the thermodynamics properties of fluids through modification of the reference fluid within the SAFT-VR framework. Within statistical mechanics, integral equation theory with the mean spherical approximation provides a way to describe the structure of anisotropic interactions and gives analytical solutions for the thermodynamics and structural properties of simple potentials. Thereafore, in this project, we developed equations of state for polar and electrolyte fluids through a combination of the SAFT-VR approach with the mean spherical approximation, in which the structure of these fluids is explicitly accounted for.

For dipolar fluids, in Chapter II, a SAFT-VR like approach, SAFT-VR+D, has been developed to study dipolar chain fluids that uses the dipolar square well fluid as the reference state. In this way, the SAFT-VR+D approach explicitly takes into account the magnitude and orientation of the dipole moment, both of which are found to affect the thermodynamics and phase behavior of dipolar square well monomer and chain fluids. In

order to gain a comprehensive understanding of the thermodynamic properties of the systems studied, and validate the SAFT-VR+D approach, both *NPT* MC and GEMC simulations were performed to obtain simulation data with which to compare the theoretical predictions. We found that the SAFT-VR+D equation with the GMSA approximation provides good predictions for the phase behavior of the dipolar monomer fluids studied, and chain fluids with a perpendicular arrangement of the dipole moments. A more accurate approximation for the radial distribution function of dipolar square well fluids (LEXP approximation) was implemented to improve the performance of the SAFT-VR+D EOS for dipolar chain fluids in which the dipole moments are parallel to the vector joining the centers of the monomers. It is found that the SAFT-VR+D with the LEXP approximation is suitable for fluids with both vertical and horizontal arrangements of the dipole moments. Furthermore, using the solution of Adelman and Deutch for polar mixtures, the SAFT-VR+D with LEXP approximation gives a good description of the thermodynamic properties of dipolar chain fluids consisting of non-dipolar segments and dipolar segments.

In chapter III, the SAFT-VR+D approach has been used to study associating fluids. To gain a comprehensive understanding of the thermodynamic properties of the systems we studied, both *NPT* MC and GEMC simulations were performed to obtain simulation data to compare to the theoretical predictions. A comparison between the theory and the *NPT* MC simulation data shows that the theory accurately describes the *PVT* and phase behavior of the fluids studied over a range of association energies and association volumes; at relative low dipole moment, the agreement is very good, however for high dipole moments (~ > a reduced dipole moment of 2), we see some discrepancy

between the theory and simulation results. Furthermore we find that the SAFT-VR+D approach provides a more accurate description of the phase behavior of water than the SAFT-VR approach.

For electrolyte fluids, in Chapter IV, the SAFT-VR+DE approach has been developed through a combination of the SAFT-VR equation and the MSA solution of the non-primitive model, in which the solvent molecules are explicitly modeled as a dipolar associating fluid. The theory has been tested through the description of the *PVT* phase behavior of several model electrolyte solutions. In order to gain a good understanding of the thermodynamic properties of the systems studied, and validate the SAFT-VR+DE approach, *NPT* MC simulations were conducted to obtain simulation data to compare to the theoretical predictions. We found that the SAFT-VR equation with the MSA solution of the non-primitive model provides good predictions for the phase behavior of the electrolyte solutions we studied. We have also compared the non-primitive model with five other models for the long-range electrostatic interactions; namely the Debye-Huckel theory, the primitive model (RPM and PM) in which the dielectric constant is obtained from the non-primitive model, the restricted non-primitive model and semi-non-primitive model. It is found that the restricted non-primitive model and the Debye-Huckel theory show the largest deviations compared with the Monte Carlo simulation data. The predictive capability of the primitive model strongly depends on the value of dielectric constant and the prediction obtained from the semi non-primitive model is close to that of non-primitive model. For the sake of the relative simplicity of the semi non-primitive model, it may be a practical replacement of the non-primitive in the development of engineering equation of state for electrolyte solution.

In chapter V, the SAFT-VR approach is extended to model isotherms of the density for several alkylmethylimidazolium ionic liquids using the primitive model within the mean spherical approximation. In our approach, ionic liquids are modeled as heteronuclear charged chain molecules composed of two homonuclear chains with positive and negative charge respectively, and the pair distribution function of ions is included into the chain term. Compared with experimental data, the approach provides a good way to correlate and predict the density of the ionic liquids studied. We also find that the SAFT-VR parameters for the cations studied can be used transferably

For polar fluids, our results have shown that the structure of the dipolar interaction does have an effect on the thermodynamics of dipolar fluids. In future work the SAFT-VR EOS may be extended to accurately model quadrupolar fluids in a similar fashion through the combination with the mean spherical approximation. It has been shown that the SAFT-VR+D approach can describe the position and orientation of dipole moments within the chain molecules. Therefore, the approach can potentially be extended to model polymers with dipolar functional groups.

For electrolyte fluids, in the SAFT-VR+DE approach we presented in Chapter IV, we have explicitly considered the solvent effect with the non-primitive model and self-association with Wertheim's theory. However, as the ion concentration increases, the ions can associate with each other and so it will be important in future work to account for ion-ion association.

VII. REFERENCES

1. Chapman, W.G., K.E. Gubbins, G. Jackson, and M. Radosz, "Saft - Equation-of-State Solution Model For Associating Fluids," Fluid Phase Equilibria, 52, 31-38 (1989).
2. Chapman, W.G., K.E. Gubbins, G. Jackson, and M. Radosz, "New Reference Equation of State For Associating Liquids," Industrial & Engineering Chemistry Research, 29, 1709-1721 (1990).
3. Wertheim, M.S., "Fluids with Highly Directional Attractive Forces.1. Statistical Thermodynamics," Journal of Statistical Physics, 35, 19-34 (1984).
4. Wertheim, M.S., "Fluids with Highly Directional Attractive Forces.2. Thermodynamic Perturbation-Theory and Integral-Equations," Journal of Statistical Physics, 35, 35-47 (1984).
5. Wertheim, M.S., "Fluids with Highly Directional Attractive Forces.3. Multiple Attraction Sites," Journal of Statistical Physics, 42, 459-476 (1986).
6. Wertheim, M.S., "Fluids with Highly Directional Attractive Forces.4. Equilibrium Polymerization," Journal of Statistical Physics, 42, 477-492 (1986).
7. Chapman, W.G., G. Jackson, and K.E. Gubbins, "Phase-Equilibria Of Associating Fluids Chain Molecules With Multiple Bonding Sites," Molecular Physics, 65, 1057-1079 (1988).
8. Economou, I.G., "Statistical associating fluid theory: A successful model for the calculation of thermodynamic and phase equilibrium properties of complex fluid mixtures," Industrial & Engineering Chemistry Research, 41, 953-962 (2002).
9. Gil Villegas, A., A. Galindo, P.J. Whitehead, S.J. Mills, G. Jackson, and A.N. Burgess, "Statistical associating fluid theory for chain molecules with attractive potentials of variable range," Journal of Chemical Physics, 106, 4168-4186 (1997).
10. Galindo, A., L.A. Davies, A. Gil-Villegas, and G. Jackson, "The thermodynamics of mixtures and the corresponding mixing rules in the SAFT-VR approach for potentials of variable range," Molecular Physics, 93, 241-252 (1998).
11. McCabe, C. and G. Jackson, "SAFT-VR modelling of the phase equilibrium of long-chain n- alkanes," Physical Chemistry Chemical Physics, 1, 2057-2064 (1999).
12. McCabe, C., A. Galindo, M.N. Garcia-Lisbona, and G. Jackson, "Examining the adsorption (vapor-liquid equilibria) of short- chain hydrocarbons in low-density polyethylene with the SAFT-VR approach," Industrial & Engineering Chemistry Research, 40, 3835-3842 (2001).
13. McCabe, C. and S.B. Kiselev, "A crossover SAFT-VR equation of state for pure fluids: preliminary results for light hydrocarbons," Fluid Phase Equilibria, 219, 3-9 (2004).
14. McCabe, C. and S.B. Kiselev, "Application of crossover theory to the SAFT-VR equation of state: SAFT-VRX for pure fluids," Industrial & Engineering Chemistry Research, 43, 2839-2851 (2004).

15. McCabe, C., A. Galindo, A. Gil-Villegas, and G. Jackson, "Predicting the high-pressure phase equilibria of binary mixtures of n-alkanes using the SAFT-VR approach," International Journal of Thermophysics, 19, 1511-1522 (1998).
16. McCabe, C., A. Gil-Villegas, and G. Jackson, "Predicting the high-pressure phase equilibria of methane plus n-hexane using the SAFT-VR approach," Journal of Physical Chemistry B, 102, 4183-4188 (1998).
17. Galindo, A., L.J. Florusse, and C.J. Peters, "Prediction of phase equilibria for binary systems of hydrogen chloride with ethane, propane and n-dodecane," Fluid Phase Equilibria, 160, 123-131 (1999).
18. Filipe, E.J.M., E. de Azevedo, L.F.G. Martins, V.A.M. Soares, J.C.G. Calado, C. McCabe, and G. Jackson, "Thermodynamics of liquid mixtures of xenon with alkanes: (xenon plus ethane) and (xenon plus propane)," Journal of Physical Chemistry B, 104, 1315-1321 (2000).
19. Filipe, E.J.M., L.F.G. Martins, J.C.G. Calado, C. McCabe, and G. Jackson, "Thermodynamics of liquid mixtures of xenon with Alkanes: (xenon plus n-butane) and (xenon plus isobutane)," Journal of Physical Chemistry B, 104, 1322-1325 (2000).
20. Filipe, E.J.M., L.M.B. Dias, J.C.G. Calado, C. McCabe, and G. Jackson, "Is xenon an "ennobled" alkane?" Physical Chemistry Chemical Physics, 4, 1618-1621 (2002).
21. Dias, L.M.B., E.J.M. Filipe, C. McCabe, and J.C.G. Calado, "Thermodynamics of liquid (xenon plus methane) mixtures," Journal of Physical Chemistry B, 108, 7377-7381 (2004).
22. Sun, L.X., H.G. Zhao, S.B. Kiselev, and C. McCabe, "Application of SAFT-VRX to binary phase behaviour: alkanes," Fluid Phase Equilibria, 228, 275-282 (2005).
23. Sun, L.X., H.G. Zhao, S.B. Kiselev, and C. McCabe, "Predicting mixture phase equilibria and critical behavior using the SAFT-VRX approach," Journal Of Physical Chemistry B, 109, 9047-9058 (2005).
24. McCabe, C., A. Galindo, A. Gil-Villegas, and G. Jackson, "Predicting the high-pressure phase equilibria of binary mixtures of perfluoro-n-alkanes plus n-alkanes using the SAFT-VR approach," Journal of Physical Chemistry B, 102, 8060-8069 (1998).
25. Bonifacio, R.P., E.J.M. Filipe, C. McCabe, M.F.C. Gomes, and A.A.H. Padua, "Predicting the solubility of xenon in n-hexane and n-perfluorohexane: a simulation and theoretical study," Molecular Physics, 100, 2547-2553 (2002).
26. Morgado, P., C. McCabe, and E.J.M. Filipe, "Modelling the phase behaviour and excess properties of alkane plus perfluoroalkane binary mixtures with the SAFT-VR approach," Fluid Phase Equilibria, 228, 389-393 (2005).
27. Blas, F.J. and A. Galindo, "Study of the high pressure phase behaviour of CO2+n-alkane mixtures using the SAFT-VR approach with transferable parameters," Fluid Phase Equilibria, 194-197, 501-509 (2002).
28. Dias, L.M.B., R.P. Bonifacio, E.J.M. Filipe, J.C.G. Calado, C. McCabe, and G. Jackson, "Liquid-vapour equilibrium of {xBF3 + (1 - x)n-butane} at 195.49 K," Fluid Phase Equilibria, 205, 163-170 (2003).

29. McCabe, C., A. Galindo, and P.T. Cummings, "Anomalies in the solubility of alkanes in near-critical water," Journal of Physical Chemistry B, 107, 12307-12314 (2003).
30. Valtz, A., A. Chapoy, C. Coquelet, P. Paricaud, and D. Richon, "Vapour-liquid equilibria in the carbon dioxide-water system, measurement and modelling from 278.2 to 318.2K," Fluid Phase Equilibria, 226, 333-344 (2004).
31. Galindo, A., A. Gil-Villegas, P.J. Whitehead, G. Jackson, and A.N. Burgess, "Prediction of phase equilibria for refrigerant mixtures of difluoromethane (HFC-32), 1,1,1,2-tetrafluoroethane (HFC-134a), and pentafluoroethane (HFC-125a) using SAFT-VR," Journal of Physical Chemistry B, 102, 7632-7639 (1998).
32. Galindo, A. and F.J. Blas, "Theoretical examination of the global fluid phase behavior and critical phenomena in carbon dioxide plus n-alkane binary mixtures," Journal of Physical Chemistry B, 106, 4503-4515 (2002).
33. Colina, C.M., A. Galindo, F.J. Blas, and K.E. Gubbins, "Phase behavior of carbon dioxide mixtures with n-alkanes and n-perfluoroalkanes," Fluid Phase Equilibria, 222, 77-85 (2004).
34. Colina, C.M. and K.E. Gubbins, "Vapor-liquid and vapor-liquid-liquid equilibria of carbon dioxide/n-perfluoroalkane/n-alkane ternary mixtures," Journal Of Physical Chemistry B, 109, 2899-2910 (2005).
35. Galindo, A., A. Gil-Villegas, G. Jackson, and A.N. Burgess, "SAFT-VRE: Phase behavior of electrolyte solutions with the statistical associating fluid theory for potentials of variable range," Journal of Physical Chemistry B, 103, 10272-10281 (1999).
36. Gil-Villegas, A., A. Galindo, and G. Jackson, "A statistical associating fluid theory for electrolyte solutions (SAFT-VRE)," Molecular Physics, 99, 531-546 (2001).
37. Patel, B.H., P. Paricaud, A. Galindo, and G.C. Maitland, "Prediction of the salting-out effect of strong electrolytes on water plus alkane solutions," Industrial & Engineering Chemistry Research, 42, 3809-3823 (2003).
38. Behzadi, B., B.H. Patel, A. Galindo, and C. Ghotbi, "Modeling electrolyte solutions with the SAFT-VR equation using Yukawa potentials and the mean-spherical approximation," Fluid Phase Equilibria, 236, 241-255 (2005).
39. Jackson, G., W.G. Chapman, and K.E. Gubbins, "Phase-Equilibria of Associating Fluids of Spherical and Chain Molecules," International Journal of Thermophysics, 9, 769-780 (1988).
40. Muller, E.A. and K.E. Gubbins, "Molecular-Based Equation of State for Associating Fluids: A Review of SAFT and Related Approaches," Ind. Eng. Chem. Res., 40, 2193-2211 (2001).
41. Economou, I.G., "Statistical Associating Fluid Theory: A successful Model for the Calculation of Thermodynamic and Phase Equilibrium Properties of Complex Fluid Mixtures," Ind. Eng. Chem. Res., 41, 953-962 (2002).
42. Chapman, W.G., S.G. Sauer, D. Ting, and A. Ghosh, "Phase behavior application of SAFT based equations of state-from associating fluids to polydispersion, polar copolymers," Fluid Phase Equilibria, (2003).

43. Gil-Villegas, A., A. Galindo, P.J. Whitehead, S.J. Mills, and G. Jackson, "Statistical associating fluid theory for chain molecules with attractive potential of variable range," J. Chem. Phys., 106, 4168-4186 (1997).
44. Galindo, A., L.A. Davies, A. Gil-Villegas, and G. Jackson, "The thermodynamics of mixtures and the corresponding mixing rules in the SAFT-VR approach for potential of variable range," Molecular Physics, 93, 241-252 (1998).
45. Chapman, W.G., K.E. Gubbins, G. Jackson, and M. Radosz, "New Reference Equation of Sate for Associating Liquids," Ind. Eng. Chem. Res., 29, 1790-1721 (1990).
46. GilVillegas, A., A. Galindo, P.J. Whitehead, S.J. Mills, G. Jackson, and A.N. Burgess, "Statistical associating fluid theory for chain molecules with attractive potentials of variable range," Journal of Chemical Physics, 106, 4168-4186 (1997).
47. Jackson, G., W.G. Chapman, and K.E. Gubbins, "Phase-Equilibria Of Associating Fluids - Spherical Molecules With Multiple Bonding Sites," Molecular Physics, 65, 1-31 (1988).
48. Kraska, T. and K.E. Gubbins, "Phase equilibria calculations with a modified SAFT equation of state.1. Pure alkanes, alkanols, and water," Industrial & Engineering Chemistry Research, 35, 4727-4737 (1996).
49. Kraska, T. and K.E. Gubbins, "Phase equilibria calculations with a modified SAFT equation of state.2. Binary mixtures of n-alkanes, 1-alkanols, and water," Industrial & Engineering Chemistry Research, 35, 4738-4746 (1996).
50. Muller, E.A. and K.E. Gubbins, "An Equation of State for Water from a Simplified Intermolecular Potential," Industrial & Engineering Chemistry Research, 34, 3662-3673 (1995).
51. Xu, K., Y.G. Li, and W.B. Liu, "Application of perturbation theory to chain and polar fluids - Pure alkanes, alkanols and water," Fluid Phase Equilibria, 142, 55-66 (1998).
52. Gubbins, K.E. and C.G. Gray, "Perturbation Theory for the Angular pair Correlation Function in Molecular Fluids," Molecular Physics, 23, 187-191 (1972).
53. Stell, G., J.C. Rasaiah, and H. Narang, "Thermodynamic Perturbation-Theory for Simple Polar Fluids.1," Molecular Physics, 23, 393-& (1972).
54. Jog, P.K. and W.G. Chapman, "Application of Wertheim's thermodynamic perturbation theory to dipolar hard sphere chains," Molecular Physics, 97, 307-319 (1999).
55. Jog, P.K., S.G. Sauer, J. Blaesing, and W.G. Chapman, "Application of dipolar chain theory to the phase behavior of polar fluids and mixtures," Industrial & Engineering Chemistry Research, 40, 4641-4648 (2001).
56. Tumakaka, F. and G. Sadowski, "Application of the Perturbed-Chain SAFT equation of state to polar systems," Fluid Phase Equilibria, 217, 233-239 (2004).
57. Dominik, A., W.G. Chapman, M. Kleiner, and G. Sadowski, "Modeling of polar systems with the perturbed-chain SAFT equation of state. Investigation of the performance of two polar terms," Industrial & Engineering Chemistry Research, 44, 6928-6938 (2005).

58. Saager, B., J. Fischer, and M. Neumann, "Reaction field simulations of monoatomic and diatomic dipolar fluids," Molecular Simulation, 27-49 (1991).
59. Saager, B. and J. Fischer, "Construction And Application Of Physically Based Equations Of State.2. The Dipolar And Quadrupolar Contributions To The Helmholtz Energy," Fluid Phase Equilibria, 72, 67-88 (1992).
60. Gross, J. and J. Vrabec, "An equation-of-state contribution for polar components: Dipolar molecules," Aiche Journal, 52, 1194-1204 (2006).
61. Wertheim, M.S., "Exact Solution of Mean Spherical Model for Fluids of Hard Spheres with Permanent Electric Dipole Moments," Journal of Chemical Physics, 55, 4291-& (1971).
62. Patey, G.N. and J.P. Valleau, "Dipolar Hard Spheres - Monte-Carlo Study," Journal Of Chemical Physics, 61, 534-540 (1974).
63. Verlet, L. and J.J. Weis, "Perturbation Theories For Polar Fluids," Molecular Physics, 28, 665-682 (1974).
64. Andersen, H.C., D. Chandler, and J.D. Weeks, "Roles of Repulsive and Attractive Forces in Liquids - Optimized Random Phase Approximation," Journal Of Chemical Physics, 56, 3812-& (1972).
65. Adelman, S.A. and J.M. Deutch, "Exact Solution of Mean Spherical Model for Simple Polar Mixtures," Journal Of Chemical Physics, 59, 3971-3980 (1973).
66. Fries, P.H. and G.N. Patey, "The Solution of the Hypernetted-Chain Approximation for Fluids of Nonspherical Particles - a General-Method with Application to Dipolar Hard-Spheres," Journal of Chemical Physics, 82, 429-440 (1985).
67. Perkyns, J.S., P.H. Fries, and G.N. Patey, "The Solution of the Reference Hypernetted-Chain Approximation for Fluids of Hard-Spheres with Dipoles and Quadrupoles," Molecular Physics, 57, 529-542 (1986).
68. Lee, P.H. and B.M. Ladanyi, "Structural and Dielectric-Properties of Dipolar Hard-Sphere Mixtures - Reference Hypernetted Chain and Pertubation Theory Results," Journal of Chemical Physics, 91, 7063-7074 (1989).
69. Gray, C.G. and K.E. Gubbins, Theory of Molecular fluids. 1984.
70. Hoye, J.S., J.L. Lebowitz, and G. Stell, "Generalized Mean Spherical Approximations for Polar and Ionic Fluids," Journal of Chemical Physics, 61, 3253-3260 (1974).
71. Stell, G. and S.F. Sun, "Generalized Mean Spherical Approximation For Charged Hard Spheres - Electrolyte Regime," Journal Of Chemical Physics, 63, 5333-5341 (1975).
72. Peng, Y., H. Zhao, and C. McCabe, "On the thermodynamics and phase behavior of heteronuclear chain molecules using the SAFT-VR approach," Molecular Physics, 104, 571-586 (2006).
73. Gray, C.G., Y.S. Sainger, C.G. Joslin, P.T. Cummings, and S. Goldman, "Computer-Simulation Of Dipolar Fluids - Dependence Of The Dielectric-Constant On System Size - A Comparative-Study Of Ewald Sum And Reaction Field Approaches," Journal Of Chemical Physics, 85, 1502-1504 (1986).
74. Barker, J.A. and R.O. Watts, "Monte-Carlo Studies of Dielectric Properties of Water-Like Models," Molecular Physics, 26, 789-792 (1973).

75. Cummings, P., I. Nezbeda, W.R. Smith, and G. Morriss, "Monte Carlo simulation results for the full pair correlation function of the hard dumbell fluid," Molecular Physics, 43, 1471 (1981).
76. Gil-Villegas, A., G. Jackson, and S.C. McGrother, "Computer simulation of dipolar liquid crystals," Journal Of Molecular Liquids, 76, 171-181 (1998).
77. Benavides, A.L., Y. Guevara, and F. Delrio, "Vapor-Liquid-Equilibrium of a Multipolar Square-Well Fluid.1. Effect of Multipolar Strengths," Physica A, 202, 420-437 (1994).
78. Garzon, B., S. Lago, and C. Vega, "Reaction Field Simulations of the Vapor-Liquid-Equilibria of Dipolar Fluids - Does the Reaction Field Dielectric-Constant Affect the Coexistence Properties," Chemical Physics Letters, 231, 366-372 (1994).
79. Smit, B., C.P. Williams, E.M. Hendriks, and S.W. Deleeuw, "Vapor Liquid Equilibria for Stockmayer Fluids," Molecular Physics, 68, 765-769 (1989).
80. Sengers, J.V. and J.M.H. Levelt Sengers, "Thermodynamic Behavior of Fluids near the Critical-Point," Annual Review of Physical Chemistry, 37, 189-222 (1986).
81. Gil-Villegas, A., A. Galindo, P.J. Whitehead, S.J. Mills, and G. Jackson, "Statistical associating fluid theory for chain molecules with attractive potentials of variable range," J. Chem. Phys., 106, 4168-4186 (1997).
82. Peng, Y., H.G. Zhao, and C. McCabe, "On the thermodynamics of diblock chain fluids from simulation and heteronuclear statistical associating fluid theory for potentials of variable range," Molecular Physics, 104, 571-586 (2006).
83. Gupta, S. and J.D. Olson, "Industrial needs in physical properties," Industrial & Engineering Chemistry Research, 42, 6359-6374 (2003).
84. Kontogeorgis, G.M., E.C. Voutsas, I.V. Yakoumis, and D.P. Tassios, "An equation of state for associating fluids," Industrial & Engineering Chemistry Research, 35, 4310-4318 (1996).
85. Kontogeorgis, G.M., I.V. Yakoumis, H. Meijer, E. Hendriks, and T. Moorwood, "Multicomponent phase equilibrium calculations for water-methanol-alkane mixtures," Fluid Phase Equilibria, 160, 201-209 (1999).
86. Voutsas, E.C., I.V. Yakoumis, and D.P. Tassios, "Prediction of phase equilibria in water/alcohol/alkane systems," Fluid Phase Equilibria, 160, 151-163 (1999).
87. Folas, G.K., G.M. Kontogeorgis, M.L. Michelsen, and E.H. Stenby, "Application of the cubic-plus-association equation of state to mixtures with polar chemicals and high pressures," Industrial & Engineering Chemistry Research, 45, 1516-1526 (2006).
88. Ikonomou, G.D. and M.D. Donohue, "Compact - A Simple Equation Of State For Associated Molecules," Fluid Phase Equilibria, 33, 61-90 (1987).
89. Ikonomou, G.D. and M.D. Donohue, "Thermodynamics Of Hydrogen-Bonded Molecules - The Associated Perturbed Anisotropic Chain Theory," Aiche Journal, 32, 1716-1725 (1986).
90. Ikonomou, G.D. and M.D. Donohue, "Extension Of The Associated Perturbed Anisotropic Chain Theory To Mixtures With More Than One Associating Component," Fluid Phase Equilibria, 39, 129-159 (1988).

91. Elliott, J.R., S.J. Suresh, and M.D. Donohue, "A Simple Equation Of State For Nonspherical And Associating Molecules," Industrial & Engineering Chemistry Research, 29, 1476-1485 (1990).
92. Visco, D.P. and D.A. Kofke, "Modeling the Monte Carlo simulation of associating fluids," Journal Of Chemical Physics, 110, 5493-5502 (1999).
93. Wierzchowski, S. and D.A. Kofke, "A general-purpose biasing scheme for Monte Carlo simulation of associating fluids," Journal Of Chemical Physics, 114, 8752-8762 (2001).
94. Chen, B. and J.I. Siepmann, "A novel Monte Carlo algorithm for simulating strongly associating fluids: Applications to water, hydrogen fluoride, and acetic acid," Journal Of Physical Chemistry B, 104, 8725-8734 (2000).
95. Chen, B. and J.I. Siepmann, "Improving the efficiency of the aggregation-volume-bias Monte Carlo algorithm," Journal Of Physical Chemistry B, 105, 11275-11282 (2001).
96. Tsangaris, D.M. and J.J. Depablo, "Bond-Bias Simulation Of Phase-Equilibria For Strongly Associating Fluids," Journal Of Chemical Physics, 101, 1477-1489 (1994).
97. Widom, B., "Some Topics in the Theory of Fluids," Journal Of Chemical Physics, 39, 2808 (1963).
98. Ghonasgi, D. and W.G. Chapman, "Theory And Simulation For Associating Fluids With 4 Bonding Sites," Molecular Physics, 79, 291-311 (1993).
99. CRC, Handbook of Chemistry and Physics. Handbook of Chemistry and Physics. 1981, Cleveland: Chemical Rubber Pub. CO.
100. Pitzer, K.S., "Thermodynamics Of Electrolytes.1. Theoretical Basis And General Equations," Journal Of Physical Chemistry, 77, 268-277 (1973).
101. Chen, C.C., H.I. Britt, J.F. Boston, and L.B. Evans, "Local Composition Model For Excess Gibbs Energy Of Electrolyte Systems.1. Single Solvent, Single Completely Dissociated Electrolyte Systems," Aiche Journal, 28, 588-596 (1982).
102. Chen, C.C. and L.B. Evans, "A Local Composition Model For The Excess Gibbs Energy Of Aqueous-Electrolyte Systems," Aiche Journal, 32, 444-454 (1986).
103. Stell, G. and J.L. Lebowitz, "Equilibirum Properties Of A System Of Charged Particles," Journal Of Chemical Physics, 49, 3706 (1968).
104. Henderson, D., "Equation Of State Of Ionic Fluids," Acs Symposium Series, 204, 47-71 (1983).
105. Henderson, D., L. Blum, and A. Tani, "Equation Of State Of Ionic Fluids," Acs Symposium Series, 300, 281-296 (1986).
106. Chan, K.Y., "Ion Dipole Model Perturbation-Theory Applied To Simple Electrolytes," Journal Of Physical Chemistry, 95, 7465-7471 (1991).
107. Jin, G. and M.D. Donohue, "An Equation Of State For Electrolyte-Solutions.1. Aqueous Systems Containing Strong Electrolytes," Industrial & Engineering Chemistry Research, 27, 1073-1084 (1988).
108. Jin, G. and M.D. Donohue, "An Equation Of State For Electrolyte-Solutions.2. Single Volatile Weak Electrolytes In Water," Industrial & Engineering Chemistry Research, 27, 1737-1743 (1988).

109. Jin, G. and M.D. Donohue, "An Equation Of State For Electrolyte-Solutions.3. Aqueous-Solutions Containing Multiple Salts," Industrial & Engineering Chemistry Research, 30, 240-248 (1991).
110. Vimalchand, P., I. Celmins, and M.D. Donohue, "Vle Calculations For Mixtures Containing Multipolar Compounds Using The Perturbed Anisotropic Chain Theory," Aiche Journal, 32, 1735-1738 (1986).
111. Rosenfeld, Y. and L. Blum, "Statistical Thermodynamics Of Charged Objects," Journal Of Physical Chemistry, 89, 5149-5151 (1985).
112. Rosenfeld, Y. and L. Blum, "Statistical-Mechanics Of Charged Objects - General-Method And Applications To Simple Systems," Journal Of Chemical Physics, 85, 1556-1566 (1986).
113. Chandler, D. and H.C. Andersen, "Optimized Cluster Expansions for Classical Fluids.2. Theory of Molecular Liquids," Journal of Chemical Physics, 57, 1930-& (1972).
114. Hirata, F. and P.J. Rossky, "An Extended Rism Equation For Molecular Polar Fluids," Chemical Physics Letters, 83, 329-334 (1981).
115. Hirata, F., P.J. Rossky, and B.M. Pettitt, "The Interionic Potential Of Mean Force In A Molecular Polar-Solvent From An Extended Rism Equation," Journal Of Chemical Physics, 78, 4133-4144 (1983).
116. Barker, J.A. and D. Henderson, "What Is Liquid - Understanding States of Matter," Reviews of Modern Physics, 48, 587-671 (1976).
117. Waisman, E. and J.L. Lebowitz, "Mean Spherical Model Integral-Equation For Charged Hard Spheres.1. Method Of Solution," Journal Of Chemical Physics, 56, 3086-& (1972).
118. Waisman, E. and J.L. Lebowitz, "Mean Spherical Model Integral-Equation For Charged Hard Spheres.2. Results," Journal Of Chemical Physics, 56, 3093-& (1972).
119. Blum, L., "Mean Spherical Model For Asymmetric Electrolytes.1. Method Of Solution," Molecular Physics, 30, 1529-1535 (1975).
120. Ball, F.X., H. Planche, W. Furst, and H. Renon, "Representation Of Deviation From Ideality In Concentrated Aqueous-Solutions Of Electrolytes Using A Mean Spherical Approximation Molecular-Model," Aiche Journal, 31, 1233-1240 (1985).
121. Lu, J.F., Y.X. Yu, and Y.G. Li, "Modification And Application Of The Mean Spherical Approximation Method," Fluid Phase Equilibria, 85, 81-100 (1993).
122. Blum, L., "Solution of a Model for Solvent-Electrolyte Interactions in Mean Spherical Approximation," Journal of Chemical Physics, 61, 2129-2133 (1974).
123. Blum, L. and J.S. Hoye, "Mean Spherical Model For Asymmetric Electrolytes.2. Thermodynamic Properties And Pair Correlation-Function," Journal Of Physical Chemistry, 81, 1311-1317 (1977).
124. Adelman, S.A. and J.M. Deutch, "Exact Solution Of Mean Spherical Model For Strong Electrolytes In Polar-Solvents," Journal Of Chemical Physics, 60, 3935-3949 (1974).
125. Blum, L. and D.Q. Wei, "Analytical Solution Of The Mean Spherical Approximation For An Arbitrary Mixture Of Ions In A Dipolar Solvent," Journal Of Chemical Physics, 87, 555-565 (1987).

126. Hoye, J.S. and G. Stell, "Ionic Solution In A Molecular Polar-Solvent," Journal Of Chemical Physics, 68, 4145-4150 (1978).
127. Hoye, J.S. and G. Stell, "Correlation-Functions For An Ionic Solution In A Polar-Solvent," Journal Of Chemical Physics, 71, 1985-1986 (1979).
128. Li, C.X., Y.G. Li, J.F. Lu, and L.Y. Yang, "Study of the ionic activity coefficients in aqueous electrolytes by the non-primitive mean spherical approximation equation," Fluid Phase Equilibria, 124, 99-110 (1996).
129. Lvov, S.N. and R.H. Wood, "Equation Of State Of Aqueous Nacl Solutions Over A Wide-Range Of Temperatures, Pressures And Concentrations," Fluid Phase Equilibria, 60, 273-287 (1990).
130. Loehe, J.R. and M.D. Donohue, "Recent advances in modeling thermodynamic properties of aqueous strong electrolyte systems," Aiche Journal, 43, 180-195 (1997).
131. Anderko, A., P.M. Wang, and M. Rafal, "Electrolyte solutions: from thermodynamic and transport property models to the simulation of industrial processes," Fluid Phase Equilibria, 194, 123-142 (2002).
132. Liu, W.B., Y.G. Li, and J.F. Lu, "A new equation of state for real aqueous ionic fluids based on electrolyte perturbation theory, mean spherical approximation and statistical associating fluid theory," Fluid Phase Equilibria, 160, 595-606 (1999).
133. Wu, J.Z. and J.M. Prausnitz, "Phase equilibria for systems containing hydrocarbons, water, and salt: An extended Peng-Robinson equation of state," Industrial & Engineering Chemistry Research, 37, 1634-1643 (1998).
134. Tan, S.P., H. Adidharma, and M. Radosz, "Statistical Associating Fluid Theory Coupled with Restricted Primitive Model to represent aqueous strong electrolutes," Industrial & Engineering Chemistry Fundamentals, 44, 4442-4452 (2005).
135. Cameretti, L.F., G. Sadowski, and J.M. Mollerup, "Modeling of aqueous electrolyte solutions with perturbed-chain statistical associated fluid theory," Industrial & Engineering Chemistry Research, 44, 3355-3362 (2005).
136. Leonard, P.J., Henderso.D, and J.A. Barker, "Perturbation Theory and Liquid Mixtures," Transactions of the Faraday Society, 66, 2439-& (1970).
137. Boublik, T., "Hard-Sphere Equation of State," Journal of Chemical Physics, 53, 471-472 (1970).
138. Mansoori, G.A., N.F. Carnahan, K.E. Starling, and T.W. Leland, "Equilibrium Thermodynamic Properties of Mixture of Hard Spheres," Journal of Chemical Physics, 54, 1523-1525 (1971).
139. Wei, D.Q. and L. Blum, "The Mean Spherical Approximation For An Arbitrary Mixture Of Ions In A Dipolar Solvent - Approximate Solution, Pair Correlation-Functions, And Thermodynamics," Journal Of Chemical Physics, 87, 2999-3007 (1987).
140. Adelman, S.A., "Effective Direct Correlation-Function - Approach To Theory Of Liquid Solutions," Journal Of Chemical Physics, 64, 724-731 (1976).
141. Barker, J.A., "Reaction Field, Screening, and Long-Range Interactions in Simulations of Ionic and Dipolar Systems," Molecular Physics, 83, 1057-1064 (1994).

142. Neumann, M., O. Steinhauser, and G.S. Pawley, "Consistent Calculation Of The Static And Frequency-Dependent Dielectric-Constant In Computer-Simulations," Molecular Physics, 52, 97-113 (1984).
143. Nymand, T.M. and P. Linse, "Ewald summation and reaction field methods for potentials with atomic charges, dipoles, and polarizabilities," Journal Of Chemical Physics, 112, 6152-6160 (2000).
144. Cummings, P.T., H.D. Cochran, J.M. Simonson, R.E. Mesmer, and S. Karaborni, "Simulation Of Supercritical Water And Of Supercritical Aqueous-Solutions," Journal Of Chemical Physics, 94, 5606-5621 (1991).
145. Zhu, S.B. and G.W. Robinson, "Molecular-Dynamics Computer-Simulation Of An Aqueous Nacl Solution - Structure," Journal Of Chemical Physics, 97, 4336-4348 (1992).
146. Bandura, A.V., S.N. Lvov, and D.D. Macdonald, "Thermodynamics of ion solvation in dipolar solvent using Monte Carlo mean reaction field simulation," Journal Of The Chemical Society-Faraday Transactions, 94, 1063-1072 (1998).
147. Holbrey, J.D. and K.R. Seddon, "Ionic liquids. Green Products and Processes," Appl. Chem., 72, 1391-1398 (1999).
148. Blanchard, L.A., D. Hancu, E.J. Beckman, and J.F. Brennecke, "Green processing using ionic liquids and CO2," Nature, 39, 28-29 (1999).
149. Earle, M.J. and K.R. Seddon, "Ionic liquids: Green solvents for the future," Pure Appl. Chem., 72, 1391-1398 (2000).
150. Carlin, R.T. and J.S. Wilkes, In Chemistry of Nonaqueous Solutions. 1994, New York: VCH Publisher Inc. 277-306.
151. Cull, S.G., J.D. Holbrey, V. Vargas-Mora, and K.R. Seddon, Room-temperature ionic liquids as replacements for organic solvents in multiphase bioprocess operations. 2000.
152. Cull, S.G., J.D. Holbrey, V. Vargas-Mora, and K.R. Seddon, "Room-temperature ionic liquids as replacement for organic solvents in multiphase bioprocess operations," Biotechnol. Bioeng., 69, 227-233 (2000).
153. Welton, T., "Room-temperature Ionic Liquids. Solvents for Synthesis and Catalysis," Chem. Rev., 99, 2071-2083 (1999).
154. Rosa, J.N., C.A.M. Afonso, and A.G. Santo, "Ionic liquids as a recyclable reaction medium for the Baylis-Hllman reaaction," Tetrahedron, 57, 4189-4193 (2001).
155. Gordon, C.M., "New developments in catalysis using ionic liquids," Appl. Catal. A-Gen, 222, 101-117 (2001).
156. Visser, A.E., R.P. Swatloski, J.G. Hudleston, and R.D. Rogers, "Room temperature ionic liquids as alternatives to organic solvents in liquid/liquid extraction of metal ions," Abstr. Pap. Am. Chem. Soc., 217, 040-IEC (1999).
157. Blanchard, L.A. and J.F. Brennecke, "Recovery of organic products from ionic liquids using supercritical carbon dioxide," Ind. Eng. Chem. Res., 40, 287-292 (2001).
158. Brennecke, J.F. and E.J. Maginn, "Ionic liquids: Innovative fluids for chemical processing," AICHE J., 47, 2384-2389 (2001).

159. Gu, Z.Y. and J.F. Brennecke, "Volume expansivities and isothermal compressibilities of imidazolium and pyridinium-based ionic liquids," Journal of Chemical and Engineering Data, 47, 339-345 (2002).
160. de Azevedo, R.G., J. Esperanca, V. Najdanovic-Visak, Z.P. Visak, H.J.R. Guedes, M.N. da Ponte, and L.P.N. Rebelo, "Thermophysical and thermodynamic properties of 1-butyl-3-methylimidazolium tetrafluoroborate and 1-butyl-3-methylimidazolium hexafluorophosphate over an extended pressure range," Journal Of Chemical And Engineering Data, 50, 997-1008 (2005).
161. Jacquemin, J., P. Husson, A.A.H. Padua, and V. Majer, "Density and viscosity of several pure and water-saturated ionic liquids," Green Chemistry, 8, 172-180 (2006).
162. Scovazzo, P., D. Camper, J. Kieft, J. Poshusta, C. Koval, and R. Noble, "Regular solution theory and CO2 gas solubility in room-temperature ionic liquids," Industrial & Engineering Chemistry Research, 43, 6855-6860 (2004).
163. Camper, D., C. Becker, C. Koval, and R. Noble, "Low pressure hydrocarbon solubility in room temperature ionic liquids containing imidazolium rings interpreted using regular solution theory," Industrial & Engineering Chemistry Research, 44, 1928-1933 (2005).
164. Camper, D., P. Scovazzo, C. Koval, and R. Noble, "Gas solubilities in room-temperature ionic liquids," Industrial & Engineering Chemistry Research, 43, 3049-3054 (2004).
165. Kato, R., M. Krummen, and J. Gmehling, "Measurement and correlation of vapor-liquid equilibria and excess enthalpies of binary systems containing ionic liquids and hydrocarbons," Fluid Phase Equilibria, 224, 47-54 (2004).
166. Kato, R. and J. Gmehling, "Systems with ionic liquids: Measurement of VLE and activity coefficients data and prediction of their thermodynamic behavior using original UNIFAC, mod. UNIFAC(D)) and COSMO-RS(O1)," Journal of chemical thermodynamics, 37, 603-619 (2005).
167. Shariati, A. and C.J. Peters, "High-pressure phase behavior of systems with ionic liquids: measurements and modeling of the binary system fluoroform+1-ethyl-3-methylimidazolium hexafluorophosphate," Journal of Supercritical Fluids, 25, 109-117 (2003).
168. Shiflett, M.B. and A. Yokozeki, "Solubilities and diffusivities of carbon dioxide in ionic liquids: [bmim][PF6] and [bmim][BF4]," Industrial & Engineering Chemistry Research, 44, 4453-4464 (2005).
169. Qin, Y. and J.M. Prausnitz, "Solubilities in ionic liquids and molten salts from a simple perturbed-hard-sphere theory," Industrial & Engineering Chemistry Research, 45, 5518-5523 (2006).
170. Kroon, M.C., E.K. Karakatsani, I.G. Economou, G.J. Witkamp, and C.J. Peters, "Modeling of the carbon dioxide solubility in imidazolium-based ionic liquids with the tPC-PSAFT equation of state," Journal Of Physical Chemistry B, 110, 9262-9269 (2006).
171. Carnahan, N.F. and K.E. Starling, "Equation of State for Nonattracting Rigid Spheres," J. Chem. Phys., 51, 635-636 (1969).

172. Daubert, T.E., R.P. Danner, H.M. Sibul, and C.C. Stebbins, Physical and Thermodynamic Properties of Pure Chemicals: Data Compilation. 1989, Washington, D. C.: Tayor & Francis.
173. Zhao, H.G. and C. McCabe, "Phase behavior of dipolar fluids from a modified statistical associating fluid theory for potentials of variable range," Journal Of Chemical Physics, 125, (2006).
174. de Azevedo, R.G., J. Esperanca, J. Szydlowski, Z.P. Visak, P.F. Pires, H.J.R. Guedes, and L.P.N. Rebelo, "Thermophysical and thermodynamic properties of ionic liquids over an extended pressure range: [bmim][NTf2] and [hmim][NTf2]," Journal Of Chemical Thermodynamics, 37, 888-899 (2005).